European Commission
E.C - Structural Funds

Ministero dell'Università e della
Ricerca Scientifica e tecnologica

Università degli
Studi di Catania

UNIVERSITÁ DEGLI STUDI DI CATANIA
DOTTORATO DI RICERCA INTERNAZIONALE
IN NEUROBIOLOGIA Ciclo XXVIII

Sedi consorziate: Università di Catania, Roma e Pavia
Sede amministrativa: Università di Catania

Dott.ssa Floriana D'Angeli

Biomolecular effects and bioclinical applications of PARPs inhibitors

TESI DI DOTTORATO

COORDINATORE: Chiar.mo Prof. Roberto Avola

TUTOR: Chiar.ma Prof.ssa V. Spina-Purrello

ANNO ACCADEMICO 2015-2016

Index

Section I

Section II

Section I

Biomolecular effects and bioclinical applications of PARPs inhibitors:

"PJ-34 inhibits PARP-1 expression and ERK phosphorylation in glioma-conditioned brain microvascular endothelial cells"

Background

1. PARPs Family

ADP-ribosyltransferases (ARTs) comprise a family of structurally conserved enzymes that catalytically cleave NAD+ and transfer the ADP-ribose moiety to acceptor residues of target proteins (Steffen J.D. et al., 2013). Originally PARP-1 was the only known enzyme with poly(ADP-ribosylation) activity, however, studies over the past decade have identified a family of as many as 17 proteins that share homology to the catalytic domain of PARP-1 (Ame, J.C. et al., 2004) (Figure 1).

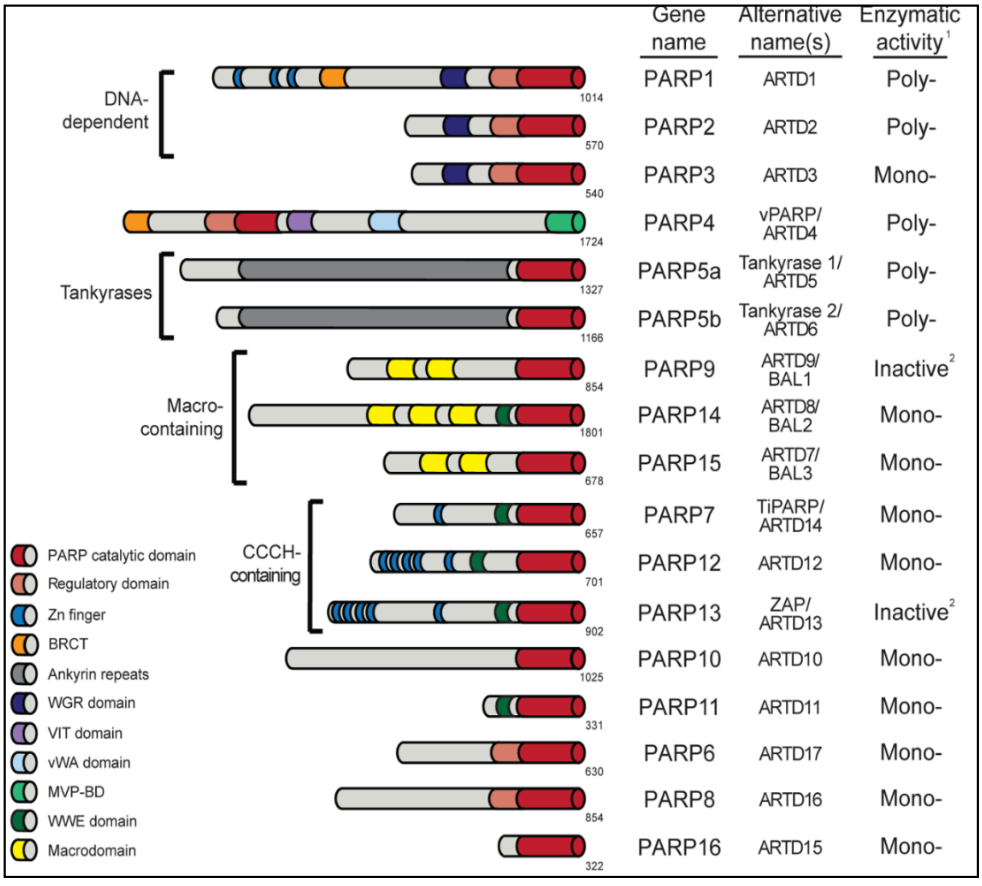

Figure 1. Schematic domain structures of human PARP proteins. Numbers to the bottom right of the protein schematic indicate the total length, in amino acids, of each protein. BRCT: BRCA1 C terminus domain; VIT: vault inter-trypsin domain; vWA: von Willebrand factor type A; MVP-BD: major vault protein binding domain. PARPs are categorized as either poly-ADP-ribosyltransferases (Poly-), mono-ADP-ribosyltransferases (Mono-) or inactive based on presence of conserved motifs and, when available, data using enzymatic assays. PARP-9 and PARP-13 lack one or more catalytic residues conserved in all other PARPs and are therefore predicted to lack catalytic activity, although it is unknown whether they still bind ADP-ribose or ADP-ribosylated proteins. (Daugherty M.D. et al., PLOS Genetics 2014).

Currently, only the first six members of this family (ARTs 1–6) are regarded as having poly(ADP-ribosyl)ation activity: PARP-1, PARP-2, PARP- 3, PARP-4 (vPARP), PARP-5a (TNKS1), and PARP-5b (TNKS2) (Figure 2). The remaining ARTs 7–17, although originally considered PARPs (PARPs 6–16) (Steffen J.D. et al., 2013), are only capable of producing mono-ADP-ribose modifications and are referred to as mono- ARTs (MARTs). ARTs 9 (PARP-9; BAL-1) and 13 (PARP-13) have yet to confirm any sort of catalytic activity like PARPs or MARTs.

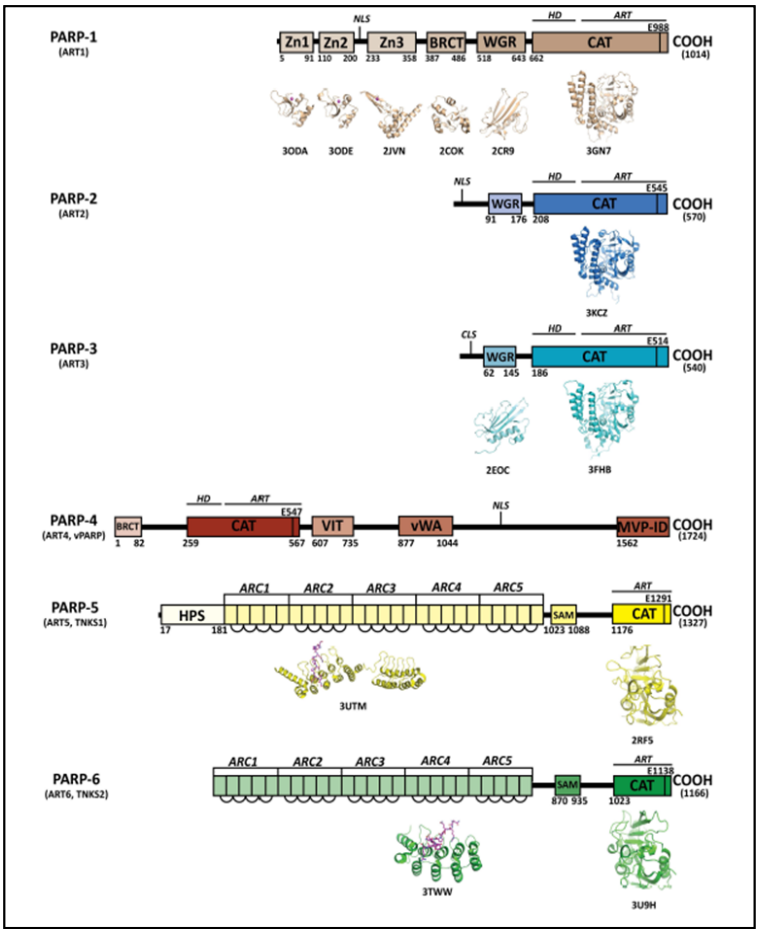

Figure 2. Domains of human PARPs. Sequence and structural representation of six PARPs. Each PARP has a catalytic domain, containing an ADP-ribosyl transferase domain (ART) and conserved catalytic glutamic acid residue. In addition, PARPs 1–4 contain a helical domain (HD) that serves in allosteric regulation. PARPs 1–3 contain a WGR domain, which is important in DNA-dependent catalytic activation. The BRCT domain (Breast Cancer Susceptibility Protein-1) C-terminus is commonly found in DNA-repair and check-point proteins: it resides in the automodification domain of PARP-1 and is also present in PARP-4. Zinc-fingers Zn1 and Zn2 of PARP-1 are important in binding DNA, while the third zinc-finger (Zn3) is important in DNA-dependent catalytic activation. Other domains and sequences represented include: centriole-localization signal (CLS), vault protein inter-alpha-trypsin (VIT), vonWillebrand type A (vWA), major vault particle interaction domain (MVP-ID), His-Pro-Ser region (HPS), ankyrin repeat clusters (ARCs), sterile alpha motif (SAM), and nuclear localization signal (NLS). (Steffen J.D. et al., Frontiers in Oncology 2013).

2. MAR- or PAR-generating PARPs

Multiple characteristics of the PARP catalytic domain are important in determining whether a PARP generates PAR or MAR modifications. These characteristics include the specific amino acid residues that bind to NAD+ and catalyse the transfer reaction, as well as structural elements that define the substrate and acceptor binding pockets (Figure 3; Table 1).

Table 1 | Enzymatic activity and cancer-relevant functions of PARPs

PARP	Alternative names	Demonstrated activity*	Predicted activity	ADP-ribose-binding domains	Cancer-related functions	Cancers to target
PARP1	PARP and ARTD1	PAR[10]	PAR	ND	DNA repair[14], ERK and NF-κB signalling[118] and heat shock response[119]	Those that are homologous recombination-deficient and those with increased ERK and NF-κB signalling
PARP2	ARTD2	PAR[120]	PAR	ND	DNA repair[120]	Those that are homologous recombination-deficient
PARP3	ARTD3	MAR[121]	PAR	ND	DNA repair[122]	ND
PARP4	VPARP and ARTD4	MAR[61]	PAR	ND	ND	ND
PARP5A	TNKS1 and ARTD5	PAR[123]	PAR	ND	Telomere maintenance[124], WNT signalling[125], proteasome regulation[126], stress granule assembly[17] and cell division[127]	Solid tumours with increased WNT signalling that are telomerase-dependent and stress granule-positive
PARP5B	TNKS2 and ARTD6	PAR[128]	PAR	ND	Telomere maintenance[128] and WNT signalling[125]	Those with increased WNT signalling and that are telomerase-dependent
PARP6	ARTD17	ND	MAR[3]	ND	Negative regulator of proliferation[62] and potential tumour-suppressive functions	Unknown
PARP7	TIPARP and ARTD14	MAR[64]	MAR	WWE domain	ND	ND
PARP8	ARTD16	ND	MAR[3]	ND	ND	ND
PARP9	BAL1 and ARTD9	No automodification activity[113]	Inactive[3]	Two macro domains	Cell migration[60]	Metastatic cancers
PARP10	ARTD10	MAR[3]	MAR	ND	Inhibits MYC[68] and NF-κB[57] signalling and is pro-apoptotic[91]	Might have potential tumour-suppressive functions; therefore, increasing its expression in tumours might be useful
PARP11	ARTD11	ND	MAR[3]	WWE domain	ND	ND
PARP12	ARTD12	MAR[17]	MAR	WWE domain	Stress granule assembly[17]	Solid tumours that are stress granule-positive
PARP13	ZAP, ZC3HAV1 and ARTD13	No automodification activity[3]	Inactive[3]	WWE domain	Stress granule assembly[17] and miRNA–RISC regulation[17,56]	Solid tumours that are stress granule-positive
PARP14	BAL2 and ARTD8	MAR[3]	MAR	Three macro domains and a WWE domain	B cell survival[102], cell migration[52] and stress granule assembly[17]	Haematopoietic malignancies and metastatic cancers
PARP15	BAL3 and ARTD7	MAR[17]	MAR	Macro domain	Stress granule assembly[17]	Solid tumours that are stress granule-positive
PARP16	ARTD15	MAR[51,70]	MAR	ND	UPR[51]	UPR-dependent tumours

Table 1. ARTD, ADP-ribosyltransferaseARTD, ADP-ribosyltransferase diphtheria-toxin-like; BAL, B aggressive lymphoma; MAR, mono(ADP-ribose); miRNA, microRNA; ND, not determined; NF-κB, nuclear factor-κB; PAR, poly(ADP-ribose); PARP, PAR polymerase; RISC, RNA-induced silencing complex; TNKS, tankyrase; UPR, unfolded protein response; WWE, Trp-Trp-Glu; ZAP, zinc finger antiviral protein; ZC3HAV1, zinc finger CCCH-type antiviral protein 1. *Catalytic activity is based on the ability of PARPs to automodify when incubated with NAD^+. (Vyas S. and Chang P., PERSPECTIVES 2014).

PAR-generating PARPs contain a His-Tyr-Glu (HYE) motif in which histidine and tyrosine residues are involved in NAD+ binding and coordination, whereas glutamate is required for PAR transfer and elongation activity (Marsischky G. T. et al., 1995). Most PARP family members lack this glutamate and instead contain leucine, isoleucine or valine and are predicted (and in some cases have been shown) to generate in vitro, MAR, using auto-modification reactions containing purified PARP and labelled NAD+ (Table 1). In addition, PARP-9 (also known as B aggressive lymphoma 1 (BAL1) and PARP-13 (also known as ZC3HAV1) lack the histidine residues and are predicted to be enzymatically inactive; they do not show auto-modification activity (Kleine H. et al., 2008; Otto H. et al., 2005) (Table 1).

Structural characteristics of the substrate and acceptor binding pockets, which affect enzymatic activity, include the donor loop (D-loop) that interacts with the substrate NAD+ and is thought to function as a 'lid' to hold NAD+ within the catalytic pocket (Wahlberg E. et al., 2012) (Figure 3). Additionally, the acceptor pocket is partly lined by the loop between β-sheets 4 and 5, which is referred to as the acceptor loop (Figure 3).

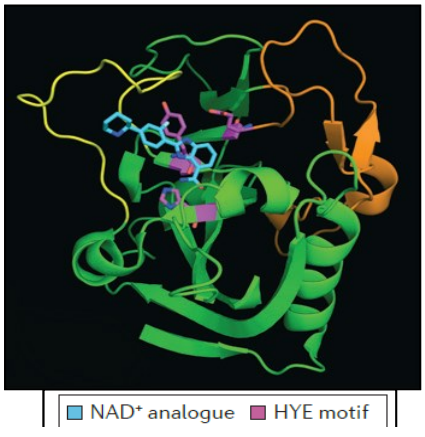

Figure 3. Sequence and structural elements of the poly(ADP-ribose) polymerase (PARP) catalytic domain. The ribbon structure shows the donor (yellow) and acceptor (orange) loops of PARP1 (protein data bank ID: 3L3M117), which shape the substrate and acceptor binding pockets, respectively. The His Tyr Glu (HYE) motif is shown in magenta. A cocrystallized NAD^+ analogue inhibitor (A927929) is shown in cyan. (Vyas S. and Chang P., PERSPECTIVES 2014).

This loop is implicated in the binding of protein substrate for MAR- and PAR-generating PARPs, or incoming ADP-ribose units for PAR-generating PARPs (Han S. and Tainer, J. A., 2002; Ruf A. et al., 1998). Both PAR and MAR function as traditional post-translational modifications, which can alter the functions of target proteins.

3. PARPs functions

PARP-1, the founding member of the PARP family, is a molecular sensor of DNA breaks, playing a key role in the spatial and temporal organization of break repair through the local synthesis of poly(ADP-ribose) (PAR) at damaged sites. Indeed, PARP-1 is activated by single- and double-strand breaks, being one enzyme critical in the base excision repair (BER) pathway (Dantzer, F. et al., 1999). In addition to its critical involvement in cellular response to DNA damage, poly(ADP-ribosyl)ation has been ascribed to regulate various biological processes such as transcription, mitotic segregation, chromatin modification, telomere homeostasis, cell proliferation, transformation, and cell death (Figure 4) (Schreiber et al., 2006). In particular, PARP-1 and, to a lesser extent, PARP-2 are important in maintaining telomere length and chromosomal stability. PARP-1 also forms part of the Groucho/TLE1 co-repressor complex, and has been implicated as a transcriptional regulator of androgen receptor expression. Other PARPs function in the repair of DSBs and in progression of mitosis (PARP-3), and some have potential roles in Wnt signalling and telomere maintenance (PARP-5 and PARP-6). PARP-1 is also a regulator of NHEJ, a mechanism of DSB repair. PARP-1 acts on mitochondria and, depending on the extent of oxidative stress, DNA damage and PARP-1 activation, different cell death pathways may be triggered.

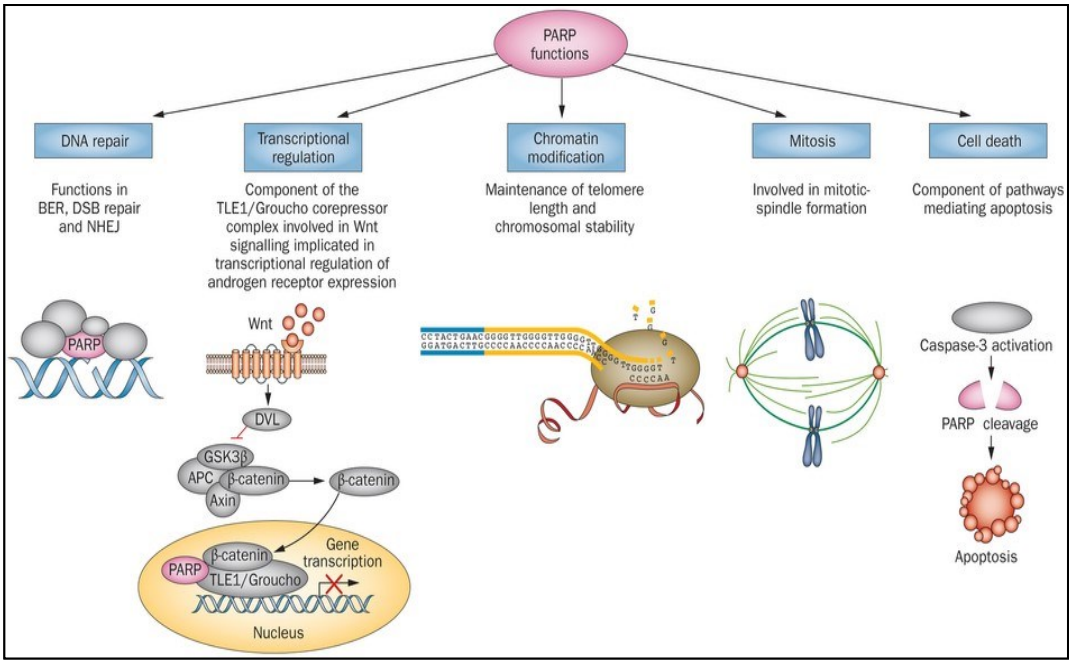

Figure 4. In addition to the classic activity of PARP in BER, the PARP family members have diverse functions in otherbiological processes, including transcriptional regulation, chromatin modification, mitosis (mitotic-spindle formation), and apoptosis, as well as intracellular trafficking, and energy metabolism (not shown). Abbreviations: APC, adenomatous polyposis coli protein; BER, base-excision repair; DSB, double-strand break; DVL, dishevelled homologue; GSK-3β, glycogen synthase kinase-3β; NHEJ, non homologous end joining; PARP, poly(ADP-ribose) polymerase; TLE1, transducin-like enhancer protein 1 (Groucho homologue). (Sonnenblick A. et al., Nat Rev Clin Oncol. 2015).

4. PARPs localization

PARP family members are localized in various cellular compartments, including nucleus, cytoplasm, mitochondria, Golgi Apparatus, endoplasmic reticulum and stress granules, although the function of many of the PARPs are unknown (Figure 5) (Krishnakumar R. and Kraus W. L., 2010). The primary nuclear PARPs are PARP-1, PARP-2 (the closest paralog to PARP-1), PARP-3, and tankyrases 1 and 2 (PARP-5a and -5b). Others PARPs have been found in the cytoplasm, although not exclusively, are v-PARP (PARP-4), PARP-6, PARP-9, the Bal proteins Bal 1-3 (PARP-13, -14, -15), and PARP-10. In addition, PARP-9 and PARP-14 exhibited enriched localization at the cell periphery. Both proteins were later confirmed to co-localize with actin filaments, motile elements of the actin cytoskeleton that are enriched at the cell

periphery. PARP-12 localizes to the Golgi apparatus, while PARP-13 is assembled in to stress granules in the cytoplasm. Finally, PARP16 exhibits reticular membrane localization, identifying it as an endoplasmic reticulum protein (Vyas S. et al., 2013).

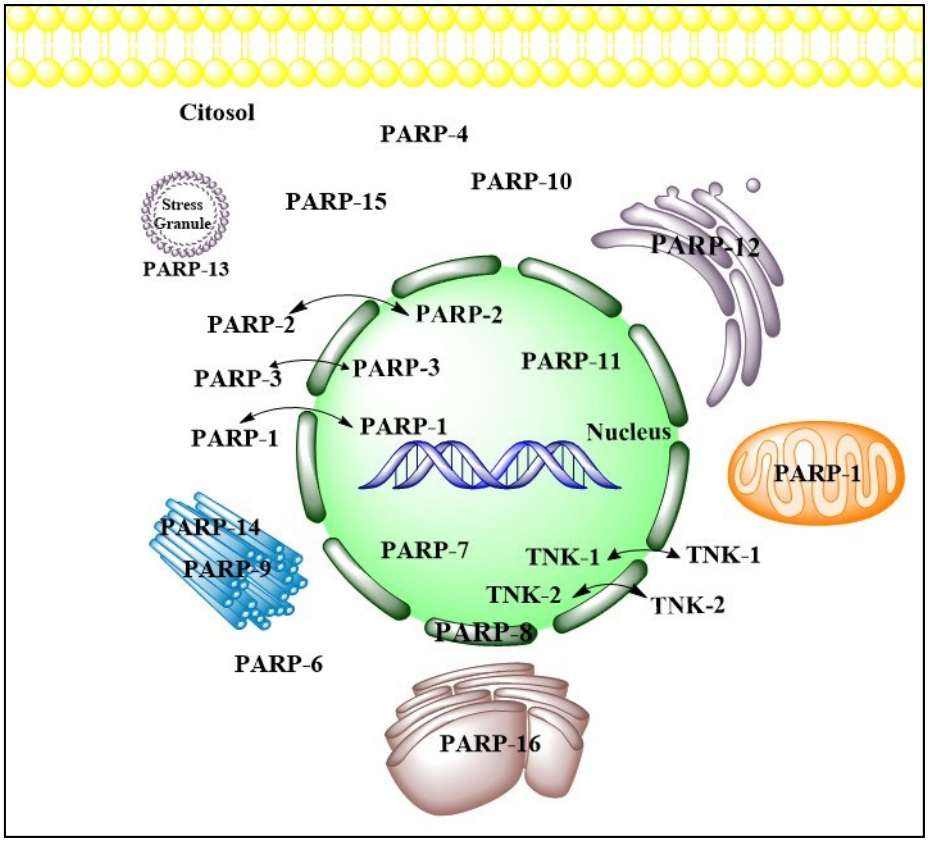

Figure 5. PARPs localization. Human PARPs have various cellular localizations. Some of them are cytoplasmic as PARP-4, PARP-6, PARP-10 and PARP-15; others are localized in the Nucleus as PARP-1, PARP-7, PARP-8 (nuclear envelope) and PARP-11. PARP-2, PARP-3 and TNK-1 and TNK-2 are localized in both cytoplasm and nucleus. PARP-9 and PARP-14 co-localize with actin filaments, while PARP-12 is localized to the Golgi. PARP-13 is assembled in to stress granules in the cytoplasm and PARP-16 exhibited reticular membrane localization.

The best-studied PARP is the founding member PARP-1 that catalyze the formation of long, branched chains of ADP-ribose known as poly-ADP-ribose (PAR) (Daugherty M.D. et al., 2014; Gibson B.A. and Kraus W.L., 2012; Hassa P.O. and Hottiger M.O., 2008; Hottiger M.O. et al., 2010; Schreiber V. et al., 2006). PARP-1 and other poly(ADP-ribosyl) transferases are localized not only in the nucleus but also in the cytoplasm (Motta et al., 2015) and in the mitochondria.

In fact, it has been recently reported that intramitochondrial poly-(ADP-ribosylation) contributes to NAD^+ depletion and cell death induced by oxidative stress in neurons (Nguewa P.A. et al., 2003).

5. PARP-1

Poly(ADP-ribose) polymerases (PARPs) are defined as cell signaling enzymes that catalyze the transfer of ADP-ribose units from NAD+ to a number of acceptor proteins. Poly(ADP-ribose) polymerase-1 (PARP-1), also known as poly(ADP-ribose) synthetase and poly(ADP-ribose) transferase, is the main member of the PARP enzyme family (Nguewa P.A. et al., 2003). PARP-1 is a highly conserved protein of ~116 kDal (D'Amours D. et al., 1999). Like many other chromatin- and transcription related proteins, it has a modular structure comprising multiple independently folded domains. The major functional units of PARP-1 are an amino-terminal DNA-binding domain (DBD), a central automodification domain (AMD), and a carboxyterminal catalytic domain (CD) (Hakme A. et al., 2008; Schreiber V. et al., 2006) (Figure 6). The DBD contains two Cys-Cys-His-Cys zinc fingers (FI/Zn1 and FII/Zn2) that mediate binding to DNA, a newly discovered third zinc binding domain (FIII/Zn3) that mediates interdomain contacts important for DNA-dependent enzyme activation (Langelier M.F. et al., 2008; Langelier M.F. et al., 2010), a nuclear localization signal (NLS), and a caspase-3 cleavage site (Hakme A. et al., 2008; Schreiber V. et al., 2006). The AMD contains a BRCT (BRCA1 C terminus) fold, which mediates protein-protein interactions (e.g., with DNA repair enzymes). The CD, which is the most conserved domain across the PARP family, contains a PARP signature motif, which binds

NAD+, as well as a ‘‘WGR’’ motif, which is named after the most conserved amino acid sequence in the motif (Trp, Gly, Arg) and has an unknown function.

Together, the structural and functional domains of PARP-1 confer the activities required for the broad range of functions of PARP-1 in the nucleus.

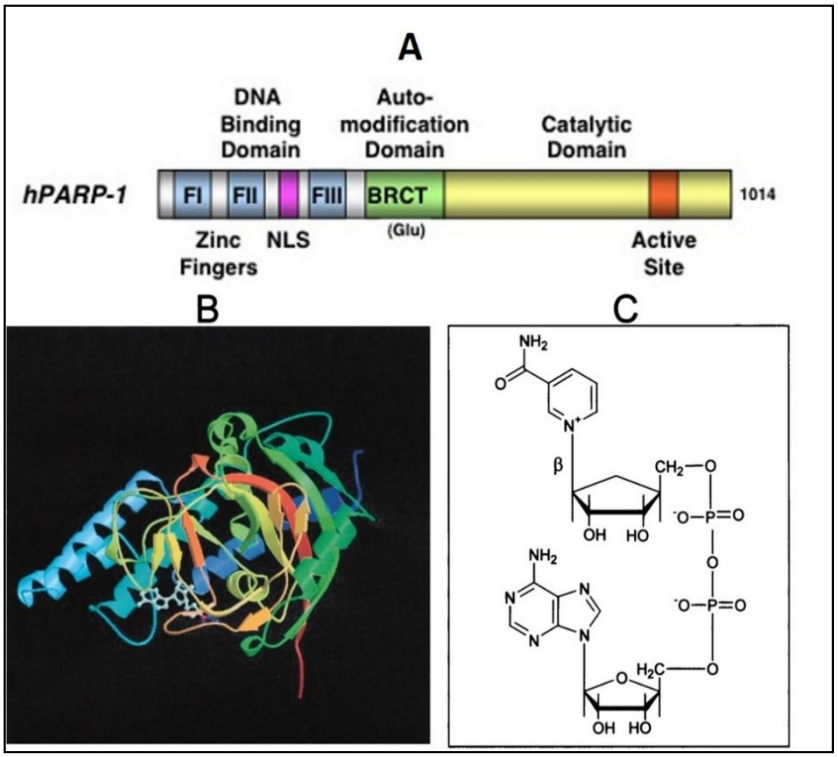

Figure 6. Structure of poly(ADP-ribose) polymerase-1 (PARP-1). A, schematic representation of the modular organization of human PARP-1 (hPARP-1). **B**, ribbon representation of chicken's PARP-1 catalytic fragment (C-terminal end, amino acids 662 to 1014), which was cocrystallized with the NAD analog carba-NAD. The ribbon diagram shows the interaction of carba-NAD (inhibitor substrate analog) with the NAD+-binding site of PARP-CF. The observed bound ADP moiety of carba-NAD is shown; it marks the acceptor site. (Adapted from Ruf A, Rolli V, de Murcia G, and Schulz GE (1998) The mechanism of the elongation and branching reaction of poly(ADP-ribose) polymerase as derived from crystal structures and mutagenesis. J Mol Biol278:57-65. Copyright © 1998 Academic Press. Used with permission.) **C**, structure of carba-NAD: the ring oxygen of the nicotinamide ribose is replaced by a methylene group, which prevents ADP-ribosyl transfer and hydrolysis of the nicotinamide moiety by cleavage of the β-glycosidic bond. (Nguewa P.A. et al., Mol Pharmacol. 2003).

6. PARP-1 and DNA repair

PARP-1 is activated by single- and double-strand breaks, being one enzyme critical in the base excision repair (BER) pathway (Dantzer F. et al., 1999). After the induction of certain types of DNA damage, PARP-1 is rapidly recruited to the altered DNA and its catalytic activity increases 10- to 500-fold, resulting in the synthesis of protein-

conjugated long branched pADPr chains (Dantzer F. et al., 1999; Haince J.F. et al., 2008; Hassa P.O. and Hottiger M.O., 2008).

The addition of pADPr interferes with the functions of modified proteins, such as histones, topoisomerase I and DNA protein kinase (DNA-PK). Notably, however, the bulk of pADPr is attached to PARP1. Once formed, this polymer could recruit hundreds of other proteins (Gagné J.P. et al., 2008; Gottschalk A.J. et al., 2009). Some of these recruited proteins, typified by XRCC1, the scaffolding protein that assembles and activates the DNA base excision repair (BER) machinery (El-Khamisy S.F. et al., 2003; Masson M. et al., 1998), bind directly to pADPr, whereas others are indirectly recruited because they interact with pADPr-binding proteins (figure 7).

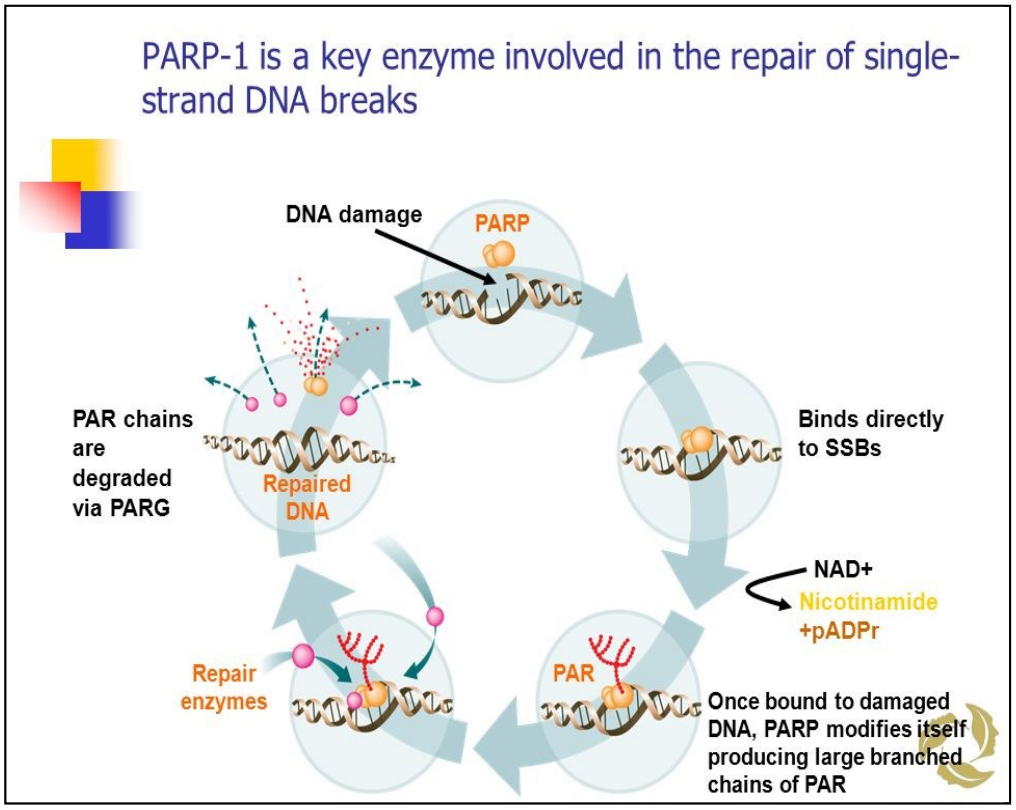

Figure 7. The biochemical pathway of poly(ADP-ribosyl)ation. PARP detects and rapidly binds to DNA strand breaks and catalyzes poly(ADP-ribosyl)ation mainly of itself using NAD+ as substrate. Upon the formation of long, branched polymers, PARP is released from DNA. Upon the formation of long, branched polymers, PARP is released from DNA and the polymers are degraded by the PARG enzyme, permitting access of the DNA repair machinery to the lesion and its repair.

At the same time, formation of pADPr diminishes the affinity of PARP1 and histones for DNA, providing a mechanism for removing PARP1 from damaged DNA and for the local modulation of chromatin compaction (Timinszky G. et al., 2009; Tulin A. and Spradling A., 2003). In vitro studies suggest that removal of PARP-1 provides access for repair proteins and suppresses further pADPr synthesis (Satoh M.S. and Lindahl T., 1992). Further polymer growth is also antagonized by two enzymes that hydrolyse pADPr, poly(ADP-ribose) glycohydrolase (PARG) and, possibly, the ADP-ribose hydrolase ARH3 (Meyer-Ficca M.L. et al., 2004; Oka S. et al., 2006). The concerted action of these enzymes removes pADPr from PARP1, restoring its ability to recognize DNA strand breaks and initiate a new round of damage signalling.

7. DNA-independent PARP-1 activation

Recent findings point to the involvement of PARP-1 activation in processes that are not necessarily related to DNA repair (Cohen-Armon M. et al., 2007). These findings showed that the C-terminal of PARP-1 containing the conserved catalytic domain of PARP enzymes (Amè J.C. et al., 2004) is involved in the interaction of PARP-1 with phosphorylated ERK-2. In cell-free systems, recombinant human PARP-1 was activated and highly auto-polyADP-ribosylated by a direct interaction with phosphorylated ERK2 constructs in the absence of DNA and ATP (one molecule of PARP-1 per two molecules of phosphorylated ERK2) (Cohen-Armon M. et al., 2007). PARP-1 activated by phosphorylated ERK2 has a higher affinity for its substrate, NAD^+, than the affinity of PARP-1 activated by nicked DNA (Cohen-Armon M. et al., 2007; Mendoza-Alvarez H. and Alvarez-Gonzalez R., 1993).

Thus, PARP-1 activated by phosphorylated ERK2 was highly auto-polyADP-ribosylated even at low NAD concentrations (nM) (Cohen-Armon M. et al., 2007).

PolyADP-ribosylated PARP-1 bound to phosphorylated ERK2 acts as a scaffold protein, dramatically enhancing ERK2-catalyzed phosphorylation of the transcription factor Elk1(Cohen-Armon M. et al., 2007).

Elk1, one of the ternary complex transcription factors, forms a ternary complex with the serum response factor (SRF) and the serum response element (SRE) in the promoter of its target genes (Buchwalter G. et al., 2004; Herdegen T. and Leah J.D. 1998). Transcription factor Elk1 is a prominent substrate of phosphorylated mitogen-activated protein kinases (MAPKs) (Buchwalter G. et al., 2004). Phosphorylation of transcription factor Elk1 activates the histone acetyl transferase (HAT) activity of CBP/p300 (Buchwalter G. et al., 2004; Li Q.J. et al., 2003). This results in core histone acetylation, and transcription of the Elk1 target gene, c-fos (Buchwalter G. et al., 2004; Li Q.J. et al., 2003) (Figure 8). ERK induced acetylation of core histones and the expression of immediate early gene c-fos were both suppressed after treatment with either PARP inhibitors or PARP-1- targeted siRNA (Cohen-Armon M. et al., 2007), indicating that PARP-1 activation mediates or significantly enhances transcription induced by ERK phosphorylate. Thus, in the absence of DNA damage, PARP-1 activation by phosphorylated ERK2 might actually mediate proliferation and differentiation regulated by the ERK phosphorylation cascade. In fact, transcription factor c-Fos protein has been implicated in cell proliferation, both in normal and in transformed cells. In view of the stimulatory effect of ERK-induced PARP-1 activation on c-fos expression (Cohen-Armon M. et al., 2007), PARP-1 activation in the ERK signalling pathway is a promising target for anti-proliferation drugs in malignancies caused by enhanced and uncontrolled activation of the ERK phosphorylation cascade.

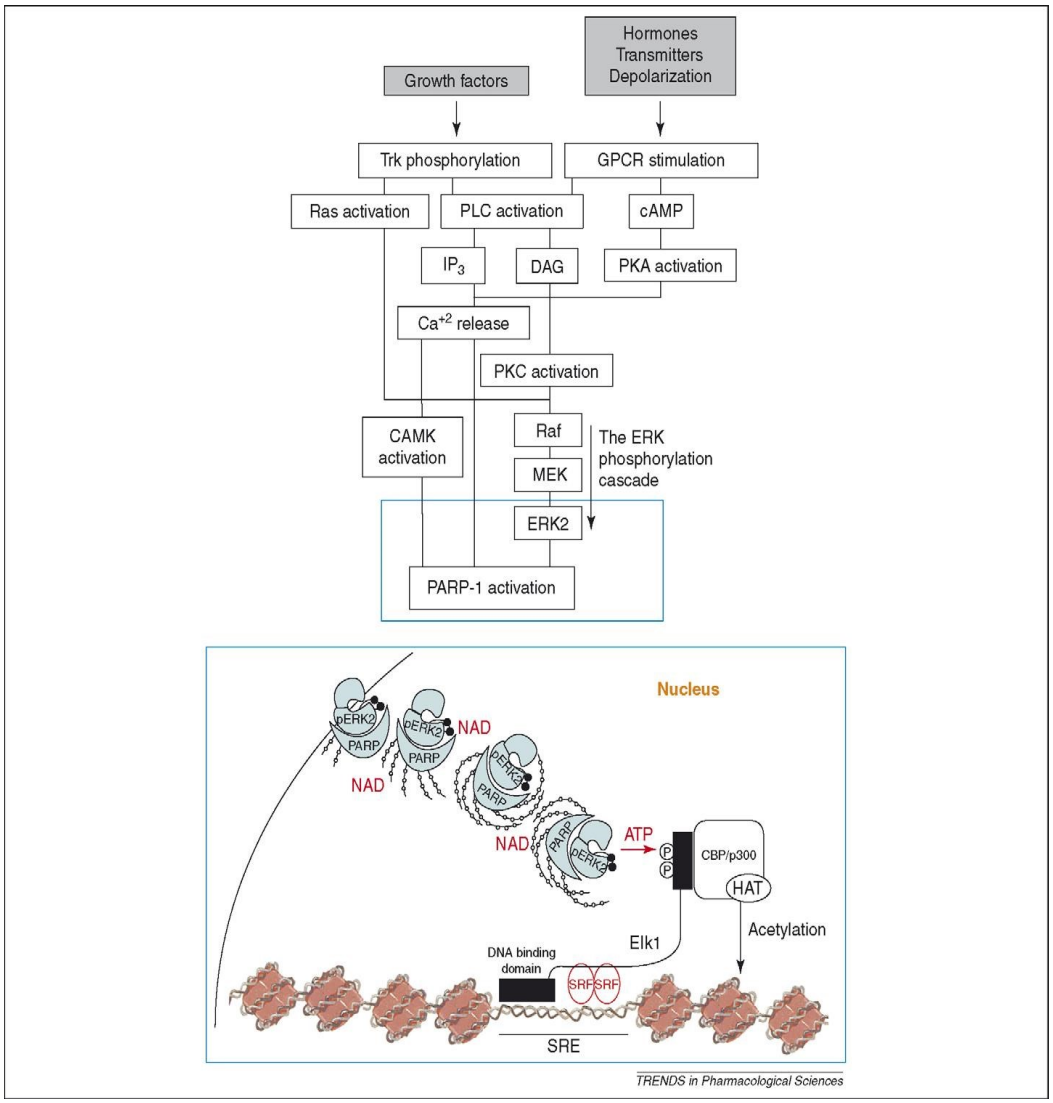

Figure 8. PARP-1 meet phosphorylated ERK2 in the nucleus. ERK is phosphorylated via diverse signal transduction mechanisms initiated by phosphorylation of receptor tyrosin kinases (Trk) or stimulation of G-protein-coupled receptors (GPCR), resulting in PLC activation, Ras activation, phosphorylation of Ca+2 dependent kinases, PKC and CAMK, and activation of the Raf1-MEK-ERK phosphorylation cascade. Phosphorylated ERK shuttles between the cytoplasm and nucleus. The interaction of phosphorylated ERK2 with PARP-1 in the nucleus enhances PARP-1 activation and auto polyADP-ribosylation. PolyADP-ribosylated PARP-1 acts as an anchoring protein for phosphorylated ERK2 in the nucleus. It also acts as a scaffold protein, enhancing ERK-catalyzed phosphorylation of transcription factor Elk1. This results in an enhanced HAT activity CBP, promoting histone acetylation and expression of Elk1 target gene, c-fos. (Cohen-Armon M. et al., Mol. Cell. 2007).

8. PARP and Angiogenesis

Angiogenesis, the process of new blood vessel formation, is crucial for the development and progression of pathophysiological changes associated with a variety of disorders, including various cancers, tumor metastases, and retinopathies.

Recently, a number of reports from various laboratories have led to a novel and unexpected effect of PARP inhibitors, showing a relationship between PARP and angiogenesis, and to the proposition of PARP inhibitors as antiangiogenic agents. So far at least five PARP inhibitors have been efficiently used in vitro (Pyriochou A. et al., 2008; Rajesh, M. et al., 2006a; Rajesh M. et al., 2006b; Tentori L. et al., 2007) to inhibit vascular endothelial growth factor (VEGF)-induced proliferation, migration, and tube formation in human umbilical vein endothelial cells (HUVECs) and in tumor models (Martin-Oliva D. et al., 2006). The PARP inhibitors 3-AB and PJ-34 have been shown to do this in HUVECs in a dose-dependent manner (Rajesh, M. et al., 2006a). Moreover, PARP inhibitors prevented the sprouting of rat aortic ring explants in an ex vivo assay of angiogenesis (Rajesh M. et al., 2006b). The PARP inhibitor PJ-34 was also shown to efficiently inhibit the chicken chorioallantoic membrane model of angiogenesis when used at low concentrations (Pyriochou A. et al., 2008).

Further, PARP activity has the ability to modulate the expression of genes involved in angiogenesis, particularly the hypoxia inducible factor (HIF), whose activity is impaired when tumors are induced either in presence of PARP inhibitor DPQ or in parp-1-knockout mice. HIF-α has been largely involved in tumor progression by promoting a global response to hypoxia, including new vessel formation. There are results suggesting that the absence of PARP-1 modulates HIF-α accumulation by reducing both NO and oxidative stress (Martinez-Romero R. et al., 2008) (Figure 9); however, the ultimate molecular link between HIF-α and PARP-1 has to date not been established clearly and further work will be necessary to unravel this mechanism.

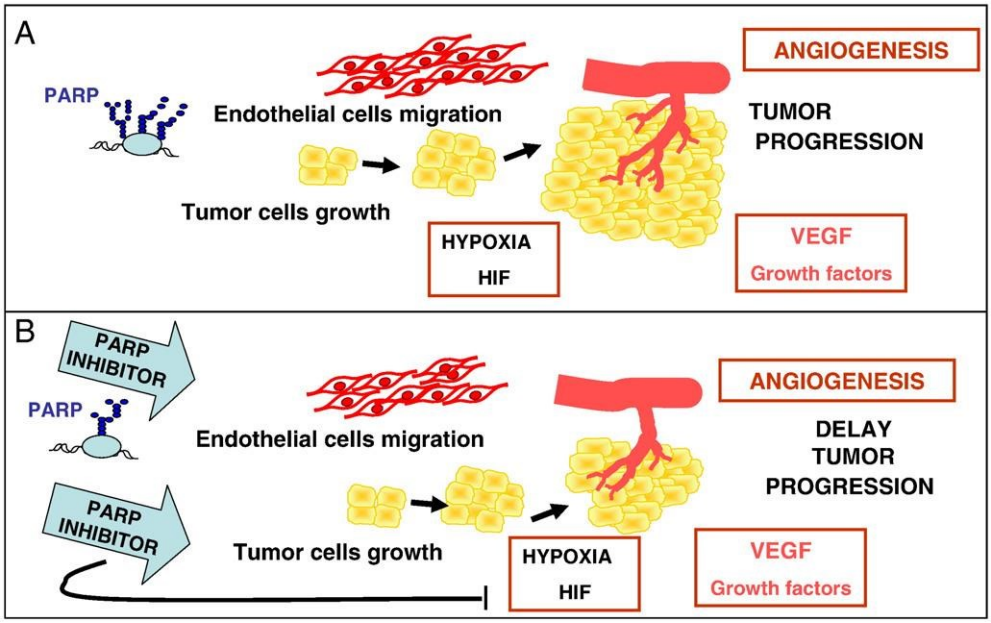

Figure 9 (A) Tumor progression. Hypoxia stimulates the expansion and remodeling of the existing vasculature to enhance blood flow to oxygen-deprived tissues. This process is accomplished primarily through the activation of HIF target genes involved in various steps of angiogenesis, such as vascular endothelial growth factor (VEGF) and other growth factors. (**B) PARP inhibitors promote a delay in tumor formation and a dramatic reduction in tumor size.** PARP inhibitors have an antiangiogenic effect, and they might be an interesting target for the treatment of cancer. (Peralta-Leal A. et al., Free Radic Biol Med. 2009).

9. PARPs Inhibitors

Most of the PARP inhibitors in development mimic the nicotinamide moiety of NAD^+. PARP catalyzes the cleavage of NAD^+ into ADP and ADP-ribose and attaches several molecules of the latter to the target protein in a process called poly(ADP-ribosyl)ation. Therefore, molecules that mimic NAD^+ block the binding of the NAD^+ to the enzyme, inhibiting PARP activity. First-generation inhibitors were developed 30 years ago: nicotinamide, benzamide, and substituted benzamide, in particular 3-aminobenzamide (3-AB), were shown to be competitive inhibitors of PARP (Peralta-Leal A. et al., 2009) (Figure 10). Initial research demonstrated that all the benzamides are more potent inhibitors than nicotinamides or nicotidamide (Purnell M.R. and Whish W.J. 1980).

However, these classical inhibitors lacked specificity and potency.

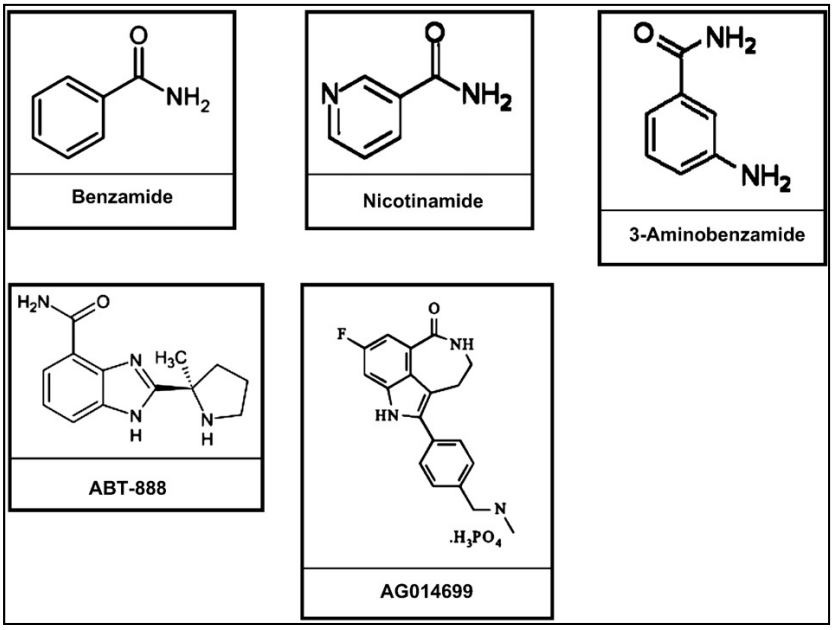

Figure 10. Inhibitors of PARP. The classical inhibitors are nicotinamide, benzamide, and substituted benzamide, in particular 3-aminobenzamide. Important inhibitors in clinical trials include ABT-888 and AG014699. (Peralta-Leal A. et al., Free Radic Biol Med. 2009).

They affect cell viability, glucose metabolism, and DNA synthesis, and in the case of 3-AB used in combination with chemotherapy or radiotherapy, millimolar concentrations are needed, which have a toxic effect (Milam K.M. and Cleaver J. E. 1984). A second generation of very potent PARP inhibitors was developed in the 1990s, producing 170 specific inhibitors. All these inhibitors may be classified as analogues of benzamide that act in the reaction between PARP and NAD+ and they are used in the micromolar range (Banasik M. et al., 1992).

A third generation of inhibitors, benzamidazoles, not only had potency but also allowed the elucidation of the PARP inhibitor structure–activity relationship. These new agents exhibit increased potency and specificity relative to earlier inhibitors (Zaremba T. and Curtin N.J., 2007). The development of specific, potent, effective, and safe PARP inhibitors has become an area of active research and much recent excitement in the PARP field.

Aim of investigation

Inhibitors of PARP-1(Poly(ADP-ribose) polymerase-1) act by competing with NAD^+, the enzyme physiological substrate, which play a protective role in many pathological conditions characterized by PARP-1 overactivation. It has been shown that PARP-1 also promotes tumor growth and progression through its DNA repair activity. Since angiogenesis is an essential requirement for these activities, we sought to determine whether PARP inhibition might affect rat brain microvascular endothelial cells (GP8.3) migration, stimulated by C6-glioma conditioned medium (CM). Through wound-healing experiments and MTT analysis, we demonstrated that PARP-1 inhibitor PJ-34 [N-(6-Oxo-5,6-dihydrophenanthridin-2-yl)-N,N-dimethylacetamide] abolishes the migratory response of GP8.3 cells and reduces their viability. PARP-1 also acts in a DNA independent way within the Extracellular-Regulated-Kinase (ERK) signaling cascade, which regulates cell proliferation and differentiation. By western analysis and confocal laser scanning microscopy (LSM), we analysed the effects of PJ-34 on PARP-1 expression, phospho-ERK and phospho-Elk-1 activation. The effect of MEK (mitogen-activated-protein-kinase-kinase) inhibitor PD98059 (2-(2-Amino-3-methoxyphenyl)-4H-1-benzopyran-4-one) on PARP-1 expression in unstimulated and in CM-stimulated GP8.3 cells was analyzed by RT-PCR. PARP-1 expression and phospho-ERK activation were significantly reduced by treatment of GP8.3 cells with PJ-34 or PD98059. By LSM, we further demonstrated that PARP-1 and phospho-ERK are coexpressed and share the same subcellular localization in GP8.3 cells, in the cytoplasm as well as in nucleoplasm. Based on these data, we propose that PARP-1 and phospho-ERK interact in the cytosol and then translocate to the nucleus, where they trigger a proliferative response.

We also propose that PARP-1 inhibition blocks CM-induced endothelial migration by interfering with ERK signal-transduction pathway.

1. Introduction

PARP-1 (E.C. 2.4.2.30) is the most thoroughly studied protein within the eukaryotic PARP family, which in mammals is comprised of eighteen members identified to date (Amè et al., 2004; Citarelli et al., 2010; D'Amours et al., 1999; Hassa et al., 2008; Hottiger et al., 2010). It catalyzes the attachment of ADP-ribose moieties from its substrate NAD+ to target proteins, modulating their molecular structure and biochemical activity. The enzyme alters chromatin structure, making damaged sites more accessible to members of the DNA Repair Apparatus: these are recruited at lesion sites and undergo ADP-ribosylation (Hassa et al., 2006; Nguewa et al., 2005). Accordingly, PARP-1 plays an important role in genome stability and expression, cell cycle regulation, cell metabolism (Lange et al., 2010). PARP-1 overactivation, with consequent NAD^+ depletion, has been related to inflammation and cell death (Gobell S. Et al., 2001; Spina-Purrello et al., 2008). In fact, its inhibition reduces severity of asthma, colitis, diabetes mellitus, experimental autoimmune encephalomyelitis, Parkinson's disease (Boulares et al., 2003; Burkart et al., 1999; Chiarugi, 2002; Eliasson et al., 1997; Iwashita et al., 2004; Jijon et al., 2000). Furthermore, PARP-1 inhibition causes a decrease in the activity of proangiogenic factors, as vascular endothelial growth factor (VEGF), transmembrane signaling protein syndecan-4 (SDC-4), platelet/endothelial cell adhesion molecule (PECAM1/CD31), and hypoxia inducible factor (HIF): this is due to a block of ERK2 target gene stimulation and ensuing reduction of angiogenesis and inflammation (Lacal et al., 2009; Martin-Oliva et al., 2006; Pyriochou et al., 2008; Tentori et al., 2008). These data suggest the implication of PARP-1 in ERK signaling in addition to its known involvement in DNA repair.

Interestingly, the activity of ERK/MEK inhibitors in blocking the ERK signaling network may be increased by PARP inhibitors (Kerr et al., 2003; Morris et al., 2013; Tai et al., 2007; Yeh et al., 2007). It is well known that glioma is characterized by an active production of proangiogenic factors (Giurdanella et al., 2011). In the present study, we performed cell culture experiments in which GP8.3 cells were incubated with CM in order to study the antiangiogenic effects of PJ-34. In fact, we are convinced that understanding endothelial cell metabolism and the signaling mechanisms that underlie angiogenesis is important, as it provides potential therapeutic targets to inhibit or enhance angiogenesis. We demonstrate here that PJ-34 significantly reduces migration and cell viability of CM-stimulated endothelial cells. To verify the involvement of PARP-1 in ERK signaling pathway, we evaluated PARP-1 expression by RT-PCR, ERK and Elk-1 phosphorylation, by western blotting analysis. In addition by LSM we demonstrated that PARP-1 and phospho-ERK are coexpressed and share the same subcellular localization in GP8.3 cells, both in the cytoplasm as in nucleoplasm. The data obtained demonstrates that PJ-34 (a classical pharmacological PARP-1 inhibitor) lowers ERK and Elk-1 phosphorylation levels, while PD98059, (a well known MEK inhibitor) downregulates PARP-1 expression, confirming an intriguing regulatory loop between PARP-1 and phospho-ERK, which mediates endothelial cell growth and migration.

2. Materials and Methods

2.1 Chemicals and antibodies

Reagent grade chemicals were purchased from Sigma Chemicals Co. (St. Louis, MO) or E. Merck (Darmstadt, Germany). MEK inhibitor PD98059 [2-(2-Amino-3-methoxyphenyl)-4H-1-benzopyran-4-one] and PARP-1 inhibitor PJ-34 [N-(6-Oxo-5,6-dihydrophenanthridin-2-yl)-N,N-dimethylacetamide.HCl] were from Calbiochem. (La Jolla, CA). Primary antibodies against PARP-1 (rabbit polyclonal antibody); rabbit polyclonal antibody against ERK1 or ERK2; mouse monoclonal antibody to phospho-ERK1/2; mouse monoclonal antibody against phospho-Elk-1; rabbit polyclonal antibody against Elk-1; mouse monoclonal antibody against actin; were purchased from Santa Cruz Biotechnology, Inc. (CA). Reagents for RT-PCR: Trizol, deoxyribonuclease 1 (DNase I Amplification Grade), High Capacity RNA-to-cDNA Kit, Power SYBR® Green PCR Master Mix, were from Lifetechnologies™, Foster-City, CA, USA).

2.2 Cell cultures

Immortalized rat brain microvascular endothelial cells GP8.3 were fed with Ham's F-10 medium supplemented with 10% fetal calf serum (FCS), 80 µg/ml heparin, 2 mM glutamine, 100U/ml penicillin, and 100 µg/ml streptomycin. The cell line was already characterized, and our cell cultures were prepared and characterized following previously described procedures (Anfuso et al., 2007). Primary microvascular endothelial cells from bovine brain (BBEC) were purchased from European Collection of Cell Cultures (ECACC).

C6 glioma (rat brain astroglioma) cells were grown in F-12 medium containing 2mM glutamine, antibiotics and 10% FCS (Anfuso et al., 2007; Giurdanella et al., 2011). C6 glioma cells were purchased from European Collection of Cell Cultures (ECACC).

2.3 Preparation of C6 glioma CMs

C6 glioma (rat brain astroglioma) cells ($1x10^6$) were seeded in a 100-mm dish with F-12 medium supplemented with heat inactivated 10% fetal calf serum (FCS) overnight. In cells cultured to sub-confluence, the medium was replaced with 1% serum F12-F10 HAM's (1:1) plus glutamine and antibiotics medium, and the tumor cells were incubated for 48 h. The culture supernatant (CM) was collected, centrifuged at 500xg for 10 min and filtered with 0.2 μm filter. The aliquots were stored at -80°C until use. In all experiments, CM was used without any dilution (Giurdanella et al., 2011).

2.4 MTT assay

To quantify cell viability, the 3-[4,5-dimethylthiazol-2-yl]-2,5-diphenyl tetrasodium bromide (MTT) assay was used (Chemicon, Temecula, CA). Controls (cells grown with 1% FCS, with or without 10μM PJ-34 for 24h) and treated cells (cells grown with CM, with or without 10μM PJ-34 added simultaneously for 24h), were seeded in 96-well plates at 3000 cells/well, to obtain optimal cell density throughout the experiment. In all assays, cells were first incubated at 37°C with MTT for 4h; then, 100μl dimethyl sulfoxide was added and absorbance was measured. The absorbance was read in a plate reader (Synergy 2-bioTek) with a test wavelength of 570 nm.

2.5 Cell migration

GP8.3 cells migration was measured using a standard wound healing assay, essentially performed as previously reported (Giurdanella et al., 2011).

To better evaluate GP8.3 cells migration in our experimental conditions, GP8.3 cells were incubated with or without (data not shown) 10 µg/ml of mitomycin C for 2 h (37°C)and then washed twice with PBS, to render them incapable of cell division (Anfuso et al., 2014).

Migration was followed by an inverted Leica DM IRB microscope equipped with CCD camera. Time zero represents the time after the scratch for all conditions: controls (cells grown with 1% FCS, with or without 10µM PJ-34 for 24h) and treated cells grown with CM, with or without 10µM PJ-34 added simultaneously.

2.6 Western analysis

PARP-1, expression, phospho-ERK and phospho-Elk1 levels were evaluated by western blot analysis. Cells were grown for 24h with 1% FCS: controls; CM, either in presence or absence of inhibitors (10µM PJ-34 or 25µM PD98059 added simultaneously), GP8.3 cells were lysed as previously described (Anfuso et al., 2007; Lupo et al., 2005). Cell lysate proteins were quantified with a bicinchoninic acid (BCA) protein assay kit (Pierce, Thermo Scientific). Immunoblots (30µg nuclear proteins and cell lysate proteins) were performed as described elsewhere (Anfuso et al., 2007). Membranes were incubated with primary antibodies against total ERK1/2 (rabbit polyclonal, 1:500 dilution), phospho-ERK (mouse monoclonal, 1:500 dilution) and PARP-1 (rabbit polyclonal, 1:500), total Elk-1 rabbit polyclonal antibody (1:100 dilution), phospho Elk-1(mouse monoclonal antibody 1:200 dilution). The membranes were then incubated with secondary antibodies for 1h at 20°C, and the immunocomplexes were detected by enhanced chemiluminescence reagent (ECL, Amersham). All blots were controlled for equal loading by actin mouse monoclonal antibody (1:500 dilution).

2.7 RT-PCR

Total RNA was extracted, quantified, DNase-treated, reverse-transcribed and amplified through real-time PCR as previously described (Barbagallo et al., 2014). PPIA was used as reference gene to normalize PCR data. Primer sequences are reported in table 1:

Table 1

Primers used for amplification of PARP1 and PPIA

Gene Name	RefSeq ID	Forward	Reverse
PARP1	NM_007415.2	CTCTCCAATCGCTTCTACAC	GTTGTCTAGCATCTCCACCT
PPIA	NM_008907.1	CAGACGCCACTGTCGCTTT	TGTCTTTGGAACTTTGTCTGCAA

2.8 Immunofluorescence analysis

To detect the expression and localization of PARP-1 and phospho-ERK, by confocal microscopy, GP8.3 cells fed with 1% FCS for 24h as follows: control; +10μM PJ-34; CM; CM+10μM PJ-34 (added simultaneously), were grown on a sterile circular microcover glass (12 mm diameter, from Electron Microscopy Sciences), and inserted on a 24-well plate. After 24h of incubation with or without CM, either in presence or absence of 10μM PJ-34, the cells were processed as previously reported (Scalia et al., 2013). GP8.3 cells were fixed with 3% paraformaldehyde in PBS (phosphate buffered saline), and permeabilized in 0,2% Triton (100-X concentration) for 10 min. The non specific-sites were blocked by incubation in 5% BSA (bovine serum albumin) and subsequently the GP8.3 cells were incubated overnight at 4°C , with the first primary rabbit polyclonal antibody against PARP1 (diluted 1:100 in PBS containing 1% BSA) in a moist chamber.

Following three washing steps with PBS, antirabbit TRITC-conjugated secondary antibody (Santa Cruz) diluted 1:100 in PBS was added for 1h at room temperature in a dark chamber.

After washing in PBS, the cells were incubated overnight at 4°C with the second primary antibody mouse monoclonal phospho-ERK (1:100 dilution in PBS containing 1% BSA). The slides were then washed with PBS and incubated for 1h at room temperature in a dark chamber with the second anti-mouse FITC-conjugated secondary antibody(Santa Cruz) diluted 1:50 in PBS containing 1% BSA. After the fluorescent labeling procedures, the slides were washed three times (5 min each) with PBS, dried on air and finally mounted up-side down on glass slides and covered with a drop of DAPI solution (Electron Microscopy Sciences) to counterstain the nucleus. Negative controls included the omission of both primary antibodies.

2.9 Cell imaging by confocal microscopy

GP8.3 cells fed with 1% FCS for 24h as follows: control;+10μM PJ-34; CM; CM+10μM PJ-34 (added simultaneously), were treated with the immunofluorescent antibodies as described above and then analyzed by confocal microscopy. Imaging was obtained using an Olympus FV1000 confocal laser scanning microscope (LSM), equipped with UV/visible lasers: 405 nm diode, multiline Argon laser (458/488/515 nm), HeNe(G/R) lasers (543/633 nm); oil immersion objective (60xO PLAPO) and spectral filtering system. Acquisition parameters were: 405 nm excitation at 32% laser power, emission filter SDM490 (band pass) 425–475 nm, PMT voltage at 390 V (channel 1, blue); 488 nm excitation at 19% laser power, emission filter SDM560, 500–540 nm, PMT voltage at 775 V (channel 2, green), and 543 nm excitation line at 21% laser power, emission filter BA560IF, PMT 730V.

Image analysis was carried out using the public domain, Java-based image processing program ImageJ (version 1.46e). Statistical analysis was performed with a one-way Anova test by using Microcal Origin (version 8.6).

2.10 Statistic Analysis

Data are expressed as mean ± standard error of the means (S.E.M.). We evaluated the statistical significance of our data by applying the one way ANOVA analysis, to assess significance of at least three sample groups from three different experiments (i.e., biological and technical triplicates). Intensity data (LSM) were analysed by one-way Anova test by using Microcal Origin (version 8.6).

3. Results

To verify the involvement of PARP-1 inhibitor PJ-34 in viability and migration of GP8.3 cells, both in basal conditions and after treatment with CM, we performed MTT analysis and wound-healing experiments. PARP-1 expression, phospho-ERK and phospho-Elk-1 levels, following inhibition by 10μM PJ-34 or 25 μM PD98059 in both conditions, were analyzed by RT-PCR or western analysis. Subcellular localization of PARP-1 and phospho-ERK was identified by electron confocal microscopy.

3.1 Viability of GP8.3 cells in presence of PJ-34 and of CM alone or with PJ-34

Viability of GP8.3 cells in our experimental conditions was assessed through MTT analysis (Fig. 1A).

A

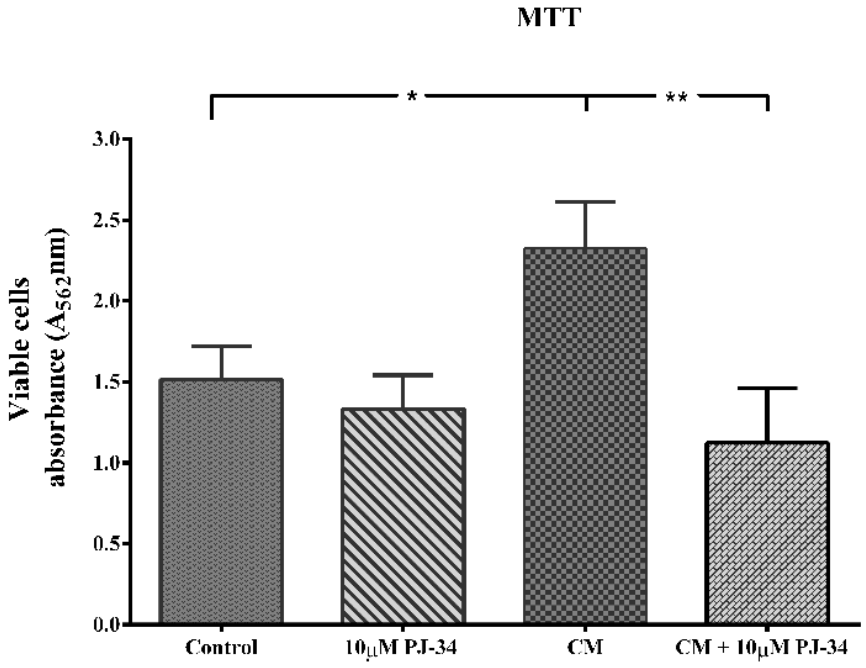

Fig. 1 Panel A. MTT assay on GP8.3 microvascular rat brain endothelial cells. GP8.3 were cultured with 1% FCS medium for 24h: control; 10μM PJ-34; CM; CM+10μM PJ-34 (added simultaneously). *P<0.001 CM vs control; **P<0.001 CM+10μM PJ-34 vs CM. Analysis

Addition of 10μM PJ-34 for 24h to culture medium containing 1% FCS, did not cause any significant effect in cell viability compared to control.

Moreover, in these experimental conditions, without addition of CM, no activation of PARP-1 was observed. Addition of CM to GP8.3 cells induced a statistically significant increase in cell viability. Interestingly, the addition of PARP-1 inhibitor PJ-34 simultaneously to CM-treated GP8.3 cells for 24h significantly reduced cell viability (Fig. 1A): this clearly confirms that the PARP-1 inhibitor is able to counteract the increase in cell viability induced by CM.

3.2 Effects of PARP-1 Inhibitor PJ-34 on stimulated GP8.3 cell migration

Fig. 1B shows representative micrographs of GP8.3 cells 24h after monolayer wounding in cells incubated with or without (data not shown) 10 µg/ml of mitomycin C for 2h (37°C) to render them incapable of cell division.

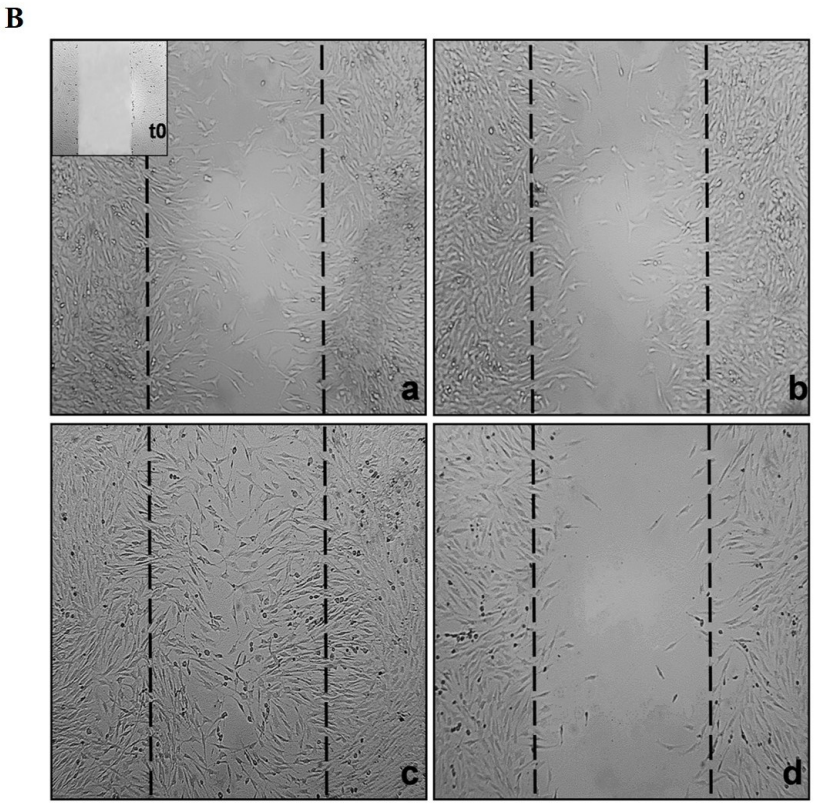

Fig. 1 Panel B. Effect of CM and PJ-34 on GP8.3 cells wound healing in vitro. To better evaluate GP8.3 migration in our experimental conditions, GP8.3 cells were cultured with 1% FCS medium for 24h and incubated with or without (data not shown) 10µg/ml of mitomycin C for 2h (37°C), to render them incapable of cell division. The small box inside panel (a) shows time 0 after scratch. GP8.3 cells were wounded as described in Materials and Methods in the following conditions: control (a); 10µM PJ-34 (b); CM (c); CM+10µM PJ-34 (d) added simultaneously.

When cell monolayer was wounded and incubated in medium containing 1% FCS, alone or in the presence of 10μM PJ-34, the migration of unstimulated GP8.3 cells partially reduced the wound size (Fig. 1B, panels a and b). The image in the small upper box shows the culture at time 0 after scratching. The wound heals in a stereotyped fashion: cells polarize toward the wound, initiate protrusion, migrate, and close the wound during a 36-48h time period. The addition of CM to cultures induced a significant enhancement of crossing cells and a faster migration of GP8.3 cells into the denuded area (Fig. 1B, panel c). GP8.3 cells treated with CM fully traversed the wound in 24h. The addition for 24h of CM+10μM PJ-34 added simultaneously, significantly arrested wound edge advancement, reproducing the same situation present at time 0 (Fig. 1B, panel d).

3.3 PARP-1 expression and PJ-34 effect

To evaluate the effect of PARP-1 inhibition, 10μM PJ-34 was added to GP8.3 cells, grown in culture medium with 1% FCS for 24h: (control+/-PJ-34). This addition caused a minor reduction of PARP-1 expression (Fig. 2A).

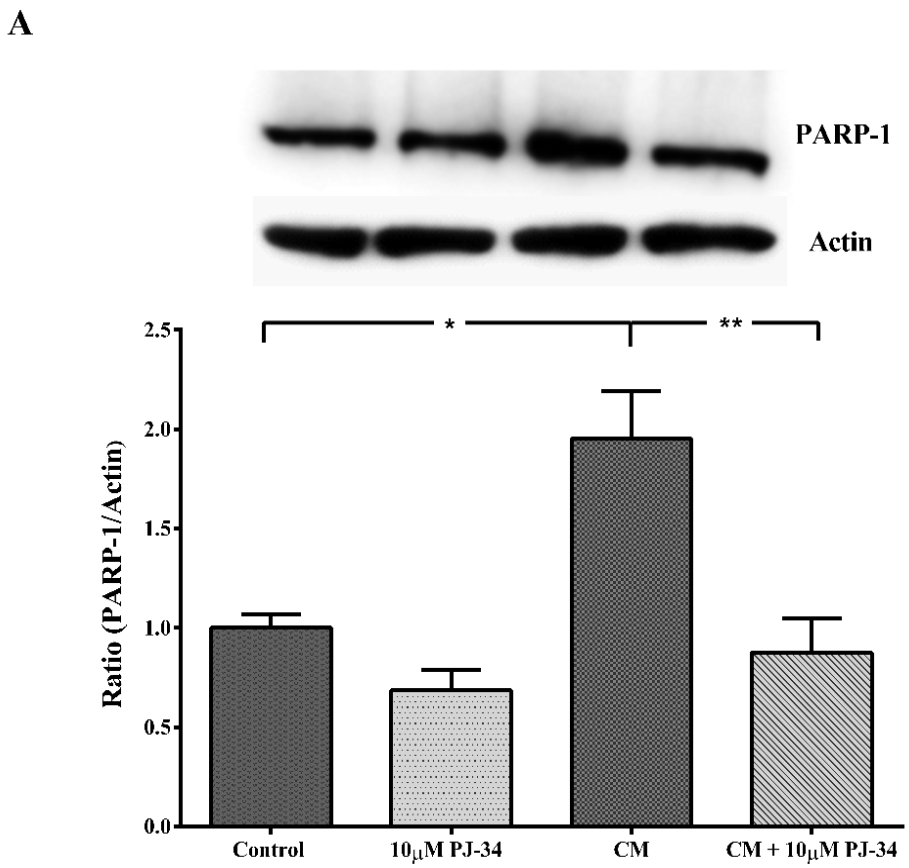

Fig. 2 Effect of PARP-1 inhibitor PJ-34 on PARP-1 expression (Panel A). GP8.3 cells were grown in culture medium containing 1% FCS for 24h: control; 10μM PJ-34; CM; CM+10μM PJ-34 (added simultaneously). Total cell lysates were blotted as reported in Materials a and Methods section. *P<0.001 CM vs control; **P<0.001 CM+10μM PJ-34 vs CM. Analysis was determined with one way ANOVA test (**P<0.001). The error bars indicate ±S.E.M. (S.E.M.=standard error of measurement).

When GP8.3 cells were fed for 24h with CM, a remarkable increase of PARP-1 expression compared to controls was observed, demonstrating the effect of growth factors present in conditioned medium (Fig. 2A). Once again, the addition of PARP-1 inhibitor to cells, added simultaneously with CM, downregulates PARP-1 level.

3.4 Modulation of phospho-ERK levels by PARP-1 inhibitor PJ-34

To verify PARP-1 activation within ERK signalling pathway, we evaluated phospho-ERK expression in endothelial cells by western analysis. Cells were grown in the presence of 1% FCS for 24h (Controls) or to CM for the same time. In both conditions, GP8.3 cells were co-treated with 10μM PJ-34 (Fig. 2 B).

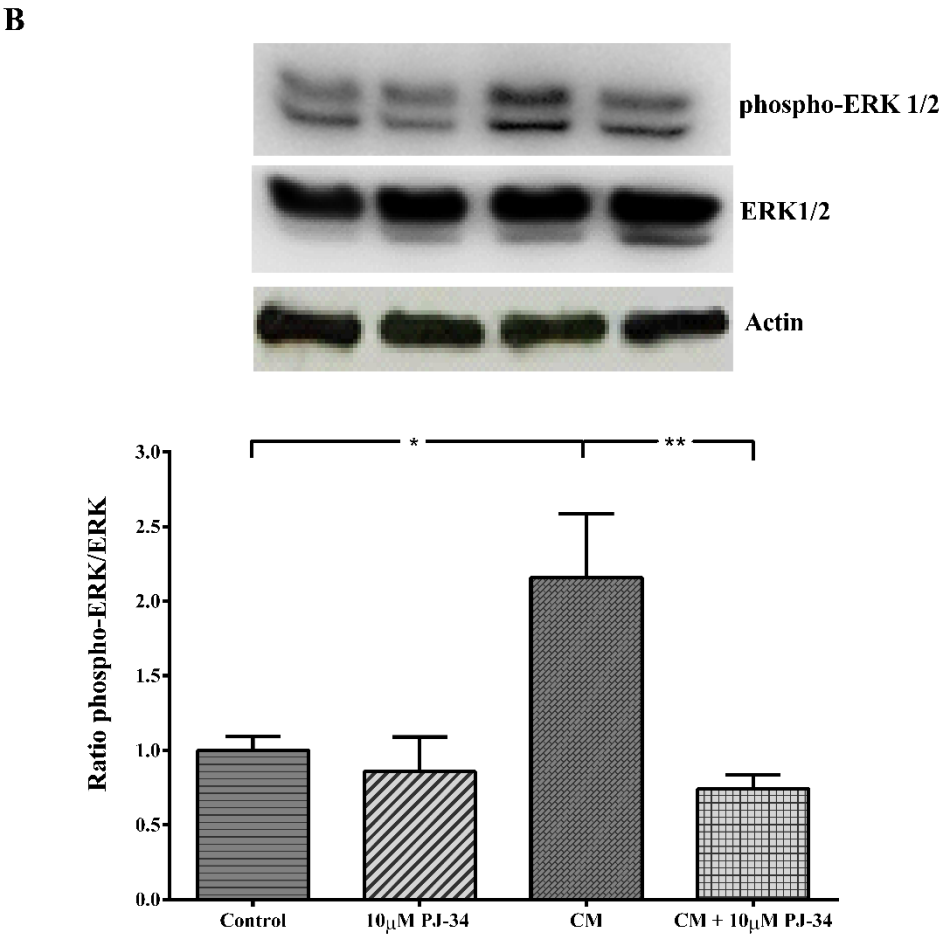

Fig. 2 Effect of PARP-1 inhibitor PJ-34 on phospho-ERK levels (Panel B). GP8.3 cells were grown in culture medium containing 1% FCS for 24h: control; 10μM PJ-34; CM; CM+10μM PJ-34 (added simultaneously). Differently from phospho-ERK, CM and PARP-1 inhibitor did not affect ERK1/2 total protein expressions. Total cell lysates were blotted as reported in Materials and Methods section. *P<0.001 CM vs control; **P<0.001 CM+10μM PJ-34 vs CM. Analysis was determined with one way ANOVA test (**P<0.001). The error bars indicate ±S.E.M. (S.E.M.=standard error of measurement).

GP8.3 cells, stimulated for 24h with CM, expressed phospho-ERK at statistically significant higher levels than unstimulated GP8.3 cells (Fig. 2B).

When GP8.3 cells were treated with 10μM PJ-34, we detected reduced phospho-ERK levels in both unstimulated and CM-treated cells (Fig. 2B); this reduction was highly remarkable in GP8.3 cells maintained for 24h in presence of CM+10μM PJ-34 (Fig. 2B). CM did not induce any change in endothelial ERK1/2 total protein expression (Fig. 2B).

3.5 Modulation of phospho-Elk-1 levels by PARP-1 inhibitor PJ-34

Through western blot analysis, we evaluate the effect of PJ-34 on phospho-Elk-1 levels (Fig. 2C).

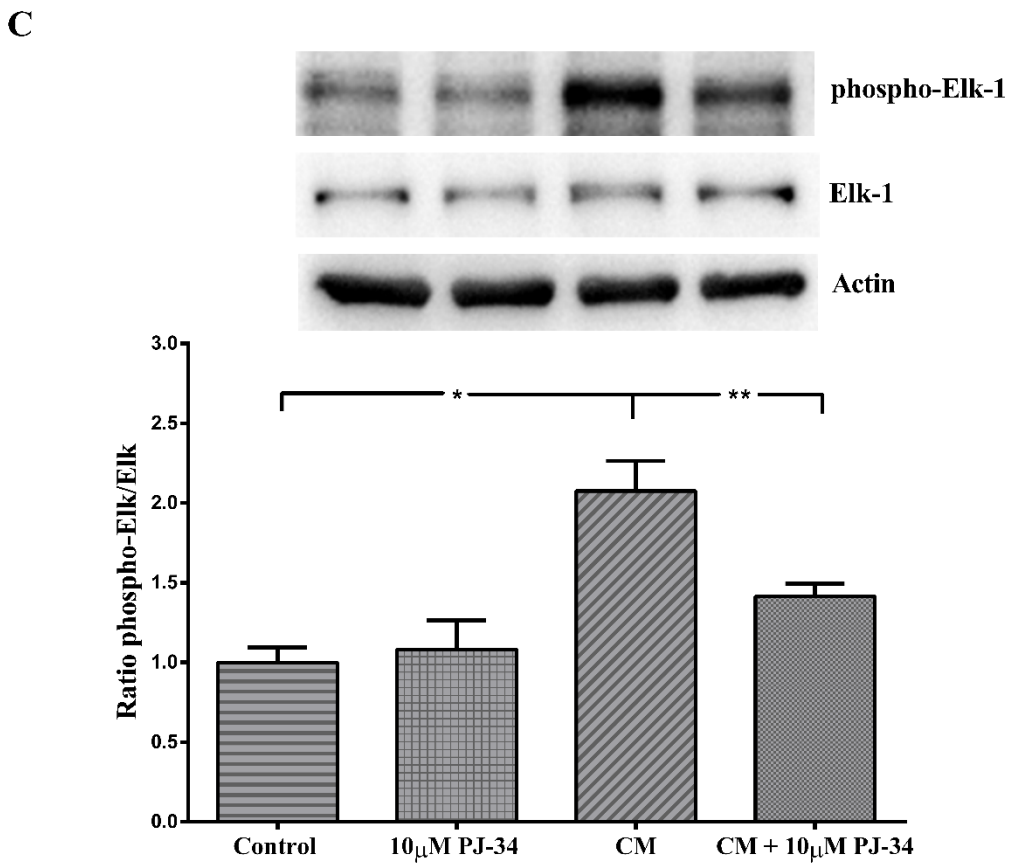

Fig. 2 Effect of PARP-1 inhibitor PJ-34 on phospho-Elk-1 levels (Panel C). GP8.3 cells were grown in culture medium containing 1% FCS for 24h: control; 10μM PJ-34; CM; CM+10μM PJ-34 (added simultaneously). Differently from phospho-Elk-1, CM and PARP-1 inhibitor did not affect Elk-1 total protein expressions. Total cell lysates were blotted as reported in Materials and Methods section. *P<0.001 CM vs control; **P<0.001 CM+10μM PJ-34 vs CM. Analysis was determined with one way ANOVA test (**P<0.001). The error bars indicate ±S.E.M. (S.E.M.=standard error of measurement).

A double fold increase, compared to control was obtained, when CM was added to GP8.3 cells for 24h. On the other hand, a significative reduction of phospho-Elk-1 level was observed in presence of 10µM PJ-34, added simultaneously with CM for 24h. It is clear that, PARP-1 inhibitor is able to modulate phopho-Elk-1 activation, suggesting an interesting involvement of PARP-1 in Elk-1 phosphorylation.

3.6 Effects of MEK inhibitor PD98059 on PARP-1 mRNA levels and on PARP-1 protein expression

To confirm the possible interaction between PARP-1 and phospho-ERK, we tested in cells grown in the same experimental conditions, PD98059 (25µM) on PARP-1 expression using RT-PCR and western analysis approach (Fig. 3A and 3B respectively).

A

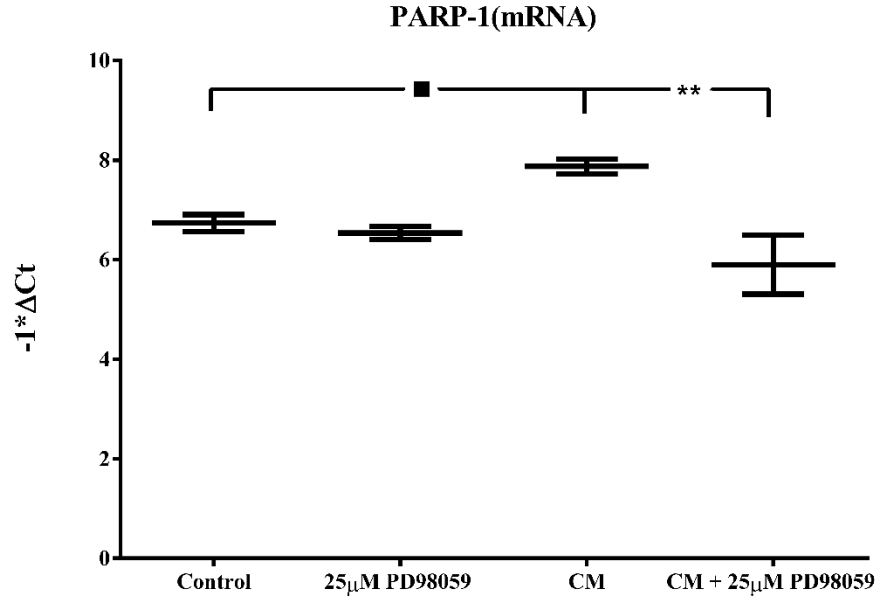

Fig. 3 Effect of MEK inhibitor PD98059 on PARP-1 mRNA level (Panel A). RT-PCR was performed as described in Materials and Methods section. GP8.3 cells were grown in culture medium containing 1% FCS for 24h: control; 25µM PD98059; CM; CM+25µM PD98059, added simultaneously. Panel A: Box plots with whiskers from minimum to maximum represent -1*(ΔCt) values. ▪P<0.05 CM vs control; **P<0.001 CM+25µM PD98059 vs CM.

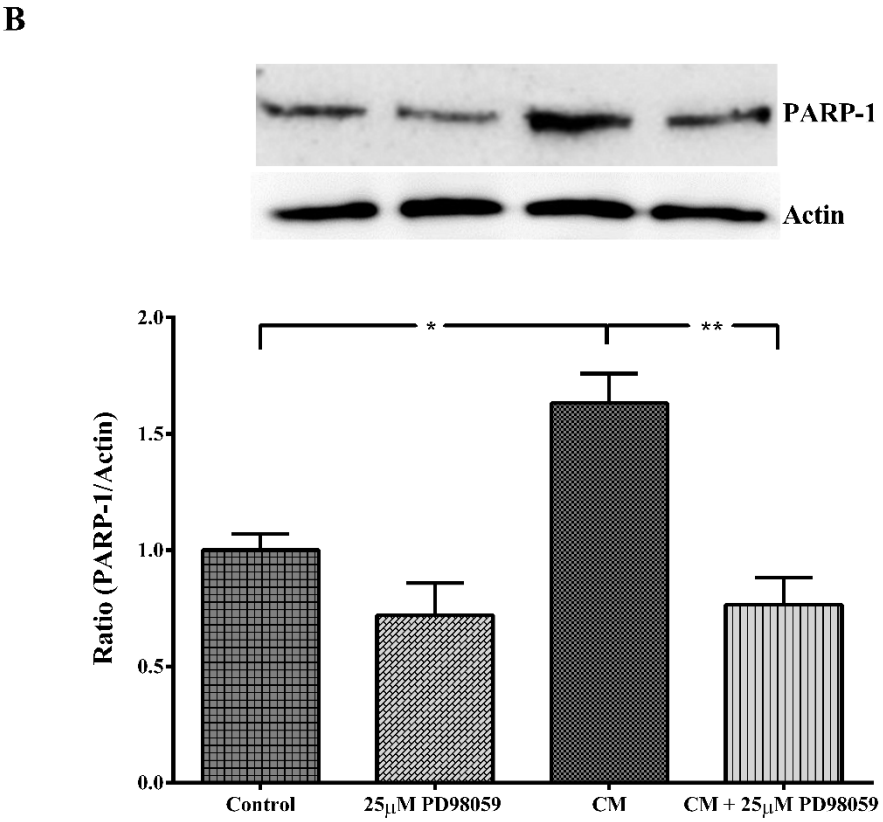

Fig. 4 Effect of MEK inhibitor PD98059 on PARP-1 protein expression (Panel B). Total cell lysate immunoblottings were performed as described in Materials and Methods section. GP8.3 cells were grown in culture medium containing 1% FCS for 24h: control; 25μM PD98059; CM; CM+25μM PD98059, added simultaneously.
Panel B: *P<0.001 CM vs control; **P<0.001 CM+25μM PD98059 vs CM. Analysis was determined with one way ANOVA test. The error bars indicate ±S.E.M. (S.E.M.=standard error of measurement).

PARP-1 mRNA resulted significantly differentially expressed (DE) in GP8.3 cells exposed for 24h to CM, compared to the controls. PARP-1 mRNA resulted even more significantly DE in cells exposed to CM+PD98059 compared to CM (Fig. 3A). A remarkable increase of PARP-1 expression was achieved when GP8.3 cells were cultured for 24h with CM (Fig. 3B). This increase was reversed in presence of 25μM PD98059 (added simultaneously with CM). This downregulation by PD98059 on PARP-1 expression strongly suggests that the two proteins PARP-1 and phospho-ERK may interact. On the other hand, a slight decrease compared to control was obtained when PD98059 was added to the GP8.3 cells for 24h (Fig. 3B).

3.7 Laser scanning microscopy

We investigated the interaction between PARP-1 and phospho-ERK by a laser scanning microscopy using double fluorescence antibodies (respectively, green emission for phospho-ERK and red for PARP-1).

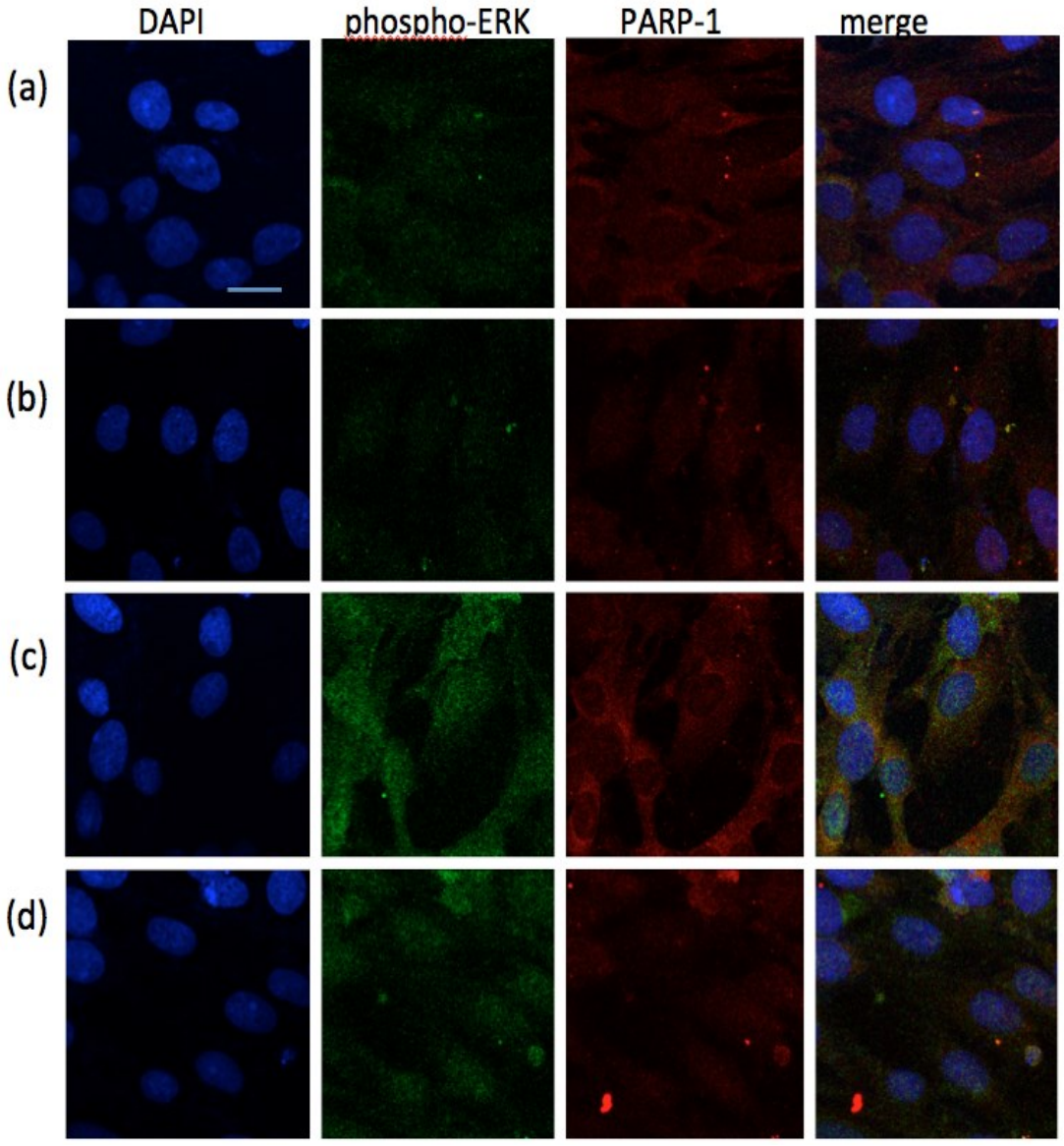

Fig. 5. Confocal LSM of phospho-ERK and PARP-1 expression and localization in GP8.3 cells. GP8.3 cells were cultured in medium containing 1% FCS for 24h: control (a); 10□M PJ-34 (b); CM (c); CM+10□M PJ-34 (d), (added simultaneously), as described in Materials and Methods. Cell monolayers were washed, fixed, permeabilized and stained with a rabbit polyclonal PARP-1 antibody (coupled to a red fluorescent-labeled secondary antibody), and a mouse monoclonal phospho-ERK antibody (coupled to a green fluorescent-labeled secondary antibody). The blue fluorescence is due to the labeling with DAPI to counterstain the nucleus. The merge shows the co-localization of the three dyes. The images were recorded at the following conditions of excitation/emission wavelengths: 405/425-475 nm (blue); 488/500-540 nm (green); 543/560-700 nm (red). Scale bar = 20μm.

Fig. 4 displays representative fluorescence images of the cells dye-labeled in the nucleus and in cytoplasm: in control (Fig. 4 panel a) GP8.3 immunofluorescence signal for PARP1(red) or phospho-ERK (green) are almost detectable in both the cytoplasm and in the nucleus. No significant variation of fluorescence was detected in control+PJ-34 (Fig. 4 panel b).

The CM-culture condition very efficiently enhances the fluorescence intensity red (TRITC secondary antibody) for PARP-1 and green (FITC secondary antibody) for phospho-ERK. The treatment with CM+PJ-34 significantly decreases fluorescence (Fig. 4 panel d). Such effect is more evident for phospho-ERK than PARP-1 labeling (see merged fluorescence images).

Quantitative analysis of confocal micrographs was carried out to analyze the fluorescence differences recorded for the two secondary antibodies FITC and TRITC, with subcellular resolution at the level of intra and extra-nuclear regions (Fig. 5a and 5b). The mean values of fluorescence measured for phospho-ERK indicate a significant increase of intensities by CM as well as a significant decrease of fluorescence upon the simultaneous addition of CM and PJ-34, both inside and outside the nuclei (Fig. 5a). A similar trend was found for the PARP-1 labeled-samples (Fig. 5b). What it is relevant to note is the comparable PARP-1 expression inside and outside the nucleus in presence of CM. PARP-1 expression is drastically reduced below control values in CM+PJ-34 (both added simultaneously), mainly inside the nucleus.

Furthermore, phospho-ERK levels were much higher outside the nucleus in GP8.3 cells grown with CM; the addition of PJ-34 simultaneously with CM to the cells for 24h, caused a significant reduction of phospho-ERK levels, demonstrating once again the effect of PJ-34 also on ERK phosphorylation (Fig. 5a).

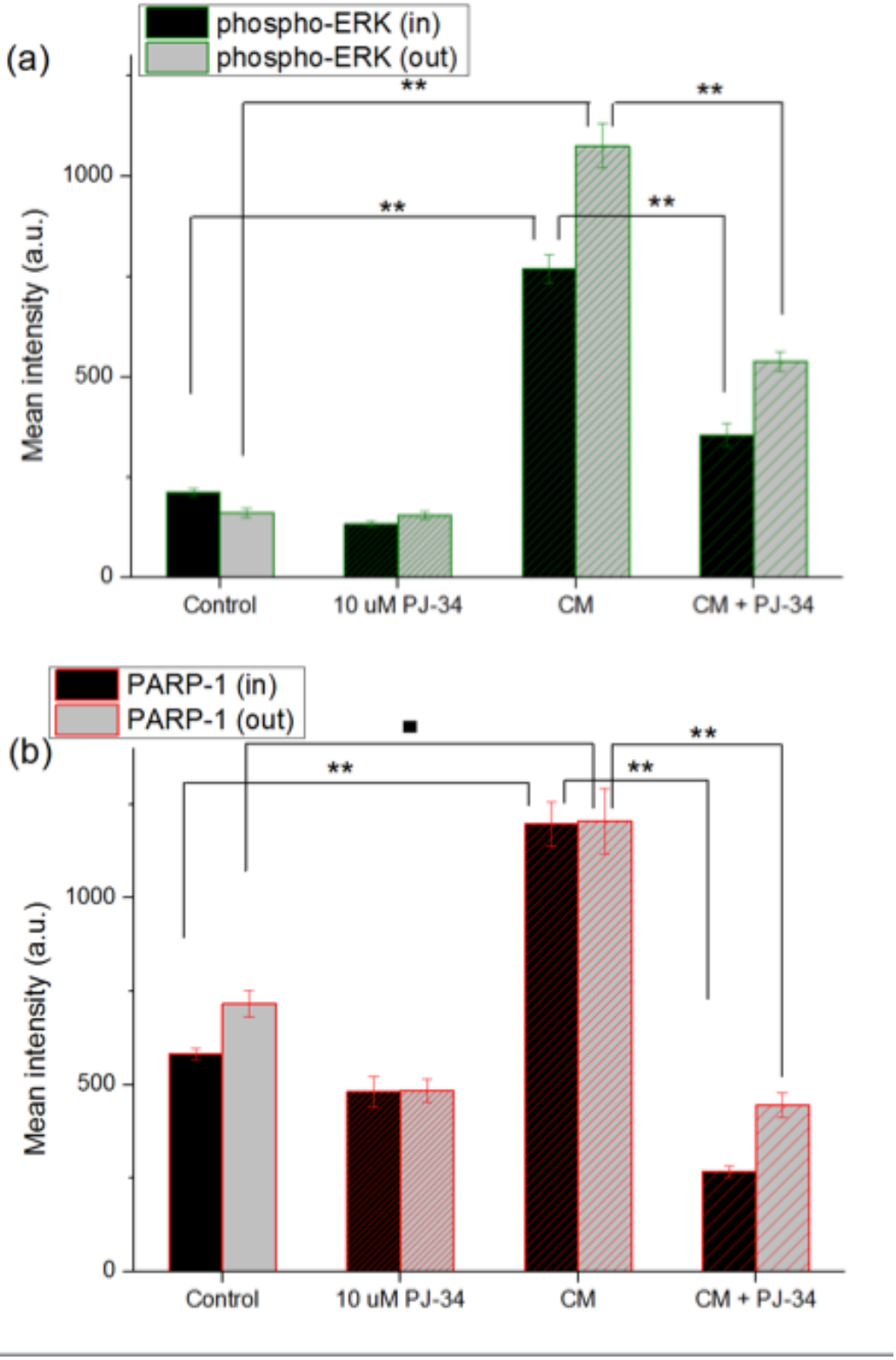

Fig. 5. Quantitative analysis of Confocal LSM data. The graph shows mean intensity values (a.u.) of phospho-ERK (a) and PARP-1 (b) fluorescence inside (in) and outside (out) the nuclear areas, as measured on the confocal LSM . GP8.3 cells were grown in culture medium containing 1% FCS for 24h: control; 10μM PJ-34; CM; CM+10μM PJ-34 (added simultaneously), respectively (a) for phospho-ERK, (b) for PARP-1. One-way analysis of variance (ANOVA; ▪P<0.05, **P<0.001) was performed by using the data from 4–6 randomly chosen fields and a minimum of 10 cells in each field. The error bars indicate ± S.E.M. (S.E.M.=standard error of measurement).

3.8 PARP-1 and phospho-ERK interaction

In Fig. 6 we propose a model based on our data . PARP-1 activation by phosphorylated ERK could contribute to the mechanism of proliferation and migration induced by the MAPK cascade of ERK, and Elk-1 (Fig. 6). Activated PARP-1 increases ERK-catalyzed Elk1 phosphorylation. This leads to an increases of migration, proliferation and vascular permeability. Based on our LMS analysis (Fig. 4 and Fig. 5), we propose that PARP-1 and phospho-ERK interact in the cytosol before their migration into the nucleus (Fig. 6).

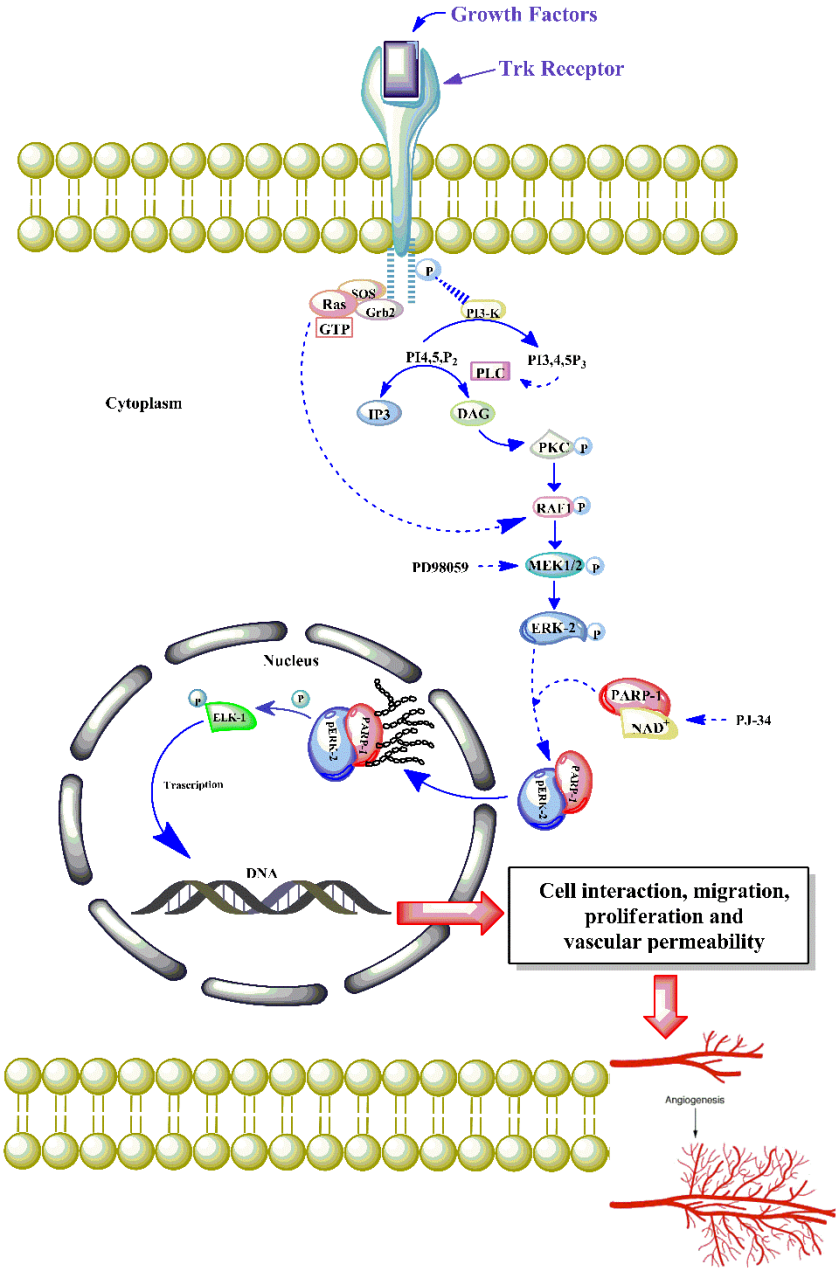

Fig. 6 PARP-1 interacts with phosphorylated ERK in the cytosol and then the complex migrates in the nucleoplasm (a schematic model). Binding of a growth factor to tyrosine kinase receptors leads to their phosphorylation and ensuing activation of ERK transduction pathway. In our model, we propose that PARP-1 and phosphorylated ERK (phospho-ERK) interact in the cytosol before their migration to the nucleus. Here, PARP-1 bound to phospho-ERK is activated by auto-polyADP-ribosylation and behaves as a scaffold protein, promoting ERK-catalyzed phosphorylation of Elk1. This signaling cascade induces endothelial proliferation, migration and vascular permeability.

4. Discussion

PARP-1 is the most extensively investigated among eighteen PARP family members; it is activated by single and double-strand DNA breaks. Its activity is critical within the base excision repair (BER) pathway (D'Amours et al., 1999; Dantzer et al., 1999; Peralta-Leal et al., 2009). Recently, PARP-1 activation in processes unrelated to DNA repair has attracted much interest. It has been demonstrated that phosphorylated ERK2 interacts with a conserved catalytic domain of PARP-1 C-terminal domain (Choen-Armon et al., 2007). In cell-free systems devoid of DNA and ATP, recombinant human PARP-1 was demonstrated to be activated and highly auto-polyADP-ribosylated by direct interaction with phosphorylated ERK2 constructs, even at low nanomolar NAD+ concentrations (Choen-Armon et al., 2007; Mendoza-Alvarez and Alvarez-Gonzalez, 1993). Binding of polyADP-ribosylated PARP-1 to phosphorylated ERK2 markedly enhances phosphorylation of the transcription factor Elk1 by ERK2 (Weaver and Yang, 2013). It is well established that the activation of CBP/p300 is a consequence of Elk1 phosphorylation. One of the Elk1 target genes is c-fos, whose transcription results from core histone acetylation (Buchwalter et al., 2004; Herdegen and Leah. 1998; Li et al., 2003). After treatment with either PARP-1 inhibitors or PARP-1 targeted siRNAs, the expression of ERK and c-fos were both repressed: this demonstrates that PARP-1 activation is involved in ERK transcription (Choen-Armon 2007; Choen-Armon et al., 2007). Even in the absence of DNA damage, PARP-1 activation by phosphorylated ERK2 could contribute to the mechanism of proliferation and migration induced by the MAPK (mitogen-activated protein kinase) cascade at ERK level (Weaver and Yang, 2013).

PARP-1 inhibitors could find a potential therapeutic application as anti-proliferative agents within the signal transduction pathway, which leads to PARP-1 activation by ERK and modulates c-fos expression (Choen-Armon et al., 2007). The pathway described above involves PARP-1 in a wide range of signaling transduction networks, including angiogenesis. In human umbilical vein endothelial cells (HUVECs), PARP-1 inhibitors were able to counteract in a dose-dependent manner migration, proliferation, and tube formation induced by VEGF (Pyriochou et al, 2008; Rajesh et al., 2006a; Rajesh et al., 2006b; Rodriguez et al., 2013;Tentori et al., 2007). Furthermore, the expression of genes involved in angiogenesis, as the hypoxia inducible factor (HIF), can be modulated by PARP-1 activity. HIF is a transcription factor expressed in tumors following oxygen deprivation: this allows new blood vessels formation (Peralta-Leal, A.et al., 2009). It has been reported that in presence of PARP-1 inhibitor DPQ [3,4-Dihydro-5-[4-(1-piperidinyl) butoxy]-1(2H)-isoquinoline] or in PARP-1 knockout mice, the hypoxia inducible factor (HIF) activity is reduced as well as the size of the tumor (Martin-Oliva et al., 2006; Peralta-Leal, A.et al., 2009). In our previous studies, we demonstrated the effects of DPQ and PJ-34 on human glioblastoma (GBM) cells in a proinflammatory state induced by Lipopolysaccharide (LPS) and Interferon-γ (INF-γ). In that case, we demonstrated that DPQ and PJ-34 reduced cell inflammation and damage following PARP-1 overexpression, while they increased cell survival, similar to other well characterized drugs (Scalia et al., 2013). In addition, the use of PARP inhibitors in multidrug regimens also prevents inflammation associated to diverse side effects of traditional chemotherapeutics (Korkmaz et al., 2008; Vyas and Chang, 2014).

Moreover, two related features of cancer such as proliferative signaling and metastasis can be inhibited when PARP-1 activity is blocked (Huang et al., 2001; Ohanna et al., 2011; Simbulan-Rosenthal et al., 1998). Our data demonstrates the interaction between PARP-1 and phospho-ERK, supporting what is actually known in literature (Inbar-Rozensal et al., 2009). On the basis of our confocal results, quantitative fluorescence analysis by LSM demonstrates that phospho-ERK increases in presence of CM, whereas it decreases upon the addition of PJ-34, both inside and outside the nuclei (Fig. 5a). A similar trend was also detected for PARP-1 (Fig. 5b). What is relevant to note is the comparable PARP-1 expression inside and outsite the nucleus in presence of CM. PARP-1 expression is drastically reduced in CM+PJ-34, mainly inside the nucleus. We speculate that PARP-1 and phospho-ERK interact in the cytosol, where they are colocalized, and then they migrate into the nucleus as a complex, where they trigger a cellular response. Furthermore, we report here evidence that PARP-1 inhibitor PJ-34 acts as an antiangiogenic agent: through a wounding technique and cell viability assay on GP8.3 cells, we clearly showed the effects of PARP-1 inhibition on cell migration and viability in a glioma tumor environment. It is well known that an effective system of microcirculation is needed for the growth of tumors. This process is due to a production of an extensive range of angiogenic molecules, such as growth factors, pro-inflammatory factors, angiogenic enzymes, cytokines, chemokines and endothelial receptors (Giurdanella et al., 2011; Tentori et al. 2007; Tentori et al. 2014). The most aggressive form of malignant astrocytoma is glioblastoma, characterized by a highly abnormal vasculature. Analysis carried out on supernatants from highly-invasive glioma cells showed the presence of several proangiogenic factors, whose activity may be effectively counteracted by antiangiogenic molecules as PJ-34 and PD98059.

It is well emphasized that modulating the accessibility to DNA through the modification of chromatin structure, PARP-1 can alter gene expression (Ba and Garg, 2011). In addition it has been reported that the activity of the DNA methyltransferase 1 Dnmt1 is regulated by PARP-1 expression (Caiafa et al., 2009; Caiafa and Zlatanova, 2009). Concomitant binding of PARP-1 to multiple nucleosomes allowed the formation of a supranucleosomal structure and caused chromatin packing and transcription repression (Kim et al., 2004). Instead, PARylation of core histones implies charge repulsion, which is responsible for chromatin relaxation allowing the transcription machinery to access DNA (Kraus and Lis, 2003; Krishnakumar and Kraus, 2010). PARP-1 possesses two different activities, protein binding and enzymatic functions: pharmacological inhibition of PARP-1 influences both (Ba and Garg, 2011; Weaver and Yang, 2013). This bring us to the question of how PARP inhibitors can modify the activity and expression of many proteins, and how in our experimental model they can negatively modulate PARP-1 expression, phospho-ERK, and phospho-Elk-1 levels. It is noteworthy that our RT-PCR experiments demonstrated that PD 98059 (MEK inhibitor) downmodulates PARP-1 mRNA expression in the presence of CM (Fig. 3A). In any case, more studies are needed to better understand the molecular mechanism underlying the action of PARP-1 and MEK inhibitors.

5. Conclusion

Our results demonstrate the interaction between PARP-1 and phospho-ERK, supporting the hypothesis that this pathway could be implicated in tumor-induced endothelial cells migration and proliferation. By demonstrating here that PARP-1 inhibitors efficiently reduce phospho-ERK levels and MEK inhibitors show similar effects on PARP-1, our data could represent an interesting contribution to this field. Accordingly, it may be proposed that also MEK inhibitors deserve to be appropriately tested in clinical trials.

References

Amè J.C., Spenlehauer C., de Murcia G., 2004. The PARP superfamily. Bioessays 26, 882–893.

Anfuso C.D., Lupo G., Romeo L., Giurdanella G., Motta C., Pascale A., Tirolo C., Marchetti B., Alberghina M., 2007. Endothelial cell-pericyte cocultures induce PLA2 protein expression through activation of PKCα and the MAPK/ERK cascade. J. Lipid Res. 48, 782–793

Anfuso C.D., Motta C., Giurdanella G., Arena V., Alberghina M., Lupo G., 2014. Endothelial PKCa-MAPK/ERK-phospholipase A2 pathway activation as a response of glioma in a triple culture model. A new role for pericytes? Biochimie 99, 77–87

Ba X. and Garg N.J., 2011. Signaling mechanism of poly(ADP-Ribose) polymerase-1 (PARP-1) in inflammatory diseases. Am. J. Pathol. 178, 946–955

Banasik M., Komura H., Shimoyama M., Ueda K., 1992. Specific inhibitors of poly(ADP-ribose) synthetase and mono(ADP-ribosyl)transferase. J Biol Chem. 267(3):1569-75

Barbagallo D., Condorelli A.G., Piro S., Parrinello N., Fløyel T., Ragusa M., Rabuazzo A.M., Størling J., Purrello F., Di Pietro C., Purrello M., 2014. CEBPA exerts a specific and biologically important proapoptotic role in pancreatic β cells through its downstream network targets. Mol. Biol. Cell. 15, 2333–2341

Boulares A.H., Zoltoski A.J., Sherif Z.A., Jolly P., Massaro D., Smulson M.E., 2003. Gene knockout or pharmacological inhibition of poly(ADP-ribose) polymerase-1 prevents lung inflammation in a murine model of asthma. Am. J. Respir. Cell. Mol. Biol. 28, 322–329

Buchwalter G., Gross C., Wasylyk B., 2004. Ets ternary complex transcription factors. Gene 324, 1–14

Burkart V., Wang Z.Q., Radons J., Heller B., Herceg Z., Stingl L., Wagner E.F., Kolb H., 1999. Mice lacking the poly(ADP-ribose)polymerase gene are resistant to pancreatic beta-cell destruction and diabetes development induced by streptozocin. Nat. Med. 5, 314–319

Caiafa P. and Zlatanova J., 2009. CCCTC-binding factor meets poly(ADP-ribose) polymerase-1. J. Cell. Physiol. 219, 265–270

Caiafa P., Guastafierro T., Zampieri M., 2009. Epigenetics: poly(ADP-ribosyl)ation of PARP-1 regulates genomic methylation patterns. FASEB J. 23, 672–678

Chiarugi A., 2002. Inhibitors of poly(ADP-ribose) polymerase-1 suppress transcriptional activation in lymphocytes and ameliorate autoimmune encephalomyelitis in rats. Br. J. Pharmacol. 137, 761–770

Citarelli M., Teotia S., Lamb R.S., 2010. Evolutionary history of the poly(ADP-ribose)polymerase gene family in eukaryotes. BMC Evol. Biol. 10, 1–26

Cohen-Armon M., 2007. PARP-1 activation in the ERK signalin pathway. Trends Pharmacol. Sci. 28, 556-560

Cohen-Armon M., Visochek L., Rozensal D., Kalal A., Geistrikh I., Rodika K., Bendetz-Nezer S., Yao Z., Seger R., 2007. DNA-independent PARP-1 activation by phosphorylated ERK2 increases Elk1 activity: a link to histone acetylation. Mol. Cell. 25, 297–308

D'Amours D., Desnoyers S., D'Silva I., Poirier G.G., 1999. Poly(ADP-ribosyl)ation reactions in the regulation of nuclear functions. Biochem. J. 342, 249–268

Dantzer F., Schreiber V., Niedergang C., Trucco C., Flatter E., De La Rubia G., Oliver J., Rolli V., Menissier-de Murcia J., de Murcia G., 1999. Involvement of poly (ADP-ribose) polymerase in base excision repair. Biochimie 81:69–75

Daugherty M.D., Young J.M., Kerns J.A., Malik H.S., 2014. Rapid evolution of PARP genes suggests a broad role for ADP-ribosylation in host-virus conflicts. PLoS Genet. 10(5):e1004403

Eliasson M.J., Sampei K., Mandir A.S., Hurn P.D., Traystman R.J., Bao J., Pieper A., Wang Z.Q., Dawson T.M., Snyder S.H., Dawson V.L., 1997. Poly(ADP-ribose) polymerase gene disruption renders mice resistant to cerebral ischemia. Nat. Med. 3, 1089–1095

El-Khamisy S.F., Masutani M., Suzuki H., Caldecott K.W., 2003. A requirement for PARP-1 for the assembly or stability of XRCC1 nuclear foci at sites of oxidative DNA damage. Nucleic Acids Res 31:5526–5533

Gagné J.P., Isabelle M., Lo K.S., Bourassa S., Hendzel M.J., Dawson V.L., Dawson T.M., Poirier G.G., 2008. Proteome-wide identification of poly(ADP-ribose) binding proteins and poly(ADP-ribose)-associated protein complexes. Nucleic Acids Res. 36(22):6959-76

Gibson B.A. and Kraus W.L., 2012 New insights into the molecular and cellular functions of poly(ADP-ribose) and PARPs. Nat Rev Mol Cell Biol 13: 411–424

Giurdanella G., Motta C., Muriana, S., Arena V., Anfuso C. D., Lupo G., Alberghina M., 2011. Cytosolic and calcium-independent phospholipase A2 mediate glioma-enhanced proangiogenic activity of brain endothelial cells. Microvasc. Res. 81, 1–17.

Gobeil S., Boucher, C.C. Nadeau, D. Poirier G.G., 2001. Characterization of the necrotic cleavage of poly(ADP-ribose) polymerase (PARP-1): implication of lysosomal proteases. Cell Death Differ. 8, 588–594.

Gottschalk A.J., Timinszky G., Kong S.E., Jin J., Cai Y., Swanson S.K., Washburn M.P., Florens L., Ladurner A.G., Conaway J.W., Conaway R.C., 2009. Poly(ADP-ribosyl)ation directs recruitment and activation of an ATP-dependent chromatin remodeler. Proc Natl Acad Sci U S A. 106(33):13770-4

Haddad M., Rhinn H., Bloquel C., Coqueran B., Szabó C., Plotkine M., Scherman D., Margaill I., 2006. Anti-inflammatory effects of PJ34, a poly(ADP-ribose)polymerase inhibitor, in transient focal cerebral ischemia in mice. Br. J. Pharmacol. 149, 23–30.

Haince J.F., McDonald D., Rodrigue A., Déry U., Masson J.Y., Hendzel M.J., Poirier G.G., 2008. PARP1-dependent kinetics of recruitment of MRE11 and NBS1 proteins to multiple DNA damage sites. J Biol Chem. 283(2):1197-208

Hakme A., Wong H.K., Dantzer F., Schreiber V., 2008. The expanding field of poly(ADP-ribosyl)ation reactions. 'Protein Modifications: Beyond the Usual Suspects' Review Series. EMBO Rep. 9, 1094–1100.

Han S. and Tainer J.A., 2002. The ARTT motif and a unified structural understanding of substrate recognition in ADP-ribosylating bacterial toxins and eukaryotic ADP-ribosyltransferases. Int J Med Microbiol. 291(6-7):523-9

Hassa P.O. and Hottiger M.O., 2008. The diverse biological roles of mammalian PARPS, a small but powerful family of poly-ADP-ribose polymerases. Front. Biosci. 13, 3046–3082.

Hassa P.O., Haenni S.S., Elser M., Hottiger M.O., 2006. Nuclear ADP-ribosylation reactions in mammalian cells: where are we today and where are we going? Microbiol. Mol. Biol. Rev. 70, 789–829.

Herdegen T. and Leah J.D., 1998. Inducible and constitutive transcription factors in the mammalian nervous system: control of gene expression by Jun, Fos and Krox and CREB/ATF proteins. Brain Res Brain Res Rev. 28, 370–490.

Hottiger M.O., Hassa P.O., Lüscher B., Schüler H., Koch-Nolte F., 2010. Toward a unified nomenclature for mammalian ADP-ribosyltransferases. Trends Biochem. Sci. 35, 208–219.

Huang S., Pettaway C.A., Uehara H., Bucana C.D., Fidler I.J., 2001. Blockade of NF-kappa B activity in human prostate cancer cells is associated with suppression of angiogenesis, invasion, and metastasis. Oncogene 20, 4188–4197.

Inbar-Rozensal D., Castiel A., Visochek L., Castel D., Dantzer F., Izraeli S., Cohen-Armon M., 2009. A selective eradication of human nonhereditary breast cancer cells by phenanthridine-derived polyADP-ribose polymerase inhibitors. Breast Cancer Res. 11: R78.

Iwashita A., Tojo N., Matsuura S., Yamazaki S., Kamijo K., Ishida J., Yamamoto H., Hattori K., Matsuoka N., Mutoh S., 2004. A novel and potent poly(ADP-ribose) polymerase-1 inhibitor, FR247304 (5-chloro-2- [3-(4-phenyl-3,6-dihydro-1(2H)-pyridinyl)propyl]-4(3H)-quinazo linone), attenuates neuronal damage in in vitro and in vivo models of cerebral ischemia. J. Pharmacol. Exp. Ther. 310, 425–436.

Jijon H.B., Churchill T., Malfair D., Wessler A., Jewell L.D., Parsons H.G., Madsen K.L., 2000. Inhibition of poly(ADP-ribose)polymerase attenuates inflammation in a model of chronic colitis. Am. J. Physiol. Gastrointest. Liver Physiol. 279, 641–651.

Kerr A.H.J., James J.A., Smith M.A., Willson C., Court E.L., Smith J.G., 2003. An investigation of the MEK/ERK inhibitor U0126 in acute myeloid leukemia. Ann. NY Acad. Sci. 1010, 86–89.

Kim M.Y., Mauro S., Gévry N., Lis J.T., Kraus W.L., 2004. NAD+-dependent modulation of chromatin structure and transcription by nucleosome binding properties of PARP-1. Cell 119, 803–814.

Kleine H., Poreba E., Lesniewicz K., Hassa P.O., Hottiger M.O., Litchfield D.W., Shilton B.H., Lüscher B., 2008. Substrate-assisted catalysis by PARP10 limits its activity to mono-ADP-ribosylation. Mol. Cell 32, 57–69

Korkmaz A., Kurt B., Yildirim I., Basal S., Topal T., Sadir S., Oter S., 2008. Effects of poly(ADP-ribose)polymerase inhibition in bladder damage caused by cyclophosphamide in rats. Exp. Biol. Med. (Maywood) 233, 338–343.

Kraus W.L. and Lis J.T., 2003. PARP goes transcription. Cell 113, 677–83.

Krishnakumar R. and Kraus W.L., 2010. PARP-1 regulates chromatin structure and transcription through a KDM5B-dependent pathway. Mol. Cell. 39, 736–749.

Lacal P.M., Tentori L., Muzi A., Ruffini F., Dorio A.S., Xu W., Arcelli D., Zhang J., Graziani G., 2009. Pharmacological inhibition of poly(ADP-ribose) polymerase activity down-regulates the expression of syndecan-4 and Id-1 in endothelial cells. Int. J. Oncol. 34, 861–872.

Lange M., Connelly D., Traber D.L., Hamahata A., Nakano Y., Esechie A., Jonkam C., von Borzyskowski S., Traber L.D., Schmalstieg F.C., Herndon D.N, Enkhbaatar P., 2010. Time course of nitric oxide synthases, nitrosative stress, and poly(ADP ribosylation) in an ovine sepsis model. Crit. Care 14, 1–10.

Langelier M.F., Ruhl D.D., Planck J.L., Kraus W.L., Pascal J.M. 2010. The Zn3 domain of human poly(ADP-ribose) polymerase-1 (PARP-1) functions in both DNA-dependent poly(ADP-ribose) synthesis activity and chromatin compaction. J. Biol. Chem. 285, 18877–18887

Langelier M.F., Servent K.M., Rogers E.E., Pascal J.M., 2008. A third zinc-binding domain of human poly(ADP-ribose) polymerase-1 coordinates DNA-dependent enzyme activation. J. Biol. Chem. 283, 4105–4114

Lavarone E., Puppin C., Passon N., Filetti S., Russo D., Damante G., 2013. The PARP inhibitor PJ34 modifies proliferation, NIS expression and epigenetic marks in thyroid cancer cell lines. Mol. Cell. Endocrinol. 365, 1–10.

Li Q.J., Yang S.H., Maeda Y., Sladek F.M., Sharrocks A.D., Martins-Green M., 2003. MAP kinase phosphorylation-dependent activation of Elk-1 leads to activation of the co-activator p300. EMBO J. 15, 281–291.

Lupo G., Nicotra A., Giurdanella G., Anfuso C.D., Romeo L., Biondi G., Tirolo C., Marchetti B., Ragusa N., Alberghina M., 2005. Activation of phospholipase A2 and MAP kinases by oxidized low-density lipoproteins in immortalized GP8.39 endothelial cells. Biochim. Biophys. Acta 1753, 135–150.

Marsischky G.T., Wilson B.A., Collier R.J., 1995. Role of glutamic acid 988 of human poly-ADP-ribose polymerase in polymer formation. Evidence for active site similarities to the ADP-ribosylating toxins. J Biol Chem. 270(7):3247-54

Martinez-Romero R., Martinez-Lara E., Aguilar-Quesada R., Peralta A., Oliver F. J., Siles E., 2008. PARP-1 modulates deferoxamine-induced HIF-1alpha accumulation through the regulation of nitric oxide and oxidative stress. J. Cell. Biochem. 104:2248–2260

Martin-Oliva D., Aguilar-Quesada R., O'valle F., Muñoz-Gámez J.A., Martínez-Romero R., García Del Moral R., Ruiz de Almodóvar J.M., Villuendas R., Piris M.A., Oliver F.J., 2006. Inhibition of poly(ADP-ribose) polymerase modulates tumor-related gene expression, including hypoxia-inducible factor-1 activation, during skin carcinogenesis. Cancer Res. 66, 5744–5756.

Masson M., Niedergang C., Schreiber V., Muller S., Menissier-de Murcia J., de Murcia G., 1998. XRCC1 is specifically associated with poly(ADP-ribose) polymerase and negatively regulates its activity following DNA damage. Mol Cell Biol. (6):3563-71

Mendoza-Alvarez H. and Alvarez-Gonzalez R., 1993. PolyADP-ribose polymerase is a catalytic dimer and the automodification reaction is intramolecular. J. Biol. Chem. 268, 22575–22580.

Meyer-Ficca M.L., Meyer R.G., Coyle D.L., Jacobson E.L., Jacobson M.K., 2004. Human poly(ADP-ribose)glycohydrolase is expressed in alternative splice variants yielding isoforms that localize to different cell compartments. Exp Cell Res 297:521–532.

Milam K.M. and Cleaver J. E. 1984. Inhibitors of poly(adenosine diphosphate-ribose) synthesis: effect on other metabolic processes. Science 223:589–591

Morris E.J., Jha S., Restaino C.R., Dayananth P., Zhu H., Cooper A., Carr D., Deng Y., Jin W., Black S., Long B., Liu J., Dinunzio E., Windsor W., Zhang R., Zhao S., Angagaw M.H., Pinheiro E.M., Desai J., Xiao L., Shipps G., Hruza A., Wang J., Kelly J., Paliwal S., Gao X., Babu B.S., Zhu L., Daublain P., Zhang L., Lutterbach B.A., Pelletier M.R., Philippar U., Siliphaivanh P., Witter D., Kirschmeier P., Bishop W.R., Hicklin D,. Gilliland D.G, Jayaraman L., Zawel L., Fawell S., Samatar A.A., 2013. Discovery of a novel ERK inhibitor with activity in models of acquired resistance to BRAF and MEK inhibitors. Cancer Discov. 3, 742–750.

Motta C., D'Angeli F., Scalia M., Satriano C., Barbagallo D., Naletova I., Anfuso C.D., Lupo G., Spina-Purrello V., 2015. PJ-34 inhibits PARP-1 expression and ERK phosphorylation in glioma-conditioned brain microvascular endothelial cells. Eur J Pharmacol. 761:55-64

Naura A.S., Datta R., Hans C.P., Zerfaoui M., Rezk B.M., Errami Y., Oumouna M., Matrougui K., Boulares A.H., 2009. Reciprocal regulation of iNOS and PARP-1 during allergen induced eosinophilia. Eur. Respir. J. 33, 252–262.

Nguewa P.A., Fuertes M.A., Alonso C., Perez J.M., 2003. Pharmacological modulation of Poly(ADP-ribose) polymerase-mediated cell death: exploitation in cancer chemotherapy. Mol Pharmacol. 64(5):1007-14

Nguewa P.A., Fuertes M.A., Valladares B., Alonso C., Pérez J.M., 2005. Poly(ADP-ribose) polymerases: homology, structural domains and functions. Novel therapeutical applications. Prog. Biophys. Mol. Biol. 88, 143–172.

Ohanna M., Giuliano S., Bonet C., Imbert V., Hofman V., Zangari J., Bille K., Robert C., Bressac-de Paillerets B., Hofman P., Rocchi S., Peyron J.F, Lacourm J.P., Ballotti R., Bertolotto C., 2011. Senescent cells develop a PARP-1 and nuclear factor-{kappa}B-associated secretome (PNAS). Genes Dev. 25, 1245–1261.

Oka S., Kato J., Moss J., 2006. Identification and characterization of a mammalian 39-kDa poly(ADP-ribose)glycohydrolase. J Biol Chem 281:705–713

Otto H., Reche P.A., Bazan F., Dittmar K., Haag F., Koch-Nolte F., 2005. In silico characterization of the family of PARP-like poly(ADP-ribosyl)transferases (pARTs). BMC Genomics 6:139

Peralta-Leal A., Rodríguez-Vargas J.M., Aguilar-Quesada R., Rodríguez M.I., Linares J.L., de Almodóvar M.R., Oliver F.J., 2009. PARP inhibitors: new partners in the therapy of cancer and inflammatory diseases. Free Radic. Biol. Med. 47, 132–136.

Purnell M.R. and Whish W.J. 1980. Novel inhibitors of poly(ADP-ribose) synthetase. Biochem. J. 185:775–777

Pyriochou A., Olah G., Deitch E.A., Szabo C., Papapetropoulos A., 2008. Inhibition of angiogenesis by the poly(ADP-ribose)polymerase inhibitor PJ-34. Int. J. Mol. Med. 22, 113–118.

Rajesh M., Mukhopadhyay P., Batkai S., Godlewski G., Hasko G., Liaudet L., Pacher P., 2006 a. Pharmacological inhibition of poly(ADP-ribose) polymerase inhibits angiogenesis. Biochem. Biophys. Res. Commun. 350, 352–357.

Rajesh M., Mukhopadhyay P., Godlewski G., Bátkai S., Haskó G., Liaudet L., Pacher P., 2006 b. Poly(ADP-ribose)polymerase inhibition decreases angiogenesis. Biochem. Bio-phys. Res. Commun. 350, 1056–1062.

Rodriguez M.I., Peralta-Leal A., O'Valle F., Rodriguez-Vargas J.M., Gonzalez-Flores A., Majuelos-Melguizo J., Lopez L., Serrano S., Garcıa de Herreros A., Rodrıguez-Manzaneque J.C., Fernandez R., del Moral R.G., de Almodovar J.M., Oliver F.J., 2013. PARP-1 regulates metastatic melanoma through modulation of vimentin-induced malignant transformation. PLoS Genet. 9, e1003531.

Ruf A., Rolli V., de Murcia G., Schulz G.E., 1998. The mechanism of the elongation and branching reaction of poly(ADP-ribose) polymerase as derived from crystal structures and mutagenesis. J Mol Biol. 278(1):57-65

Satoh M.S. and Lindahl T., 1992. Role of poly(ADP-ribose) formation in DNA repair. Nature 356:356–358.

Scalia M., Satriano C., Greca R., Giuffrida-Stella A.M., Rizzarelli E., Spina-Purrello V., 2013. PARP-1 inhibitors DPQ and PJ-34 negatively modulate proinflammatory commitment of human glioblastoma cells. Neurochem. Res. 38, 50–58

Schreiber V., Dantzer F., Ame J.C., de Murcia G., 2006. Poly(ADPribose): novel functions for an old molecule. Nat. Rev. Mol. Cell Biol. 7, 517–528

Simbulan-Rosenthal C.M., Rosenthal D.S., Iyer S., Boulares A.H., Smulson M.E., 1998. Transient poly(ADP-ribosyl)ation of nuclear proteins and role of poly(ADP- ribose)polymerase in the early stages of apoptosis. J. Biol. Chem. 273, 13703–13712.

Spina-Purrello V., Patti D., Giuffrida-Stella A.M., Nicoletti V.G., 2008. Parp and cell death or protection in rat primary astroglial cell cultures under LPS/IFNγ induced proinflammatory conditions. Neurochem. Res. 33, 2583–2592.

Steffen J.D., Brody J.R., Armen R.S., Pascal J.M., 2013. Structural Implications for Selective Targeting of PARPs. Front Oncol. 20;3:301

Steffen J.D., Brody J.R., Armen R.S., Pascal J.M., 2013. Structural Implications for Selective Targeting of PARPs. Front Oncol. 20;3:301

Suarez-Pinzon W.L., Mabley J.G., Power R., Szabó C., Rabinovitch A., 2003. Poly (ADP-ribose) polymerase inhibition prevents spontaneous and recurrent autoimmune diabetes in NOD mice by inducing apoptosis of islet-infiltrating leukocytes. Diabetes. 52(7):1683-8

Tai Y.T., Fulciniti M., Hideshima T., Song W., Leiba M., Li X.F., Rumizen M., Burger P., Morrison A., Podar K., Chauhan D., Tassone P., Richardson P., Munshi N.C., Ghobrial I.M., Anderson K.C., 2007. Targeting MEK induces myeloma-cell cytotoxicity and inhibits osteoclastogenesis. Blood 110, 1656–1663.

Tentori L., Lacal P.M., Muzi A., Dorio A.S., Leonetti C., Scarsella M., Ruffini F., Xu W., Min W., Stoppacciaro A., Colarossi C., Wang Z.Q., Zhang J., Graziani G., 2007. Poly(ADP-ribose)polymerase (PARP) inhibition or PARP-1 gene deletion reduces angiogenesis. Eur. J. Cancer 43, 2124–2133.

Tentori L., Muzi A., Dorio A.S., Bultrini S., Mazzon E., Lacal P.M., Shah G.M., Zhang J., Navarra P., Nocentini G., Cuzzocrea S., Graziani G., 2008. Stable depletion of poly(ADP-ribose)polymerase-1 reduces in vivo melanoma growth and increases chemosensitivity. Eur. J. Cancer 44, 1302–1314.

Tentori L., Ricci-Vitiani L., Muzi A., Ciccarone F., Pelacchi F., Calabrese R., Runci D., Pallini R., Caiafa P., Graziani G., 2014. Pharmacological inhibition of poly(ADP-ribose) polymerase-1 modulates resistance of human glioblastoma stem cells to temozolomide. BMC Cancer 14, 151.

Timinszky G., Till S., Hassa P.O., Hothorn M., Kustatscher G., Nijmeijer B., Colombelli J., Altmeyer M., Stelzer E.H., Scheffzek K., Hottiger M.O., Ladurner A.G., 2009. A macrodomain-containing histone rearranges chromatin upon sensing PARP1 activation. Nat Struct Mol Biol. 16(9):923-9

Tulin A. and Spradling A., 2003. Chromatin loosening by poly(ADP)-ribose polymerase (PARP) at Drosophila puff loci. Science 299:560–562

Vyas S. and Chang P., 2014. New PARP targets for cancer therapy. Nat. Rev. Cancer 14, 502-509.

Vyas S., Chesarone-Cataldo M., Todorova T., Huang Y., Chang P., 2013. A systematic analysis of the PARP protein family identifies new functions critical for cell physiology. Nat Commun. 4: 2240

Wahlberg E., Karlberg T., Kouznetsova E., Markova N., Macchiarulo A., Thorsell A.G., Pol E., Frostell Å., Ekblad T., Öncü D., Kull B., Robertson G.M., Pellicciari R., Schüler H., Weigelt J., 2012. Family-wide chemical profiling and structural analysis of PARP and tankyrase inhibitors. Nat Biotechnol. 30(3):283-8

Weaver A.N., Yang E.S., 2013. Beyond DNA repair: additional functions of PARP-1 in cancer. Front. Oncol. 3, 1–11

Yeh T.C., Marsh V., Bernat B.A., Ballard J., Colwell H., Evans R.J., Parry J., Smith D., Brandhuber B.J., Gross S., Marlow A., Hurley B., Lyssikatos J., Lee P.A., Winkler J.D., Koch K., Wallace E., 2007. Biological characterization of ARRY-142886(AZD6244), a potent, highly selective mitogen activated protein kinase kinase1/2 inhibitor. Clin. Cancer Res. 13, 1576–1583

Zaremba T. and Curtin N.J., 2007. PARP inhibitor development for systemic cancer targeting. Anticancer Agents Med Chem. 7:515–523

Section II

Biomolecular effects and bioclinical applications of PARPs inhibitors:

"PARP-14 acts as pro-survival molecule in the murine pancreatic α-TC1 cells in an in vitro model of immune-mediated diabetes"

Background

1. Macro PARPs

The diversity of PAR functions is a consequence of the variety of the functional domains combined to the PARP domain in each PARP family member. PARP-9, PARP-14, and PARP-15 belong to the subfamily of macro-PARPs (Figure 1).

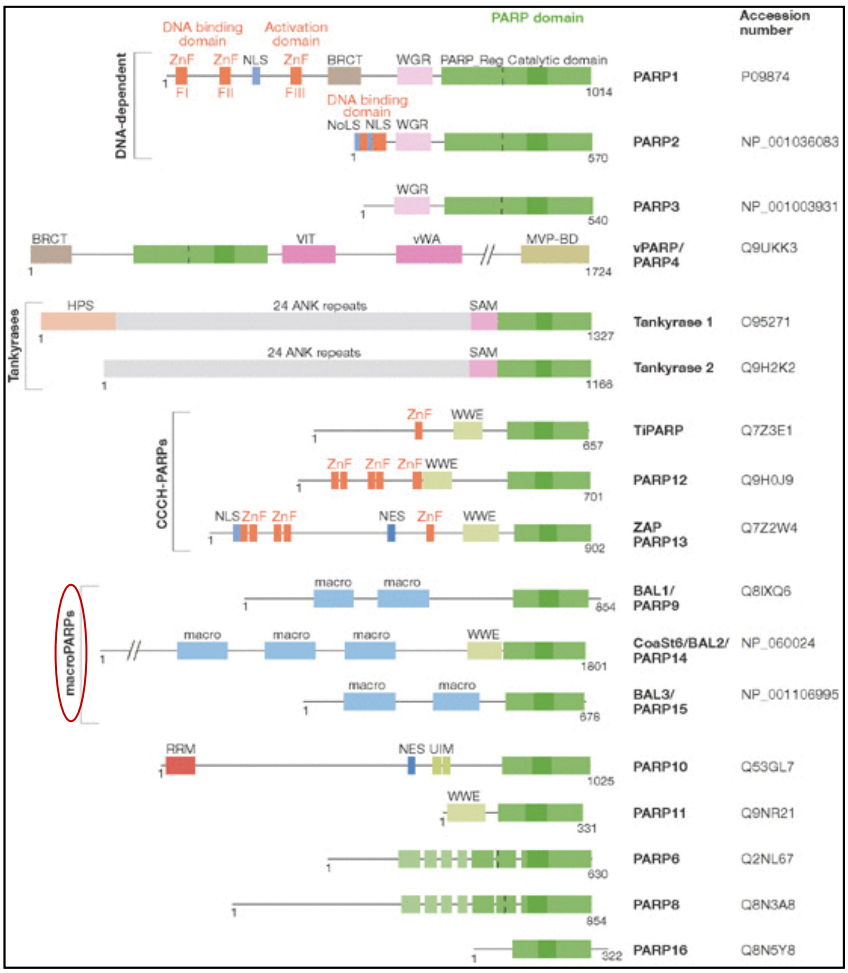

Figure 1. Domain architecture of human poly(ADP-ribose) polymerase family members. Within each putative PARP domain, the region that is homologous to residues 859–908 of PARP1 the PARP signature is indicated by a darker colour. BRCT, SAM, UIM, MVP-BD, VWA and ANK are protein-interaction modules. ANK, ankyrin; BRCT, BRCA1-carboxy-terminus; HPS, homopolymeric runs of His, Pro and Ser; macro, domain involved in ADP-ribose and poly(ADP-ribose) binding; MVP-BD, MVP-binding; NES, nuclear export signal; N(o)LS, nuclear (nucleolar) localization signal; PARP, poly(ADP-ribose) polymerase; PARP_Reg, putative regulatory domain; RRM, RNA-binding motif; SAM, sterile α-motif; TiPARP, 2,3,7,8-tetrachlorodibenzo-p-dioxin-inducible poly(ADP-ribose) polymerase; UIM, ubiquitin-interacting motif; VIT, vault inter-α-trypsin; vPARP, vault poly(ADP-ribose) polymerase; vWA, von Willebrand factor type A; WGR, conserved W, G and R residues; WWE, conserved W, W and E residues; ZnF, DNA or RNA binding zinc fingers (except PARP1 ZnFIII, which coordinates DNA-dependent enzyme activation). (Hakmé A. et al., EMBO Rep. 2008).

2. Macro PARP: PARP-14

In addition to containing the PARP catalytic domain, PARP-14 contains three copies of the macro domains that were first identified in the non-classical histone macroH2A (mH2A) (Mehrotra P. et al., 2011). Like core histone H2A, mH2A is also associated with nucleosomes and replaces H2A in three percent of vertebrate nucleosomes (Ladurner A.G., 2003).

mH2A participates in the inactivation of the X chromosome (Xi) and depletion of mH2A in female cells results in the reactivation of genes on Xi (Chadwick B.P., 2001; Costanzi C. and Pehrson J.R., 1998). There is some evidence that macro domains associate with histone deacetylases (HDACs). Thus, mH2A may participate in transcriptional repression by recruiting HDACs (Chakravarthy S. et al., 2005). All of these observations indicate that macro domains are transcription repressors rather than activators. It is possible that the macro domains found in PARP-14 may also function to repress transcription. However, Mehrotra et al. showed that PARP-14 enhances Stat6-dependent transcription instead of repressing it (Goenka S. and Boothby M., 2006). To reconcile this paradox, they hypothesized that PARP-14 does function as a repressor first by recruiting HDAC 2 and 3. However, in the presence of IL-4 the ADP-ribosyl transferase activity of PARP-14 is activated, which results in relieving its repressive function. In 2009, Cho et al. demonstrated that PARP-14 mediates IL-4–induced B-cell protection against apoptosis after irradiation or growth factor withdrawal. Furthermore, the induction of several B-cell survival factors (Pim-1; Mcl-1) by IL-4 depended on PARP-14, assuming a protective role of the PARP-14 (Cho S.H. et al., 2009).

3. PARP-14 acts as a pro-survival signal in multiple myeloma

In 2013 Barbarulo et al. showed a protective role of PARP-14 in multiple myeloma (MM), a neoplasm of terminally differentiated B cells, characterized by accumulation of clonal, long-lived plasma cells in the bone marrow (BM) and extramedullary sites (Barbarulo A. et al., 2013). In particular, they demonstrated that JNK-2 is constitutively active in myeloma cells and inhibits the pro-apoptotic activity of JNK-1 through effects on PARP-14, thus promoting survival in myeloma cells (figure 2).

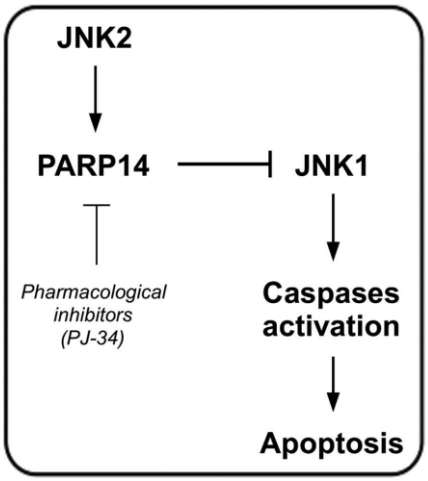

Figure 2. Schematic model for JNK2-dependent myeloma cell survival. JNK-2 suppresses basal apoptosis in myeloma cells via PARP14. Constitutive JNK-2 activity regulates levels of PARP-14, which in turn inhibits JNK-1, thereby suppressing the activation of endogenous apoptotic pathways. (Barbarulo et al., Oncogene 2013).

According to their hypothesis, PARP-14 acts as a physiological downstream effector of the JNK-2-dependent pro-survival signal by binding to JNK1 and inhibiting its activity. They also find that expression of PARP-14 correlates with disease progression and poor prognosis in MM. Therefore, this study describes a novel regulatory pathway in myeloma cells through which JNK-2 promotes survival and suggests that selective inhibition of PARP-14 might be of therapeutic value.

4. The 2nd generation PARP inhibitors: PJ-34 acts as pan PARP inhibitor

PARPs have important cellular roles that include preserving genomic integrity, telomere maintenance, transcriptional regulation, and cell fate determination. The diverse biological roles of PARPs have made them attractive therapeutic targets, which have fuelled the pursuit of small molecule PARP inhibitors. Nicotinamide (NA) and 3-aminobenzamide (3-AB) (Figure 3) were the first compounds used to inhibit poly(ADP-ribosylation).

Figure 3. Structure of nicotinamide and 3-aminobenzamide.

Nicotinamide (pyridin-3-carboxylic acid amide) inhibits the conversion of NAD into ADP-ribose (Clark J.B. and Pinder S., 1969; Clark J.B. et al., 1971; Giansanti et al., 2010) and, when administered in S phase, affects the rate of DNA replication (Colyer R.A. et al., 1973), possibly interfering with nucleotide synthesis (Purnell M.R. and Whish W.J., 1980). Benzamide (benzoic acid amide), which mimics the nicotinamide moiety of NAD, was recognized as a promising inhibitor (Shall S., 1975) and further used as a lead compound to produce derivatives with new residues in the 3-position, including 3-aminobenzamide and M-methoxybenzamide. Instrumental information for structure–activity studies was obtained through the crystal structure of the catalytic domain of chicken PARP-1 (Ruf A. et al., 1996), and the consequent identification of the site of interaction between inhibitors and NAD-binding region (Ruf A. et al., 1998).

The cyclization of an open benzamide structure or the creation of a further ring system on the existing cyclic amide allowed the development of 2nd generation PARP inhibitors, including the well known molecule PJ-34 (Figure 4). However, further studies leaded to the development of several third generation molecules, which have been or are being evaluated in clinical trials following two two distinct approaches: 1) targeting cells that are genetically predisposed to die when PARP activity is lost; 2) combining PARP inhibition with DNA-damaging therapy to derive additional therapeutic benefit from DNA damage (Rouleau M. et al., 2010).

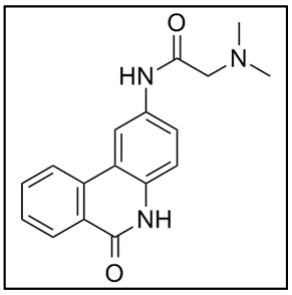

Figure 4. PJ-34 is a potent specific inhibitor of PARP-l/2 of second generation.

In the midst of the tremendous efforts that have brought PARP inhibitors to the forefront of modern chemotherapy, most clinically used PARP inhibitors bind to conserved regions that permits cross-selectivity with other PARPs containing homologous catalytic domains. One of these PARP inhibitors which is able to react with different PARPs is the potent molecule PJ-34, that, as a consequence, is often used as a pan-PARP inhibitor. Thus, the development of inhibitors specific for a single specific PARP has proven to be considerably more difficult given the high level of conservation of PARP catalytic domains (Wahlberg E. et al., 2012). Although quinazolinone and quinoxaline derivatives may be more selective for PARP-1 and PARP-2, respectively (Steffen J.D. et al., 2013), increasing specificity is an important area of focus for the future.

Additionally, it is hopeful that with an in depth understanding of the structure-function of each PARP family member, better and more specific targeting strategies will emerge. However, PARP inhibitors are likely to be useful for treating a wide variety of diseases, including cancer, (for the treatment of DNA repair deficiency-related cancer or as antiangiogenic agents) and Diabetes (Suarez-Pinzon W.L. et al, 2003).

5. Diabetes

5.1 The Pancreatic Islets

Islets of Langerhans are irregularly shaped patches of endocrine tissue located within the pancreas of most vertebrates. They are named after the German physician Paul Langerhans, who first described them in 1869. The islets consist of four distinct cell types, of which three, alpha, beta and delta cells, produce important hormones, instead the fourth component (PP cells) secretes pancreatic polypeptide (Figure 5).

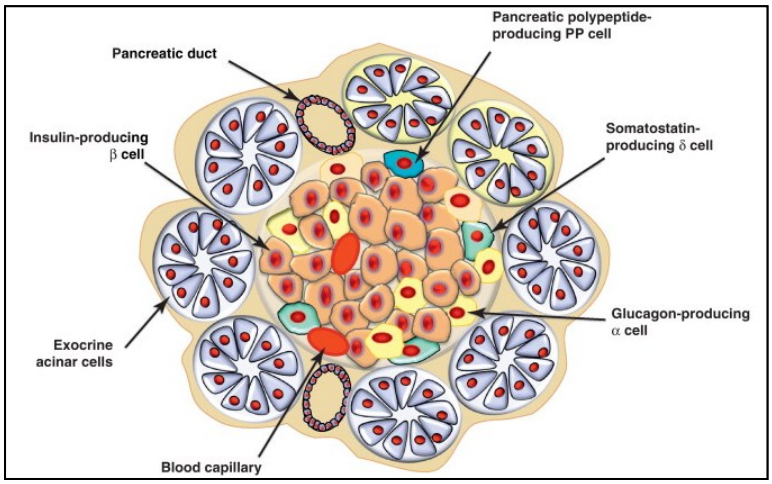

Figure 5. Schematic representation of pancreatic islets of Langerhans. Irregular microscopic structures consisting of cords of endocrine cells that are scattered throughout the pancreas among the exocrine acini. Each islet is surrounded by connective tissue fibres and penetrated by a network of capillaries. There are four major cell types. The most abundant beta cells (50-80%) secrete insulin. Alpha cells (5-20%) secrete glucagon. Delta cells (~5%) secrete somatostatin. PP cells (10-35%) secrete pancreatic polypeptide.

The most common islet cell, the beta cell, produces insulin, the major hormone in the regulation of carbohydrate, fat, and protein metabolism.

The inability of the islet cells to make insulin or the failure to produce amounts sufficient to control blood glucose level are the causes of diabetes mellitus.

5.2 Diabetes Mellitus: definition and description

Diabetes mellitus is a group of metabolic diseases characterized by hyperglycaemia resulting from defects in insulin secretion, insulin action, or both. The chronic hyperglycaemia of diabetes is associated with long-term damage, dysfunction, and failure of various organs, especially the eyes, kidneys, nerves, heart, and blood vessels. Several pathogenic processes are involved in the development of diabetes. These range from abnormalities that result in resistance to insulin action to autoimmune destruction of the β-cells of the pancreas with consequent insulin deficiency (immune-mediated diabetes).

5.3 Immune-mediated diabetes

This form of diabetes, which accounts for only 5-10% of those with diabetes, previously encompassed by the terms insulin-dependent diabetes, type I diabetes, or juvenile-onset diabetes, results from a cellular-mediated autoimmune destruction of the β-cells of the pancreas. Markers of the immune destruction of the β-cell include islet cell autoantibodies, autoantibodies to insulin, autoantibodies to glutamic acid decarboxylase, and autoantibodies to the tyrosine phosphatases IA-2 and IA-2β. One and usually more of these autoantibodies are present in 85-90% of individuals when fasting hyperglycaemia is initially detected. Autoimmune destruction of β-cells has multiple genetic predispositions and is also related to environmental factors that are still poorly defined.

5.4 Molecule effectors in immune-mediated diabetes

The immune-mediated diabetes or Type 1 diabetes mellitus (T1DM) is characterized to a strong inflammatory component. The latest studies indicate that innate immunity and inflammatory mediators have a much broader role in T1DM than initially assumed. Inflammation is a biological response that is triggered by infection, tissue injury and tissue stress or malfunction (Medzhitov R., 2008) and it might contribute to early induction and amplification of the immune assault against pancreatic β cells and, at later stages, to the stabilization and maintenance of insulitis (Eizirik D.L. et al., 2009).

5.5 Induction of Insulitis

Recognition by the mammalian immune system of invading micro-organisms depends on innate and adaptive components. The adaptive immune system recognizes antigens derived from microorganisms by highly diverse T-cell surface receptors that are formed via somatic gene recombination. The innate immune system, on the other hand, recognizes microorganisms by pattern-recognition receptors (PRRs), including Toll-like receptors (TLRs), RIG-I, MDA-5 and receptors of the nucleotide-binding oligomerization domain like receptor (NLR) family. Some components of the innate immunity response, including TLRs, contribute to the development of insulitis and T1DM in animal models. Indeed, mouse and human pancreatic islets express TLR2, TLR3, TLR4 and TLR9; of these, TLR3 and TLR4 are expressed at high levels (Giarratana N. et al., 2004; Vives-PI M. et al., 2003; Wen L. et al., 2004). The expression of TLR3 is upregulated in β cells by double-stranded RNA (dsRNA), (Rasschaert J. et al., 2005; Wen L. et al., 2004) an intermediate nucleic acid that is generated during the life cycle of most viruses.

In human islets that are infected with coxsackievirus B5 or exposed to interferon (IFN)-γ or IFN-γ and interleukin (IL)-1β, increased expression of TLR3, RIG-I and MDA-5 have been observed (Hultcrantz M. et al., 2007; Ylipaasto P. et al., 2005). Intracellular dsRNA and extracellular dsRNA, which is derived from damaged or dying cells, can both bind to TLR3 and trigger β-cell apoptosis and cytokine and chemokine production, at least in part, through activation of the transcription factors NFκB and IRF-3 (Dogusan Z. et al., 2008; Liu D. et al., 2001; Liu D. et al., 2002; Rasschaert J. et al., 2005). However, whereas the activation of these transcription factors by extracellular dsRNA is entirely dependent on TLR3, intracellular dsRNA uses alternative pathways, which might include RIG-I/MDA-5 activation (Dogusan Z. et al., 2008). Internal dsRNA triggers a massive production of type I interferons. When prolonged or excessive, such interferon release can lead to dsRNA-induced β-cell apoptosis, which is partly caused by endoplasmic reticulum (ER) stress (Dogusan Z. et al., 2008). Importantly, high levels of interferons are present in pancreatic tissue of patients with T1DM, (Foulis A.K. et al., 1987) and IFN-α contributes to viral-induced experimental diabetes (Devendra D. et al., 2005; Lang K.S., 2005). These observations suggest that activation of TLR3 and/or RIG-I and MDA-5 in β cells leads to a complex molecular response that starts by activation of the key transcription factors NFκB and IRF-3. This activation is followed by production of IFN-α and IFN-β, which leads to paracrine activation of the transcription factor STAT-1, over expression of MHC class-I antigens, further production of IFN-α and IFN-β and the release of several chemokines. The result of these combined factors is attraction of immune cells that release proinflammatory cytokines, such as IL-1β, tumor necrosis factor (TNF) and INF-γ (Figure 6).

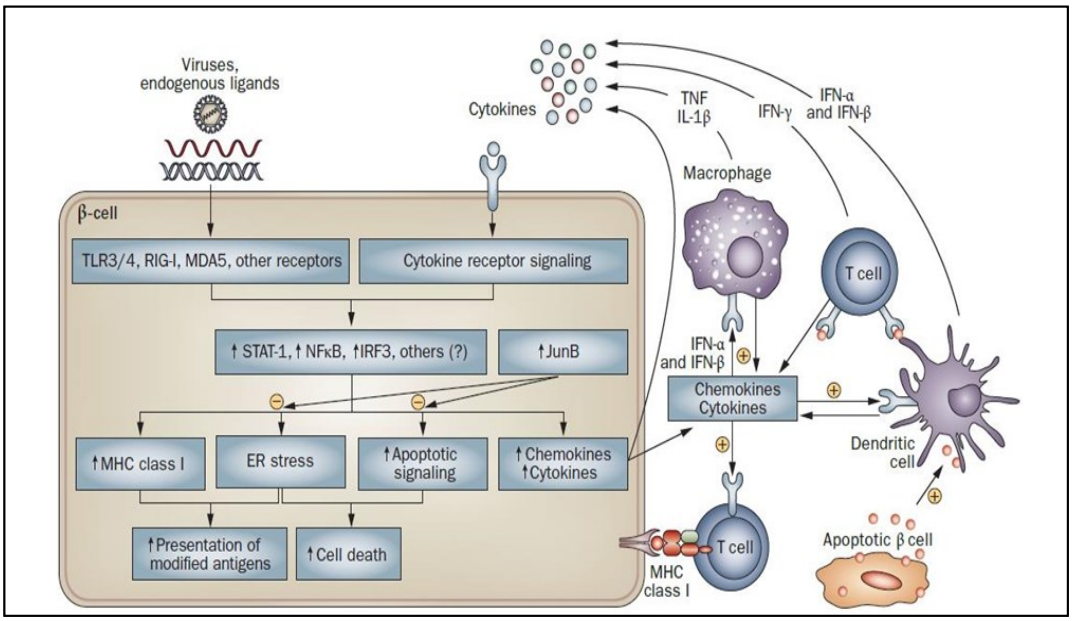

Figure 6. Interaction of β cells and immune cells leads to induction and amplification of insulitis, and the transition from innate to adaptative immune response. Recognition of endogenous and exogenous ligands by PRRs (TRL3/4, RIG-I, MDA5) leads to activation of key transcription factors, as NFκB, IRF3 and STATs. Activation of these transcription factors induces the release of chemokines and cytokines that recruit and activate immune cells, increase the β cells' expression of MHC class-I antigens (that, when associated with ER stress, might lead to presentation of modified antigens to immune cells), and activate proapoptotic signals that lead to β-cell death. Signals from dying β cells are presented by professional antigen-presenting cells that contribute to the activation of autoreactive T cells. During this local inflammation process, proinflammatory cytokines (for example, IL-1β, TNF and IFN-α/β/γ) are released by the immune cells and induce transcription factors (e.g STAT-1, NF-κB and IRF-3) in β cells that contribute to the maintenance and amplification of the network described above. This vicious circle can result in a progressive and selective destruction of pancreatic β cells. Some transcription factors might function as negative regulators of the above signaling pathways; for instance, overexpression of Jun-B prevents cytokine-induced ER stress and β-cell apoptosis. Abbreviations: ER, endoplasmic reticulum; IFN, interferon; IL, interleukin; PRR, pattern-recognition receptor; TLR, Toll-like receptor; TNF, tumor necrosis factor; +, stimulation; –, inhibition. (Eizirik D.L. et al., Endocrinology 2009).

This theory is supported by accumulating evidence that viral infections, especially enteroviruses, have a role in the etiology of T1DM (Drescher K.M. and Tracy S.M., 2008). Another possibility (which does not exclude a pathogenic role of viral infection in some individuals) is that endogenous ligands start the inflammatory process by binding to PRRs (Baccala R. et al., 2007). In line with this theory, apoptotic mouse β cells that are undergoing secondary necrosis trigger T-cell immunity through a TLR2-initiated signalling pathway.

Importantly, autoimmune diabetes in two mouse models was markedly inhibited by TLR2 deletion through impaired activation of T-cells by antigen presenting cells following β-cell injury (Kim H.S. et al., 2007). This finding indicates that β-cell death, and its detection by TLR2, is a putative trigger of the development of T1DM. From an immunological perspective, multiple pathways and diverse forms of human T1DM might exist (Eizirik D.L. and Mandrup-Poulsen T., 2001).

5.6 ER stress in β cells and antigen presentation

β-cell apoptosis is probably the main form of β-cell death in patients with T1DM (Cnop M. et al., 2005; Eizirik D. L. and Mandrup-Poulsen T., 2001). Exposure of β cells to inflammatory cytokines or to dsRNA induces ER stress, which leads to accumulation of misfolded proteins in the ER and triggers the unfolded protein response (Cardozo A.K. et al., 2005; Dogusan Z. et al., 2008; Eizirik D.L. et al., 2008; Liadis N. et al., 2005). The unfolded-protein response aims to alleviate stress on the ER and to restore homeostasis by decreasing the arrival of new proteins, increasing the amount of ER chaperones and increasing the extrusion and subsequent degradation of irreversibly misfolded proteins; when the steps described above fail, apoptosis is triggered (Figure 7) (Eizirik D.L. et al., 2008). Dying cells can transfer immunologically relevant information to dendritic cells, which signal the nature of cell death and determine the immunological outcome of phagocytosis (Albert M.L., 2004). Peptides from within the ER of dying cells can be loaded onto MHC class-I molecules in dendritic cells without further cytosolic processing (Blachère N.E. et al., 2005). In this way, dying cells provide antigen-presenting cells with an accurate representation of what happened just before their death (Albert M.L., 2004).

Although this signaling might be beneficial when viral infection has triggered apoptosis, it might have dire consequences for insulin-producing β cells. Insulin production represents nearly 50% of the total production of protein by β cells, and it accumulates in the ER during periods of increased stress. In this case, insulin accumulates (at least in part) in a misfolded configuration, which might increase its antigenicity (Eizirik D.L. et al., 2008; Scheuner D. and Kaufman R.J., 2008). High antigenicity results in increased presentation of proinsulin and insulin to antigen-presenting cells, especially in the presence of inflammation. Of note, insulin is a key antigen for autoimmune diabetes in both humans and in nonobese, diabetic (NOD) mice (Kent S.C. et al., 2005; Nakayama M. et al., 2005; Skowera A. et al., 2008; Wong F.S. et al., 1999).

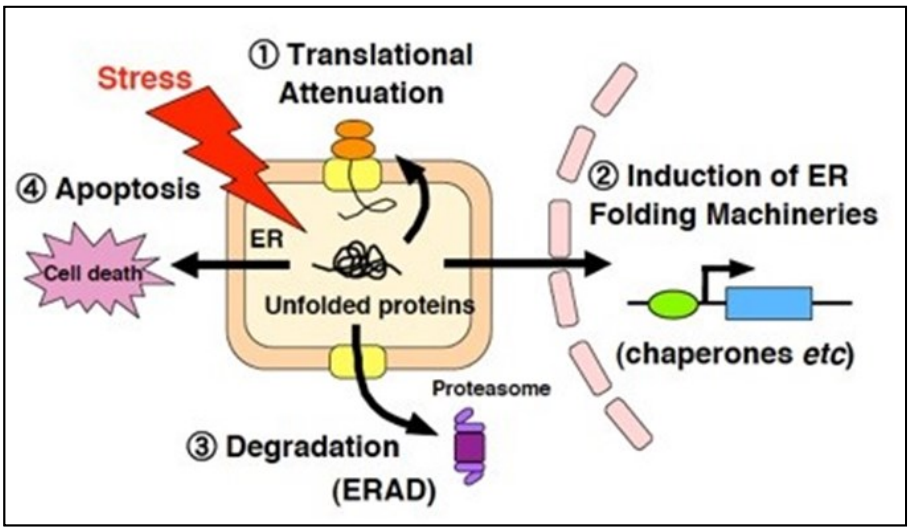

Figure 7. Schematic representation of ER stress unfolded protein response (UPR) signaling pathway. Perturbations of ER homeostasis affect protein folding and cause ER stress. ER can sense the stress and respond to it through gene expression program so called ER stress response. The ER stress response has four functional components. The first is translational attenuation, which inhibits protein synthesis, an adaptation aimed at lowering the load of client proteins the ER must process. The second is the transcriptional upregulation of the folding machineries in the ER to process client proteins. The third is enhancing degradation of misfolded protein in the ER, which is called ER-associated degradation (ERAD). The fourth is apoptosis, which occurs when the ER function is severely impaired.

5.7 Role of PARP in Type 1 Diabetes: The Okamoto model

The removal of the insulin-producing pancreatic β-cells from an animal induces a syndrome, which features many of the acute metabolic derangements of diabetes as they are known in humans. Von Mering and Minkowski in 1890 were the first to produce this form of diabetes by surgically removing the pancreas of dogs.

Alloxan in 1943 and streptozotocin in 1963 were found to be highly selective β-cytotoxins in animals and to be extremely potent diabetogenic substances. Since then, alloxan and streptozotocin have been widely used to produce diabetes in experimental animals (Okamoto H. and Takasawa S., 2002). In particular, STZ is distinctly taken up by β-cells, inducing DNA alkylation and leading to impaired β-cell function and death. In addition, STZ was also found to generate NO species, further deteriorating β-cell survival (Cobo-Vuilleumier N. and Gauthier B.R., 2012).

In the early 1980s, Okamoto and colleagues (Yamamoto H. et al., 1981) demonstrated that STZ and alloxan cause cell death by inducing DNA strand breaks and the activation of poly(ADP)-ribose synthase (PARP). PARP acts to repair the DNA breaks, consuming β-cell NAD^+ as a substrate. Consequently, there would be a sharp drop in the intracellular levels of NAD^+. The cellular NAD^+ reduction would severely impair such cellular functions as insulin synthesis and secretion and cause lethal injury to the β-cells (Figure 8). Therefore, in diabetes induction, pancreatic β-cells seem to be making a "suicide response" in their attempt to repair the damaged DNA. This NAD^+ depletion and β-cell functional impairment were dose-dependently blocked by the radical scavengers superoxide dismutase and catalase and by PARP inhibitors such as nicotinamide (Uchigata Y. et al., 1982; Uchigata Y. et al., 1983).

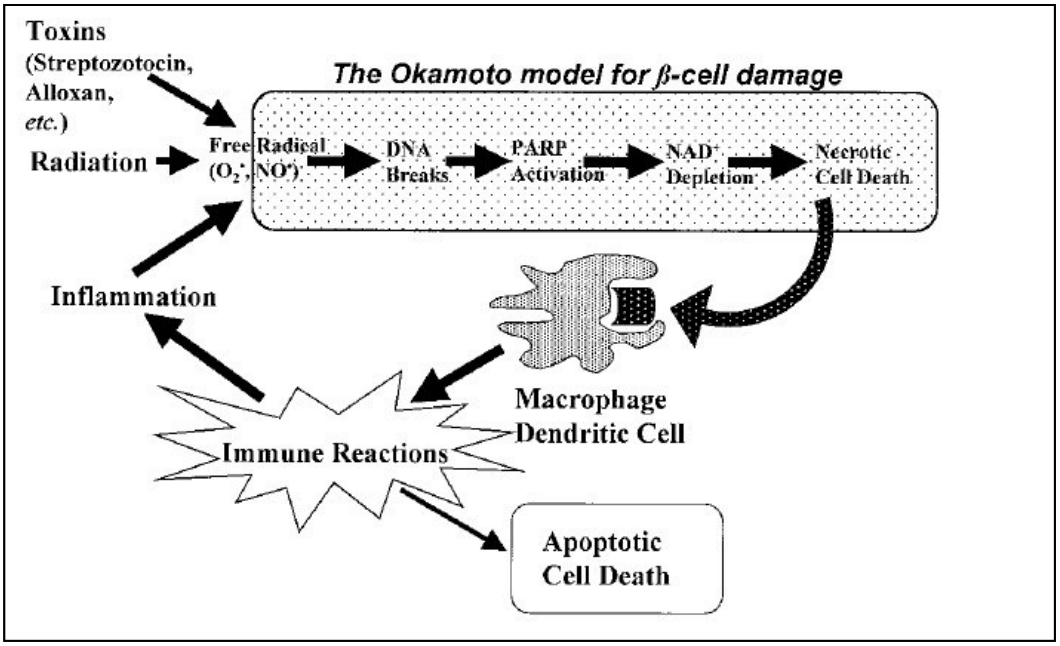

Figure 8. The Okamoto model for necrotic cell death. The Okamoto model, originally proposed as a unifying model for β-cell damage and its prevention, well explains both how autoimmunity for β-cell necrosis is initiated and how necrotic cell death is involved in various diseases in many tissues other than β-cells. Under physiological conditions, apoptotic cell death constitutively occurs for renewal and maintenance in animal bodies, whereas necrotic cells initiate and enhance (auto)immune reactions under pathological conditions. On the other hand, apoptotic cells recognized by macrophages/dendritic cells inhibit phlogistic (auto)-immune responses. For the initiation of massive and pathological apoptotic cell death, necrotic cell death, which triggers autoimmune responses in macrophages/dentritic cells, is required. (Okamoto H. and Takasawa S. Diabetes 2002).

5.8 Involvement of pancreatic α-cell in Diabetes

Glucagon-secreting α-cells are one of the main endocrine cell populations that coexist in the islet of Langerhans along with insulin-secreting β-cells. The architecture of rodent islets is characterized by the location of β-cells in the core and the non-β cells in a mantle around the insulin-secreting cell population. This cellular distribution along with several studies on microcirculation within the islet suggests that the order of paracrine interactions is from β- to α- and δ-cells (Quesada I. et al.,2008). The rich vascularization within the islet ensures a rapid sensing of plasma glucose levels by these endocrine cells, allowing an appropriate secretory response. The principal level of control on glycaemia by the islet of Langerhans depends largely on the coordinated secretion of glucagon and insulin by α- and β-cells respectively.

Both cell types respond oppositely to changes in blood glucose concentration: while hypoglycaemic conditions induce α-cell secretion, β-cells release insulin when glucose levels increase (Nadal et al. 1999, Quesada et al. 2006a). An abnormal function of these cells can generate failures in the control of glycaemia, which can lead to the development of diabetes (Dunning et al. 2005).

5.9 Glucagon secretion in mouse α-cells

Actually, diabetes is associated with disorders in the normal levels of both insulin and glucagon. An excess of glucagon plasma levels relative to those of insulin can be determinant in the higher rate of hepatic glucose output, which seems to be critical in maintaining hyperglycaemia in diabetic patients (Dunning et al. 2005). A model to explain the glucose regulation of electrical activity in mouse α-cells has been postulated in the light of recent studies (Figure 9). At low-glucose levels, the activity of KATP channels renders a membrane potential of about K 60 mV. At this voltage, T-type channels open, which depolarize the membrane potential to levels where NaC and N-type Ca2C channels are activated, leading to regenerative action potentials (Gromada et al. 2004, MacDonald et al. 2007). Ca2C entry through N-type channels induces glucagon secretion. The repolarization of action potentials is mediated by the flowing of KCA-currents. At low-glucose concentrations, this electrical activity triggers oscillatory Ca2C signals in both human and mouse a-cells in intact islets (Nadal et al. 1999, Quesada et al. 1999, 2006b). However, the increase in extracellular glucose levels rises the cytosolic ATP/ADP ratio which blocks KATP channels, depolarizing α-cells to a membrane potential range where the channels involved in action potentials become inactivated (Gromada et al. 2004, MacDonald et al. 2007).

As a consequence, electrical activity, Ca2C signals and glucagon secretion are inhibited (Figure 9).

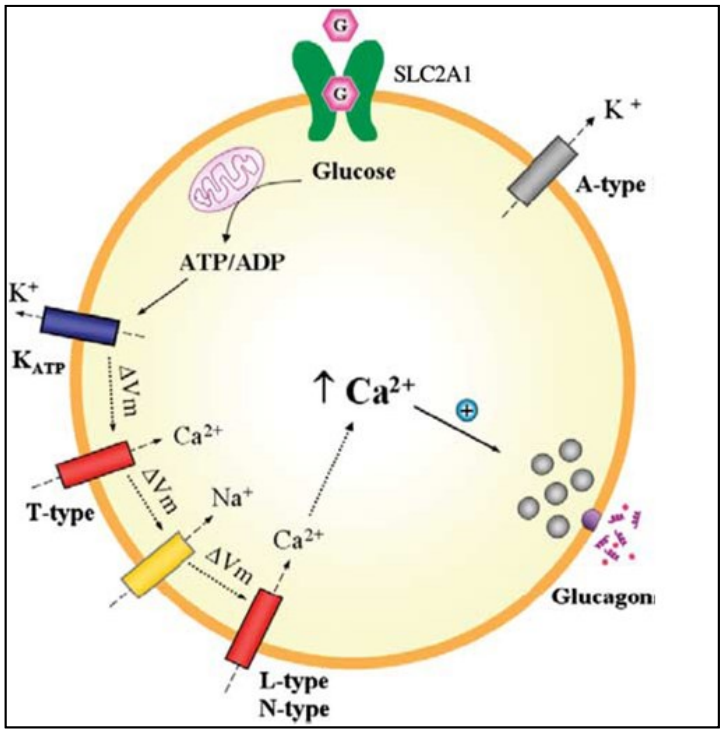

Figure 9. Schematic model for glucose-dependent regulation of glucagon secretion in the mouse α-cell. Glucose is incorporated into the α-cell by the transporter SLC2A1. At low-glucose concentrations, the moderate activity of KATP channels situates the α-cell membrane potential in a range that allows the opening of voltage-dependent T- and N-type Ca_2C channels and voltage-dependent NaC channels. Their activation triggers action potentials, Ca2C influx and exocytosis of glucagon granules. The opening of A-type KC channels is necessary for action potential repolarization. However, high-glucose concentrations elevate the intracellular ATP/ADP ratio, blocking KATP channels and depolarizing the membrane potential to a range where the inactivation of voltage-dependent channels takes place. This results in the inhibition of electrical activity, Ca2C influx and glucagon secretion. The function of L-type channels predominates when cAMP levels are elevated. See text for further details (Quesada I. et al. J Endocrinol. 2008).

Thus, glucagon release from α-cells is mainly supported by an intermediate KATP channel activity that maintains a membrane potential range able to sustain regenerative electrical activity (MacDonald et al. 2007). A similar model has been also proposed for human α-cells (MacDonald et al. 2007).

5.10 The role of α-cell in immune-mediated diabetes

More than 30 years ago, Unger & Orci (1975) proposed the bihormonal hypothesis to explain the pathophysiology of diabetes. According to this hypothesis, this metabolic disease is the result of an insulin deficiency or resistance along with an absolute or relative excess of glucagon, which can cause a higher rate of hepatic glucose production than glucose utilization, favouring hyperglycaemia. Indeed, it has been reported that, in diabetic patients, the lack of suppression of glucagon release in hyperglycaemic conditions, would contribute further to postprandial hyperglycaemia in both type 1 and type 2 diabetes (Dinneen et al. 1995, Shah et al. 2000). However, this irregular α-cell behaviour does not occur when insulin levels are adequate, suggesting that abnormalities in glucagon release are relevant for hyperglycaemia in the context of diabetes or impairment of insulin secretion or action (Shah et al. 1999). Another defect in normal glucagon secretion has important consequences in the management of hypoglycaemia. The secretory response of α-cells to low-glucose concentrations is impaired in type 1 and long-lasting type 2 diabetes, increasing the risk of episodes of severe hypoglycaemia, especially in patients treated with insulin (Cryer 2002). In this regard, iatrogenic hypoglycaemia is a situation that implies insulin excess and compromised glucose counter-regulation, and it is responsible for a major complication in diabetes treatment, increasing the morbidity and mortality of this disease (Cryer 2002). This lack of glucagon response to hypoglycaemia has been associated with multiple failures in α-cell regulation; yet, the mechanisms are still under study (Bolli et al. 1984, Cryer 2002, Zhou et al. 2007).

All these problems in the glucagon secretory response observed in diabetes have been attributed to several defects in α-cell regulation including defective glucose sensing,

loss of β-cell function, insulin resistance or autonomic malfunction. However, the mechanisms involved in α-cell pathophysiology still remain largely unknown and deserve more investigation for better design of therapeutic strategies. In this regard, although direct therapeutic approaches to correct the lack of α-cell response to hypoglycaemia are missing, several proposals have been developed to amend glucagon excess.

Aim of investigation

The poly(ADP-ribose) polymerase (PARP) are a family of proteins that use NAD^+ as their substrate to synthetize adenosine diphosphate-ribose polymers (ADPr), transferring them to acceptor proteins. PARPs family members are involved in many pathological conditions, including the inflammatory diseases. Diabetes is a chronic disease with a strong inflammatory component. The inflammation is the main cause to apoptotic death of pancreatic β-cells. The progressive loss of pancreatic β-cells leads to the onset of Diabetes. Although the pancreatic α and β cells share common endocrine precursors (Ngn3+ cells), upon differentiation they respond differently to external stimuli as proinflammatory cytokines. In particular, the pancreatic α cells are not susceptible to the inflammatory environment, proving to be resistant to apoptosis induced by inflammatory cytokines. Furthermore, in the Okamoto model, PARP-1, the most studied of PARPs family proteins, was correlated to apoptotic death of pancreatic β cells.

Therefore, in our study we hypothesized an involvement of one or more of the 17 PARP family members in the resistance of α-cells to apoptotic death, after treatment with inflammatory cytokines cocktail. Indeed, by RT-PCR, we evaluated the expression of each of PARP family member in both α-TC1.6 and β-TC1 cell lines, grown in presence or absence of inflammatory cytokines, at different time point (24h, 48h). RT-PCR results showed an overexpression of PARP-14 in α-TC1.6 cells.

It has been reported that PARP-14 promotes the survival of myeloma cells through its interaction with JNK-1. The complex PARP-14-JNK-1 prevents the apoptosis induced by JNK-1. Then, we can speculate that this protein could have a protective role also in the survival of α-TC1.6 cells exposed to inflammatory cytokines.

To evaluate the effective role of PARP-14, pancreatic α-TC1.6 and β-TC1 cells were treated with PJ-34 a pan PARP inhibitor. By MTT assay, caspase-3 assay and flow cytometry analysis we evaluated the viability of both cell lines after the treatment of cytokines in presence or absence of PJ-34. Through confocal and western blot analysis we will evaluate PARP-14 and downstream proteins expression. Finally, to demonstrate the pathway involved in the resistance of pancreatic α-TC1.6 cells exposed to inflammatory environment we also propose to perform immunoprecitation assay.

1. Introduction

The immune-mediated diabetes or Type I diabetes mellitus (T1DM) is an inflammatory disease due to β-cells destruction in the pancreatic islets by the immune system, resulting in low blood levels of insulin. However, T1DM is a complex metabolic disease which etiology involves the whole micro-environment of the pancreatic island, including the neighboring α-cells. Indeed, it has been reported that the release of glucagon by the α-cells plays a critical role in the maintenance of high levels of blood glucose (hyperglycaemia) in diabetic patients (Quesada I. et al., 2008). Concerning that, although the molecular mechanisms leading to β-cells destruction in T1DM are largely known, (Barbagallo D. et al., 2013; Cnop M. et al., 2005; Grunnet L.G. et al., 2009) to better understand the pathophysiological actions of α-cells in diabetes further studies are needed. The poly(ADP-ribose) polymerases (PARPs) are a family of proteins that catalyze the transfer of ADP-ribose polymers from their substrate NAD+ to a number of target proteins. PARP-1, the most studied of PARP family proteins, is activated by DNA breaks, being a main component of the base-excision repair pathway (D'Amours D. et al.,1999; El-Khamisy S.F., et al., 2003; Lindahl T. et al., 1995; Underhill C. et al., 2011). Thus, the inhibition of PARP-1 activity is considered a therapeutic strategy to counteract the survival of cancer cells (Brody L.C., 2005). Recently, we demonstrated that pharmacological inhibition of PARP-1 by the potent molecule PJ-34 has proven effective in reducing proliferation and migration of brain endothelial cells stimulated by conditioned medium from glioma cells (Motta C. et al., 2015), showing that PARP-1 inhibitors are able to prevent also the growth of tumours. However, recent finding showed that also the macro PARP-14, another member of PARP family, had a critical role in cancer.

Indeed, in this study Barbarulo et al. demonstrated that PARP-14 is a downstream effector of JNK-2 and upon activation it binds and inhibits the pro-apoptotic protein JNK-1, promoting the survival of myeloma plasma cells (Barbarulo A. et al., 2013). Therefore, we proposed to investigate the potential involvement of one or more PARP family members in the survival of the murine pancreatic α-TC1 cells in an in vitro model of immune-mediated diabetes. The RT-PCR results showed that, after treatment with cytokines cocktail, PARP-14 was more over-expressed in the murine pancreatic α-TC1 cells compared to murine pancreatic β-TC1 cells. Thus, in our study we demonstrate that the macro PARP-14 is a key protein of α-TC1 cells survival in an inflammatory context.

2. Materials and Methods

2.1 Cell cultures and treatment with cytokines

α-TC1.6 cells, a mouse α-cell line, were purchased from the American Type Culture Collection. Cells were maintained in DMEM (Sigma-Aldrich, Saint Louis, MO, USA) containing 10% FBS, 2 mM L-glutammin, 0,15% HEPES 15 mM, 1% non-essential amino acids, 0.02% bovine serum albumins (BSA, Sigma-Aldrich), 25 mM d-glucose (Sigma-Aldrich), 100U/ml penicillin, and 100 µg/ml streptomycin, at 37 °C, in a 5%-CO2 humidified incubator.

Mouse insulinoma cell lines β-TC1 were also from ATCC; cells were grown in DMEM with 25 mM glucose (Sigma Aldrich), supplemented with 2 mM L-Glutamine, 15% HS (horse serum), 2.5% FBS, 1% penicillin/streptomycin, in 95% humidified air-5% CO2 at 37° C. Cells were passaged once a week after trypsinization and replaced with new medium twice weekly. Treatment with cytokines (recombinant murine IL-1β, specific activity 0,1 U/ml, Preprotech, London, UK, UE; recombinant murine IFN-γ, specific activity 25 U/ml, Preprotech; recombinant murine TNF-α, specific activity 25 U/ml, Preprotech) as previously described (Barbagallo et al. 2013). α-TC1.6 and β-TC1 cells were seeded the day before treatment in 60 mm dishes at a density of 7 × 105 cells.

2.2 MTT assay

To evaluate cell viability, the 3-[4,5-dimethylthiazol-2-yl]-2,5-diphenyl tetrasodium bromide (MTT) assay was used (Chemicon, Temecula, CA). Control and treated cells (cells grown in absence or presence of cytokines (TNF-α 25 U/ml; IFN-γ 25 U/ml and IL-1β 0,1 U/ml), respectively, with or without of 10µM PJ-34), were seeded in 96-well plates at 1 x 104 cells/well, to obtain optimal cell density throughout the experiment.

In all assays, cells were first incubated at 37°C with MTT for 4h; then, 100µl dimethyl sulfoxide was added and absorbance was measured. The absorbance was read in a plate reader (Synergy 2-bioTek) with a test wavelength of 570 nm.

2.3 Apoptosis assay

Caspase-3 activity was measured in α-TC1.6 and β-TC1 cell lysates through a colorimetric protease assay (ThermoFisher) following the manufacturer's protocol. The absorbance was read in a plate reader (Synergy 2-bioTek) set at 400 nm.

2.4 Imaging Flow Cytometer analysis

Percentage of apoptotic or necrotic cells was assessed through flow cytometry. Analysis was performed with a FlowSight® Imaging Flow Cytometer. Cells were collected, washed with phosphate-buffered saline (PBS), and stained with Annexin V-FITC/propidium iodide (PI) (Sigma- AldrichW) in Annexin-V binding buffer, as specified by the manufacturer.

Data analysis was carried out using the IDEAS® Software, by which it was possible to obtain the scatter plots of each sample. In the scatter plot we can see the distribution of the acquired events, depending on their differential fluorophore labelling. Our samples were labelled with two markers: Annexin V-FITC (A) and Propidium Iodide (PI). Thus, the scatter plots are divided in four quadrants. The lower left quadrant collects vital cells (A-/PI- cells); the upper left one includes the early apoptotic cells (A+/PI- cells); the upper right one represents the late apoptotic cells (A+/PI+ cells) and the lower right one shows the necrotic cells (A-/PI+ cells). Furthermore, since the software acquires an image for every single event, the operator can easily set the edges of each quadrant looking through the photo gallery (see image below).

The FlowSight® imaging flow cytometry provides images of every labelled (Annexin V-FITC and Propidium Iodide) cell in up to 10 fluorescent channels at up to 2.000 events per second. Detailed analysis of intensity, location, and co-location of probes is achieved using IDEAS® analysis software (see image below).

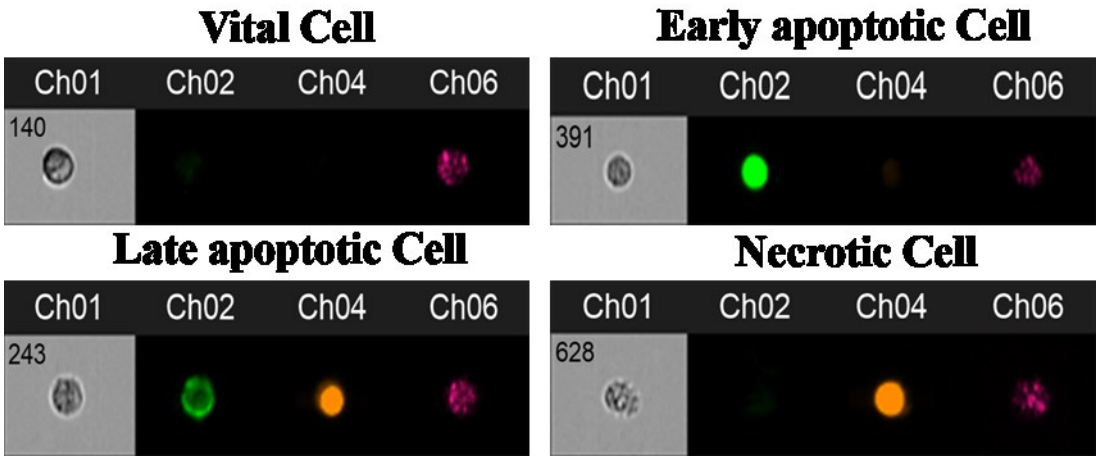

Representative images of the photo gallery of IDEAS® Software. Samples were previously labelled with Annexin V-FITC (A) and Propidium Iodide (PI) markers. The unique image collection system simultaneously produces brightfield (Ch01); two fluorescence images, one for Annexin V-FITC (Ch02) and one for Propidium Iodide (PI) (Ch04), and darkfield (side scatter) (Ch06). The FlowSight® Imaging Flow Cytometer operates at ~20X magnification allowing visualization of fluorescence from the membrane, cytoplasm, or nucleus.

The representative images of the photo gallery of our samples retrieved by IDEAS® software are reported above. A small panel shows the single event in all the different selected channels. In the small upper left panel (vital cell) the cell appears only in the first and last channel. The first channel (Ch01) represents the brightfield cell visualization. In the last channel (Ch06) it is possible to observe the darkfield (side scatter) cell view that permits the evaluation of cell granularity or internal complexity. Since this panel shows a vital cell, no image is reported in the second (Ch02) and in the third (Ch04) channels, in which we can observe the fluorescence of Annexin V-FITC and Propidium Iodide, respectively. Conversely, in the upper right panel (early apoptotic cells) the cell, in addition to Ch01 and Ch06, will appear also in Ch02 but

not in Ch04, since it is only positive to the Annexin. In the "late apoptotic cells" panel (lower on the left) the cell is positive to both dyes and so it is possible to see an image for each channel. Finally, in the "necrotic cells" panel (lower on the left) the cell is positive only to Propidium Iodide fluorescence and therefore it will appear in channels Ch01, Ch04 and Ch06.

2.5 RT-PCR

Total RNA was extracted with TRIzol (Life Technologies, Foster City, CA), according to the manufacturer's instructions. RNA quantification was performed by Qubit Fluorometer (Life Technologies). DNA contamination was removed using deoxyribonuclease 1 (DNase I Amplification Grade; Life Technologies). DNase-treated RNA was reverse transcribed by using High Capacity RNA-to cDNA Kit (Life Technologies) according to manufacturer's instructions.

Resulting cDNAs (200 ng per sample-loading port) were loaded into custom TLDAs, format 96a (Life Technologies), and amplified through a standard thermal cycling profile on an ABI PRISM 7900HT Fast Real-Time PCR System (Life Technologies). Single-gene specific assays were performed through real-time PCR by using Fast SYBR Green Master Mix (Life Technologies) according to manufacturer's instruction. To allow statistical analysis, PCRs were performed in three independent biological replicates. Primer sequences are available upon request.

2.6 Immunofluorescence

To detect the expression and localization of PARP-14 confocal microscopy analysis was performed on α-TC1.6 and β-TC1 cells (control; control +10μM PJ-34; cytokines (TNF-α 25 U/ml; IFN-γ 25 U/ml and IL-1β 0,1 U/ml) and cytokines +10μM PJ-34) grown on a sterile circular micro-cover glass (12 mm diameter, from Electron

Microscopy Sciences), inserted on a 24-well plate. After 24h of incubation with or without cytokines (TNF-α 25 U/ml; IFN-γ 25 U/ml and IL-1β 0,1 U/ml), in the presence or absence of 10μM PJ-34, the cells were processed as previously reported (Scalia M. et al., 2013). Pancreatic α-TC1.6 and β-TC1 cells were fixed with 3% paraformaldehyde in PBS (phosphate buffered saline), and permeabilized in 0,2% Triton (100-X concentration) for 10min.

The non-specific sites were blocked by incubation in 5% BSA (bovine serum albumin) and subsequently the α-TC1.6 and β-TC1 cells were incubated overnight at 4 °C, with the primary goat polyclonal antibody against PARP-14 (diluted 1:100 in PBS containing 1% BSA) in a moist chamber. Following three washing steps with PBS, anti-goat FITC-conjugated secondary antibody (Santa Cruz) diluted 1:50 in PBS containing 1% BSA was added for 1h at room temperature in a dark chamber.

After the fluorescent labeling procedures, the slides were washed three times (5 min each) with PBS, dried on air and finally mounted up-side down on glass slides and covered with a drop of DAPI solution (Electron Microscopy Sciences) to counterstain the nucleus. Negative controls included the omission of both primary antibodies.

2.7 Confocal microscopy imaging

An Olympus FV1000 confocal laser scanning microscope (LSM) was used for confocal imaging. Diode UV (405 nm, 50 mW), multiline Argon (457 nm, 488 nm, 515 nm, total 30 mW) and HeNe (543 nm, 1 mW) and HeNe(R) (633 nm, 1 mW) lasers were used. An oil immersion objective (60xO PLAPO) and spectral filtering system were used. The detector gain was fixed at a constant value and images were taken at random locations throughout the area of the samples, in sequential mode.Quantitative analysis of fluorescence was performed by using the ImageJ software (1.50i version,

NIH), in terms of the average of the mean grey value measured at least in ten equivalent regions of interest (ROIs) drawn in the cell-covered areas. The values obtained by these analyses were imported into OriginPro 8.6 program for statistical analysis for P values, calculated by using a one-way ANOVA with a Tukey multiple comparison test (*$P<0.05$).

2.8 Statistical Analysis

Data are expressed as mean ± standard deviation (S.D.) or ± standard error of the means (S.E.M.) of three experiments (i.e., biological and technical triplicates). We evaluated the statistical significance of these data by applying the Student's T-test and one-way Anova test, as described in figure legends.

3. Results

To evaluate the required cytokines concentration to induce β-cells apoptosis, we performed MTT and FACS analysis at different cytokines concentrations and different time points: 24h, 48 and 72h. To perform our experiments, we have chosen the minimal cytokines concentration (TNF-α 25 U/ml; IFN-γ 25 U/ml and IL-1β 0,1 U/ml) that was able to induce β-cells apoptosis.

3.1RT-PCR

3.1.1 PARP expression in β-TC1 cells treated with inflammatory cytokines

To study which PARP of the 16 members was differentially expressed (DE) between the pancreatic β-TC1 cells and α-TC1.6 cells, these cell lines were treated with inflammatory cytokines at concentrations mentioned above, at 24h, 48h, 72h. Indeed, through RT-PCR it was possible to evaluate the mRNA expression levels of each PARP in both cell lines in order to correlate one or more overexpressed PARPs in the pathophysiology of pancreatic cells in an inflammatory environment. The RT-PCR results of pancreatic β-TC1 cells are reported in table 1.

PARP	FC β-TC1 Cyt vs Ctrl 24h	FC β-TC1 Cyt vs Ctrl 48h	FC β-TC1 Cyt vs Ctrl 72h
PARP-1	1.37	0.67	0.94
PARP-2	1.74	0.82	0.83
PARP-3	8.2	6.05	5.34
PARP-4	1.57	1.41	1.52
TNKS-1	1.53	0.81	0.77
TNKS-2	1.1	1.23	1.16
PARP-6	1.64	1.11	0.96
PARP-7	1.06	0.65	0.84
PARP-8	1.72	1.21	1.29
PARP-9	21.41	35.48	36,05
PARP-10	5.95	3.83	2.57
PARP-11	5.53	5.43	5.84
PARP-12	4.28	2.61	2.61
PARG	1.29	1.06	1
PARP-14	129.99	122.48	127.91
PARP-16	1.68	1.66	2.41

Table 1. Fold change values of 16 PARP family members in murine pancreatic β-TC1 lines. In this table are reported fold change values of each PARP, comparing PARP ΔCt values of treated cells (TNF-α 25 U/ml; IFN-γ 25 U/ml and IL-1β 0,1 U/ml) against PARP ΔCt values of steady state cells (controls), at 24h, 48h and 72h.

In table 1 are reported the fold change of 16 PARPs members. What is important to note is that mRNA levels of PARP-3, PARP-9, PARP-11 and PARP-14 are significantly differentially expressed (DE) in β-TC1 cells exposed to inflammatory stimuli, compared to the controls.

3.1.2 PARP expression in α-TC1.6 cells treated with inflammatory cytokines

To verify which of 16 PARPs members are DE between pancreatic β-TC1 and α-TC1.6 cells, we also analyzed the expression of all PARPs members in α-TC1.6 cells trough RT-PCR. Pancreatic α-TC1.6 cells were treated with the same cytokines concentrations of β-TC1 cells, for 24h, 48h, 72h. The data are reported in table 2.

PARP	FC α-TC1.6 Cyt vs Ctrl 24h	FC α-TC1.6 Cyt vs Ctrl 48h	FC α-TC1.6 Cyt vs Ctrl 72h
PARP1	0.79	0.98	1.78
PARP2	0.66	0.98	1.51
PARP3	2.65	5.19	5.71
PARP4	0.55	1.27	2.36
TNKS1	0.45	0.82	1.47
TNKS2	0.55	1.02	1.49
PARP6	0.79	1	1.42
PARP7	0.64	1.02	0.96
PARP8	0.52	1.38	1.65
PARP9	19.94	27.88	31.02
PARP10	4.86	3.95	5.42
PARP11	5.77	3.28	3.74
PARP12	2.79	4.27	4.74
PARG	0.63	1.11	1.41
PARP14	2356.68	2102.50	2363.6
PARP16	0.91	1.62	2.07

Table 2. Fold change values of 16 PARP family members in murine pancreatic α-TC1.6 cells lines. In this table are reported fold change values of each PARP, comparing PARP ΔCt values of treated cells (TNF-α 25 U/ml; IFN-γ 25 U/ml and IL-1β 0,1 U/ml) against PARP ΔCt values of steady state cells (controls), at 24h, 48h and 72h.

In table 2 we can observe that PARP-3, PARP-9 and PARP-11 expression levels are similar in both cells lines. Therefore, these PARPs can't be considered involved in the pathophysiology of none of the two cell lines (e.g. in apoptotic β-TC1 cells death or in α-TC1.6 cells survival), in a context of an inflammatory environment. However, after inflammatory stimuli, pancreatic α-TC1.6 cells express higher levels of PARP-14 mRNA compared to β-TC1 cells, which could suggest a protective role of this PARP versus inflammatory insults.

3.1.3 mRNA expression of PARP-14 on pancreatic β-TC1 and α-TC1.6 cells

The RT-PCR analysis on β-TC1 and α-TC1.6 cells shows the expression level of PARP-14 mRNA, which was differentially expressed between the two cell lines, as it was reported in tables 1 and 2 (figure 1).

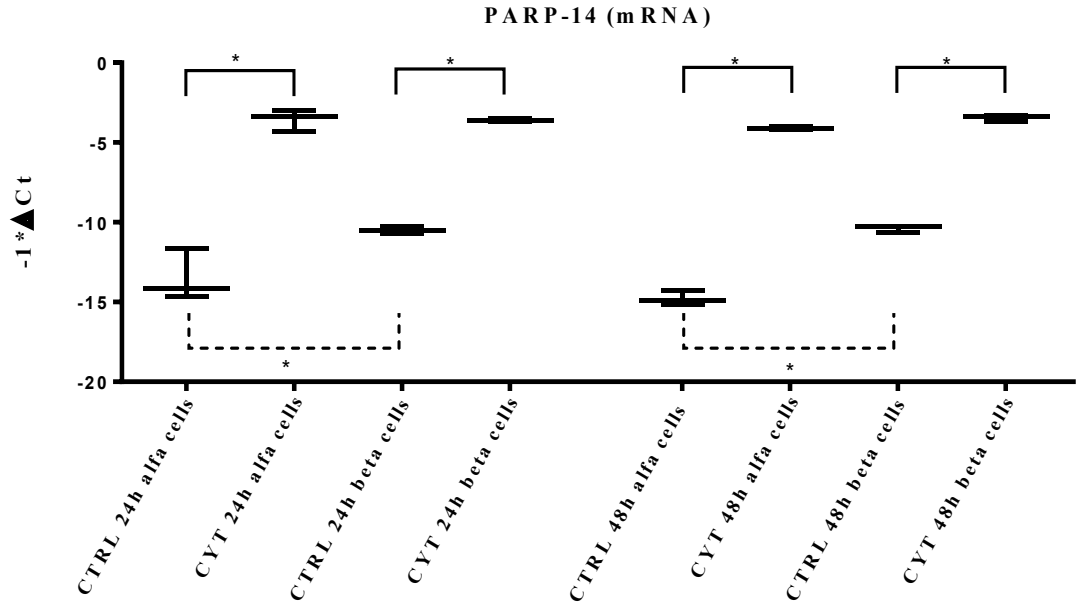

Figure 1. PARP-14 mRNA expression on β-TC1 and α-TC1.6 cells after 24h and 48h of treatment with inflammatory cytokines. Cytokines treatment induces a statistically increment of PARP-14 mRNA after 24h and 48h in both cell lines. Box plots with whiskers from minimum to maximum represent -1*(ΔCt) values. *P<0.01 Cyt vs control. Analysis was determined with one-way ANOVA test. The error bars indicate ± SD (S.D.= standard deviation).

As shown in figure 1, the treatments, at 24h and 48h, with cytokines induced a significant increase of PARP-14 mRNA expression level in both cell lines. However, the basal level of PARP-14 mRNA of α-TC1.6 cells was lower than for β-TC1 cells. After the treatment with cytokines the amount of PARP-14 mRNA was the same for both cell lines. According to this results, after treatment, the increase of PARP-14 mRNA was higher in α-TC1.6 cells. Furthermore, since the trend of PARP-14 mRNA expression at 48h and 72h was equal, we tested only two time points: 24h and 48h.

3.2 Confocal microscopy analysis

To analyze the expression of PARP-14 protein in murine pancreatic α-TC1.6 and β-TC1 cells treated with or without cytokines (TNF-α 25 U/ml; IFN-γ 25 U/ml and IL-1β 0,1 U/ml) for 24h and 48h we performed confocal microscopy analysis. The results are reported in figure 2A and B and in figure 3.

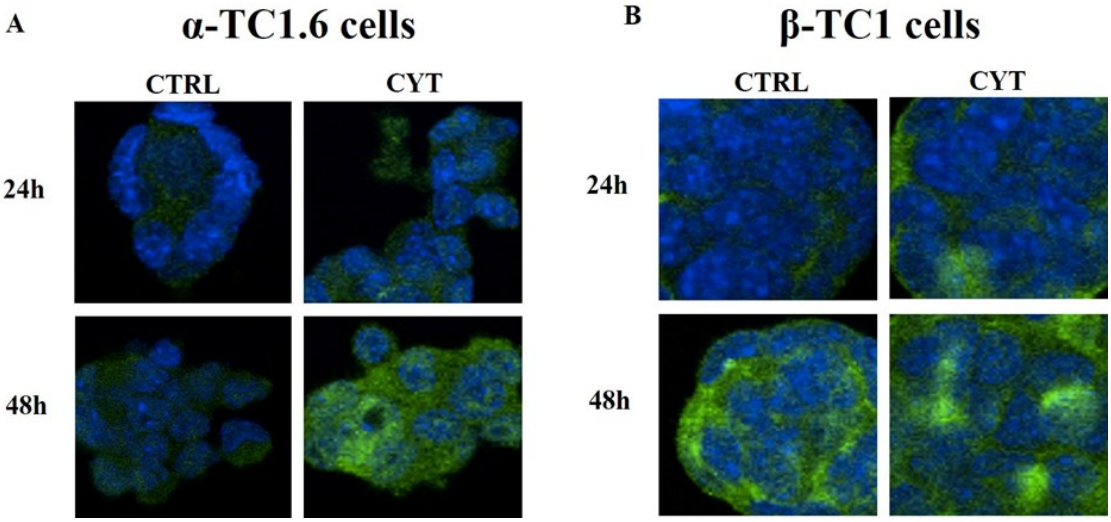

Figure 2 A and B. Confocal LSM of PARP-14 expression in pancreatic α-TC1.6 and β-TC1 cells. Pancreatic α-TC1.6 and β-TC1 cells were cultured with normal medium: control or with medium containing cytokines (TNF-α 25 U/ml; IFN-γ 25 U/ml and IL-1β 0,1 U/ml added simultaneously). Cell monolayers were washed, fixed, permeabilized and stained with a goat polyclonal PARP-14 antibody (coupled to a green fluorescent-labeled secondary antibody). The blue fluorescence is due to the labeling with DAPI to counterstain the nucleus. The merge shows the co-localization of the two dyes. The images were recorded at the following conditions of excitation/emission wavelengths: 405/425-475 nm (blue); 488/500-540 nm (green). Scale bar = 20 μm.

PARP-14 protein expression was investigated by laser scanning microscopy using a green fluorescent labelled antibody (FITC secondary antibody). In panel A, we can observe PARP-14 immunofluorescence in α-TC1.6 cells, grown for 24 and 48h, with normal culture medium (Control) or in presence of inflammatory cytokines: TNF-α 25 U/ml; IFN-γ 25 U/ml and IL-1β 0,1 U/ml added simultaneously (Cytokines). In both time points, cytokines treatment was able to induce very efficiently the immunofluorescence signal for PARP-14, compared to the control. Conversely, in β-TC1 cells (panel B) the immunofluorescence signal for PARP-14 was high already at basal levels. Thus, in presence of cytokines the fluorescence intensity for PARP-14 was higher at 24h, instead similar to the control at 48h.

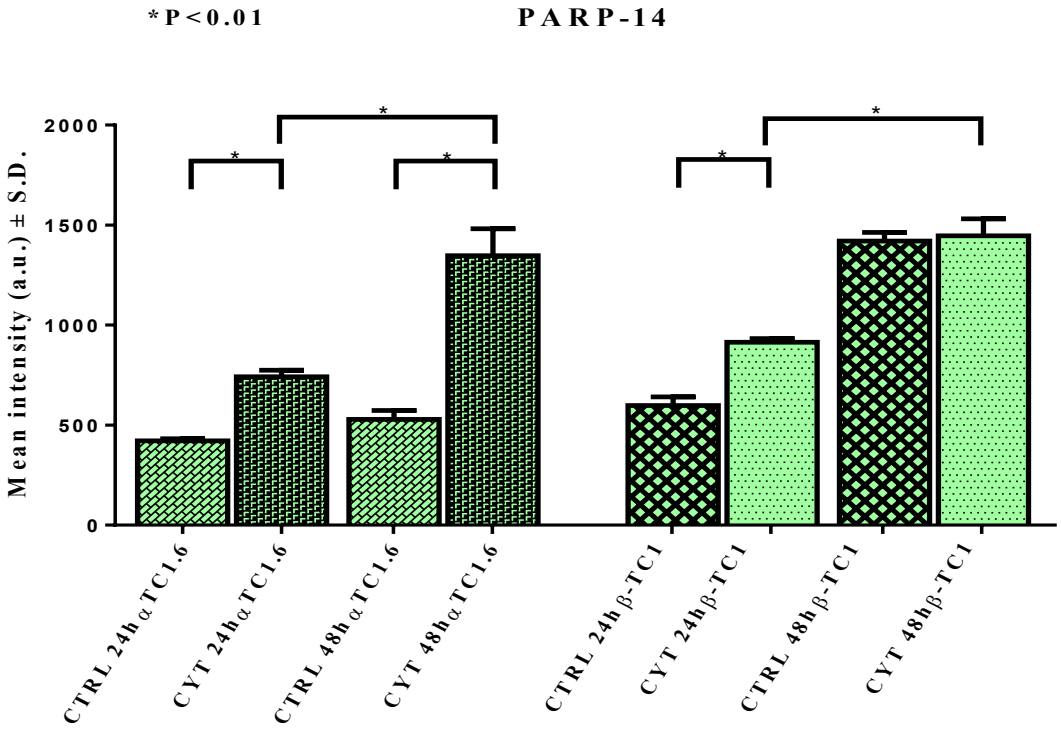

Figure 3. The graph shows mean intensity values (a.u.) of PARP-14. The pancreatic α-TC1.6 and β-TC1cells were grown with normal culture medium (control) or with normal medium containing cytokines cocktail (TNF-α 25 U/ml; IFN-γ 25 U/ml and IL-1β 0,1 U/ml added simultaneously), for 24h and 48h. In the graph the quantitative analysis of Parp-14 emission as calculated by the averaged grey mean values +/- S.D. of at least 10 measurements for each sample. Intensity data (LSM) were analyzed by Student's T-test *P <0.01

Quantitative analysis of confocal micrographs was carried out to analyze the fluorescence recorded for the FITC secondary antibodies, (figure 3). In pancreatic α-TC1.6 cells, the mean values of fluorescence measured for PARP-14 indicate a statistically significant increase of intensities after both 24h and 48h of cytokines treatment (TNF-α 25 U/ml; IFN-γ 25 U/ml and IL-1β 0,1 U/ml added simultaneously), compared to the control. A statistically significant increase was found for PARP-14 also in β-TC1cells after 24h of treatment with cytokines. At 48h, the intensity of fluorescence measured was similar in β-TC1cells treated with cytokines compared to the control. In both cell lines there was a statistically significant increase of the intensity of fluorescence for the PARP-14 at 48h compared to intensity measured at 24h. As shown in Figure 3, the amount of PARP-14 protein more than doubled following α-TC1.6 cells treatment with the cytokine cocktail for 48h.

3.3 Cell Viability

To verify the involvement of PARP-14 in α-TC1.6 cells survival we performed MTT assay. β-TC1 and α-TC1.6 cells were treated with cytokines (TNF-α 25 U/ml; IFN-γ 25 U/ml and IL-1β 0,1 U/ml) in presence or absence of 10μM PJ-34, for 24h, 48h. The result of viability of the two cell lines are reported below (figure 4 and 5).

3.3.1 Effect of PJ-34 on α-TC1.6 cells viability

MTT analysis was performed on α-TC1.6 cells to evaluate the effect of the treatment with cytokines (TNF-α 25 U/ml; IFN-γ 25 U/ml and IL-1β 0,1 U/ml) on cell viability of α-TC1.6 cells, at 24h and 48h. Moreover, PJ-34 a pan-PARP inhibitor that could inhibit PARP-14 activity, was added to the cytokines (TNF-α 25 U/ml; IFN-γ 25 U/ml and IL-1β 0,1 U/ml) to study the role of PARP-14 on α-TC1.6 cells viability after 24h and 48h of treatment (figure 4).

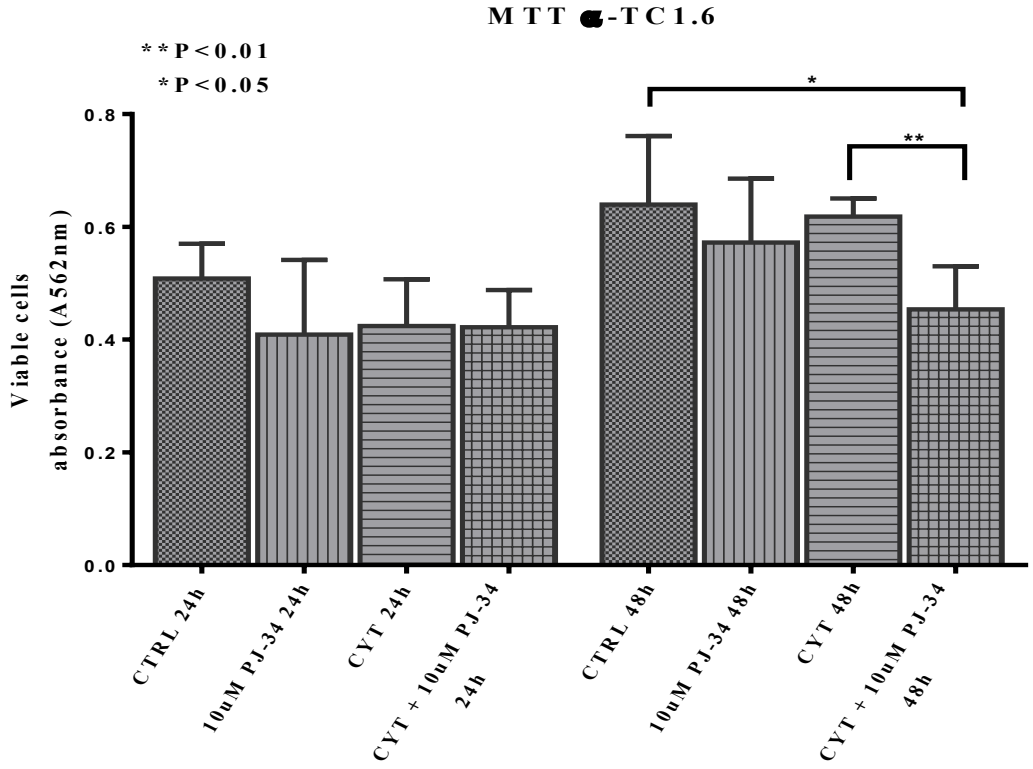

Figure 4. MTT assay on pancreatic α-TC1.6 cells. Histograms show cell viability of α-TC1.6 at steady state (control) or after treatment with cytokines (TNF-α 25 U/ml; IFN-γ 25 U/ml and IL-1β 0,1 U/ml) added simultaneously, in presence or absence of 10μM PJ-34, at 24h and 48h. Statistical analysis was performed by Student's T-test *P <0.05; **P <0.01. The error bars indicate ± SD (S.D.= standard deviation).

Figure 1 shows the effect of pancreatic α-TC1.6 cells viability at 24h and 48h after treatment with cytokines (TNF-α 25 U/ml; IFN-γ 25 U/ml and IL-1β 0,1 U/ml), added simultaneously, in presence or absence of 10μM PJ-34. Cytokines treatment did not induce any change on α-TC1.6 cells viability in both time points. This result confirms that α-TC1.6 cells are resistant to inflammatory stimuli similarly of what occurs in immune-mediated diabetes. After 48h, the addiction of 10μM PJ-34 to the cytokines cocktail (TNF-α 25 U/ml; IFN-γ 25 U/ml and IL-1β 0,1 U/ml) was able to reduce significantly α-TC1.6 cells viability compared to control and to the treatment with cytokines (TNF-α 25 U/ml; IFN-γ 25 U/ml and IL-1β 0,1 U/ml) alone, supporting the hypothesis that PARP-14 could have a protective role in α-TC1.6 cells against inflammatory stimuli.

However, the addiction of 10μM PJ-34 to the culture medium of the α-TC1.6 cells did not affect the α-TC1.6 cells viability, probably because in this condition any PARP was activated and its inhibitor could not act.

3.3.2 Effect of PJ-34 on β-TC1.6 cells viability

Viability of β-TC1 cells after treatment with cytokines (TNF-α 25 U/ml; IFN-γ 25 U/ml and IL-1β 0,1 U/ml), added simultaneously, with or without the addiction of 10μM PJ-34, at 24h and 48h, was evaluated through MTT assay (figure 5).

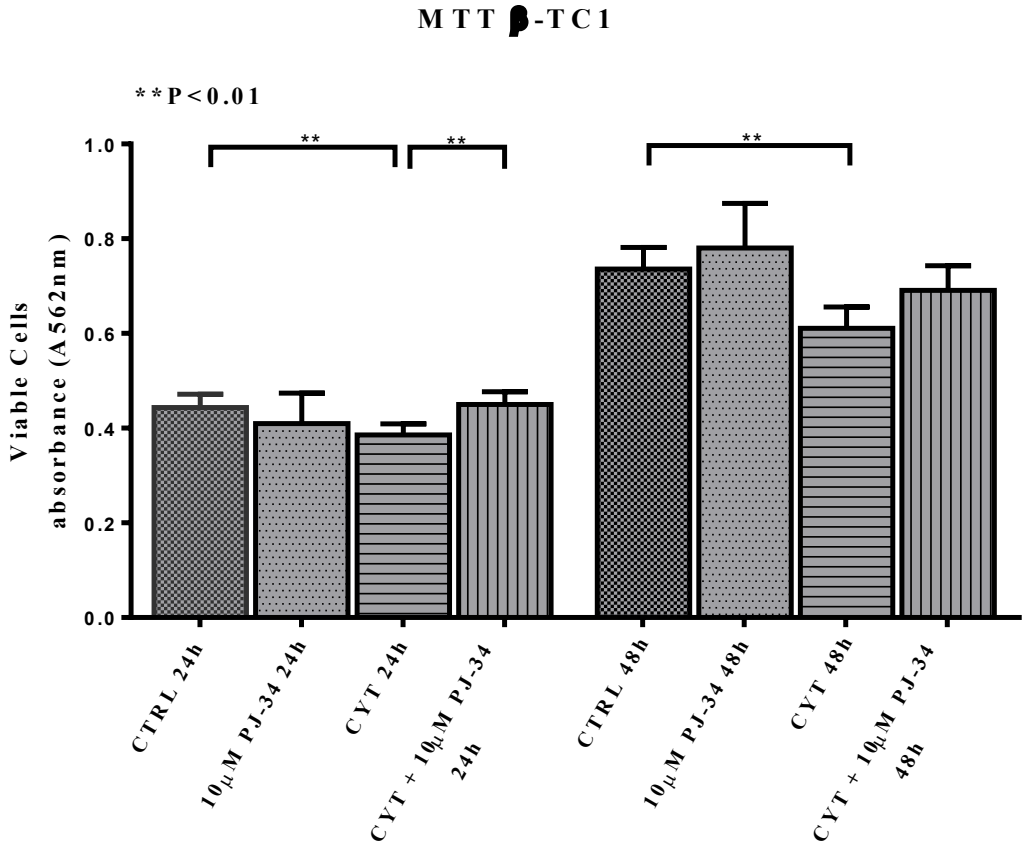

Figure 5. MTT assay on pancreatic β-TC1 cells. Histograms show cell viability of β-TC1 at steady state (control) or after treatment with cytokines (TNF-α 25 U/ml; IFN-γ 25 U/ml and IL-1β 0,1 U/ml) in presence or absence of 10μM PJ-34, at 24h and 48h. Statistical analysis was performed by Student's T-test **P <0.01. The error bars indicate ± SD (S.D.= standard deviation).

The murine pancreatic β-TC1 cell line is very susceptible to the cytokines treatment, at both 24h and 48h.

In fact, the exposure to inflammatory cytokines (TNF-α 25 U/ml; IFN-γ 25 U/ml and IL-1β 0,1 U/ml) induced a significant reduction of β-TC1 cells viability compared to the control. The addiction of 10μM PJ-34 to the cytokines (TNF-α 25 U/ml; IFN-γ 25 U/ml and IL-1β 0,1 U/ml), added simultaneously, restored β-TC1 cells viability to the control values at 24h as well as 48h. Similarly to the α-TC1.6 cells PJ-34, added to the normal medium had not effect on β-TC1 cells viability and this could be explained with the same hypothesis expressed for the α-TC1.6 cells.

3.4 Apoptosis assay

To further evaluate the role of PARP-14 in α-TC1.6 cells survival, after treatment, for 24h and 48h, with inflammatory cytokines (TNF-α 25 U/ml; IFN-γ 25 U/ml and IL-1β 0,1 U/ml), added simultaneously, we performed a Caspase-3 assay. Through this analysis we evaluated the caspase-3 activity in α-TC1.6 and β-TC1 cells lines, before and after treatment with inflammatory cytokines (TNF-α 25 U/ml; IFN-γ 25 U/ml and IL-1β 0,1 U/ml), in presence or absence of 10μM PJ-34, at 24h and 48h (figure 3 and 4).

3.4.1 Caspase-3 activity on α-TC1.6 cells treated with cytokines, in presence or absence of PJ-34

The lysates obtained from pancreatic α-TC1.6 cells were used to perform apoptosis test. Caspase-3 assay is a colorimetric assay that allows to evaluate the activity of the enzyme. The absorbance values are directly proportional to the ability of caspase-3 to cleave its substrate (Figure 6).

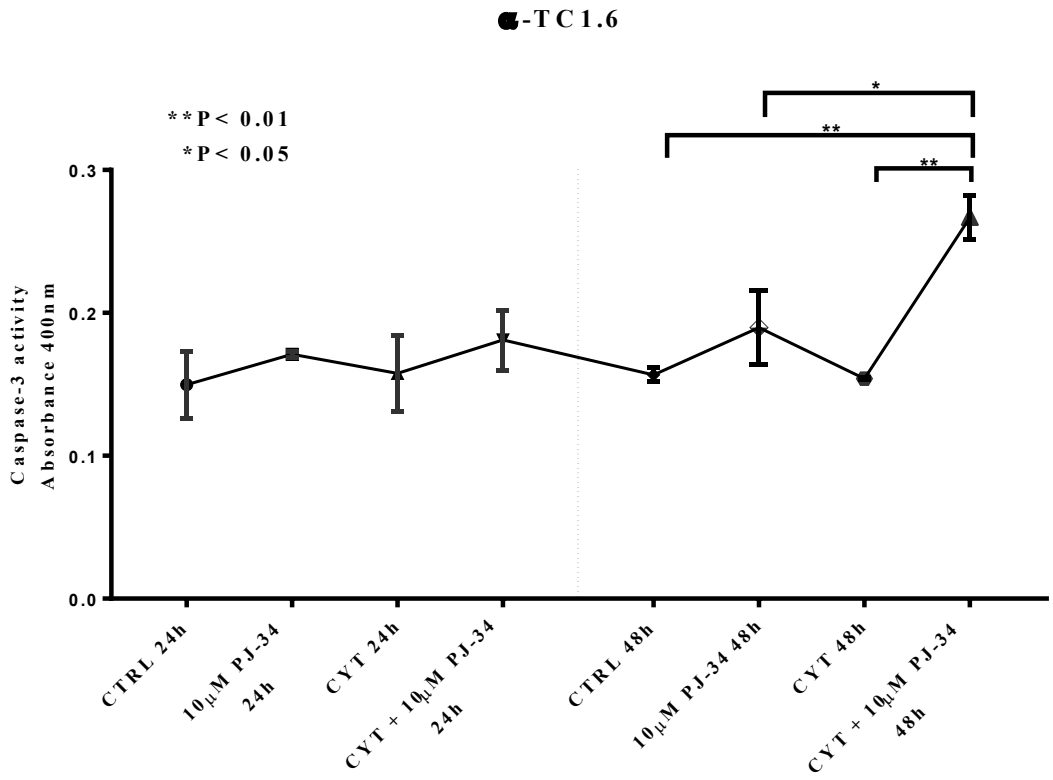

Figure 6. Caspase 3 activity of α-TC1.6 cells. α-TC1.6 cells were treated for 24h and 48h with cytokines (TNF-α 25 U/ml; IFN-γ 25 U/ml and IL-1β 0,1 U/ml), added simultaneously, in presence or absence of 10μM PJ-34. Statistical analysis was performed by Student's T-test *P <0.05; **P <0.01. The error bars indicate ± SD (S.D.= standard deviation).

The graphic reported in figure 6 shows the caspase-3 activity of α-TC1.6 cells treated with cytokines (TNF-α 25 U/ml; IFN-γ 25 U/ml and IL-1β 0,1 U/ml), in presence or absence 10μM PJ-34, at 24h and 48h. According to the MTT assay results, at 24h after treatment with cytokines (TNF-α 25 U/ml; IFN-γ 25 U/ml and IL-1β 0,1 U/ml), the caspase-3 activity was equal to the control.

The addiction of 10μM PJ-34 to the culture medium or to the medium with cytokines (TNF-α 25 U/ml; IFN-γ 25 U/ml and IL-1β 0,1 U/ml) determined a small increase of caspase-3 activity. This could be due to the fact that PJ-34 is able to inhibit catalytic activity of the PARPs, enzymes involved in different cellular function. Therefore, its addiction lead to a small increase of the caspase-3 activity, indicating cell suffering, more in presence of cytokines.

At 48h the trend of the caspase-3 activity was similar to the 24h. However, the addiction of 10μM PJ-34 to the cytokines cocktail (TNF-α 25 U/ml; IFN-γ 25 U/ml and IL-1β 0,1 U/ml) determined a significant enhancement of caspase-3 activity compared to the control, the PJ-34 condition and to the treatment with the cytokines alone (TNF-α 25 U/ml; IFN-γ 25 U/ml and IL-1β 0,1 U/ml), indicating that, in presence of inflammatory stimuli, the inhibition of PARP-14 causes the apoptotic death of α-TC1.6 cells. Thus, this result supports our hypothesis about the protective role of PARP-14 on pancreatic α-TC1.6 cells against inflammatory insult.

3.4.2 Caspase-3 activity on β-TC1 cells treated with cytokines, in presence or absence of PJ-34

To demonstrate that the overexpression of PARP-14 is involved in the resistance of apoptotic α-TC1.6 cells death we performed our experiments also in β-TC1 cells. Indeed, this cell line is very susceptible to apoptotic death after exposition to inflammatory stimuli. Therefore, it was interesting to evaluate the caspase-3 activity on β-TC1 cells and verify the effect of treatment with 10μM PJ-34, at 24h and 48h (figure 7).

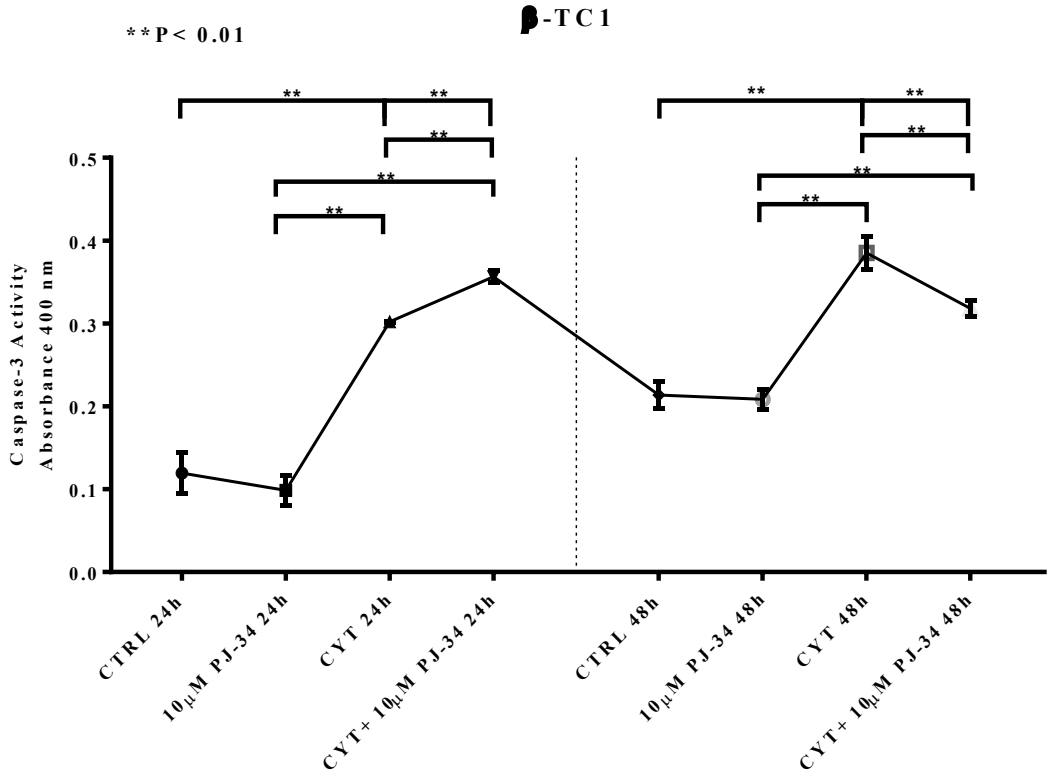

Figure 7. Caspase 3 activity on β-TC1 cells. β-TC1 cells were treated for 24h and 48h with cytokines (TNF-α 25 U/ml; IFN-γ 25 U/ml and IL-1β 0,1 U/ml), in presence or absence of 10μM PJ-34. Statistical analysis was performed by Student's T-test **P <0.01. The error bars indicate ± SD (S.D.= standard deviation).

β-TC1 cells were exposed to the same experimental conditions used for α-TC1.6 cells. The treatment, for 24h, with cytokines (TNF-α 25 U/ml; IFN-γ 25 U/ml and IL-1β 0,1 U/ml), induced a significant increase of the caspase-3 activity compared to the control and PJ-34 condition. The addiction of 10μM PJ-34 to the culture medium did not affect the caspase-3 activity compared to the control. On the other hand, the addiction of this inhibitor to the medium containing inflammatory cytokines (TNF-α 25 U/ml; IFN-γ 25 U/ml and IL-1β 0,1 U/ml) cause a statistically significant enhancement of caspase-3 activity. The trend of the graphic, after 48h of treatments, was the same of the 24h, accept for the effect of the cytokines (TNF-α 25 U/ml; IFN-γ 25 U/ml and IL-1β 0,1 U/ml) with 10μM PJ-34. In this case, the inhibitor PJ-34 caused a statistically significant reduction of caspase-3 activity.

These results confirm the susceptibility, to the apoptotic death, of pancreatic β-TC1 cells growing in presence of inflammatory cytokines.

In addiction we can observe a double effect of the PARP inhibitor PJ-34 added to the medium with cytokines (TNF-α 25 U/ml; IFN-γ 25 U/ml and IL-1β 0,1 U/ml). In fact, at 24h it promotes the apoptotic death of β-TC1 cells, conversely at 48h it seems to have a protective effect, reducing the caspase-3 activity of β-TC1 cells.

3.5 Flow Cytometry

To further analyze the role of PARP-14 in the α-TC1.6 cells survival we performed a flow cytometry analysis on pancreatic α-TC1.6 and β-TC1 cell lines, treated with the same cytokines concentration, in presence or absence of 10μM PJ-34, for 24h and 48h. Representative data of the Annexin V-FITC/propidium iodide (PI) flow cytometry results are shown in figure 8a-b and 9a-b.

3.5.1 Effect of PJ-34 on apoptotic α-TC1.6 cells death: flow cytometry analysis

Apoptosis of α-TC1.6 cells was analysed by flow cytometry. This technique allows to study, for each condition (control, 10μM PJ-34, cytokines (TNF-α 25 U/ml; IFN-γ 25 U/ml and IL-1β 0,1 U/ml) and cytokines + 10μM PJ-34), the rate of the vital cells, the early apoptotic cells, the late apoptotic cells and the necrotic cells. The results of flow cytometry are shown in Figure 8a and 8b.

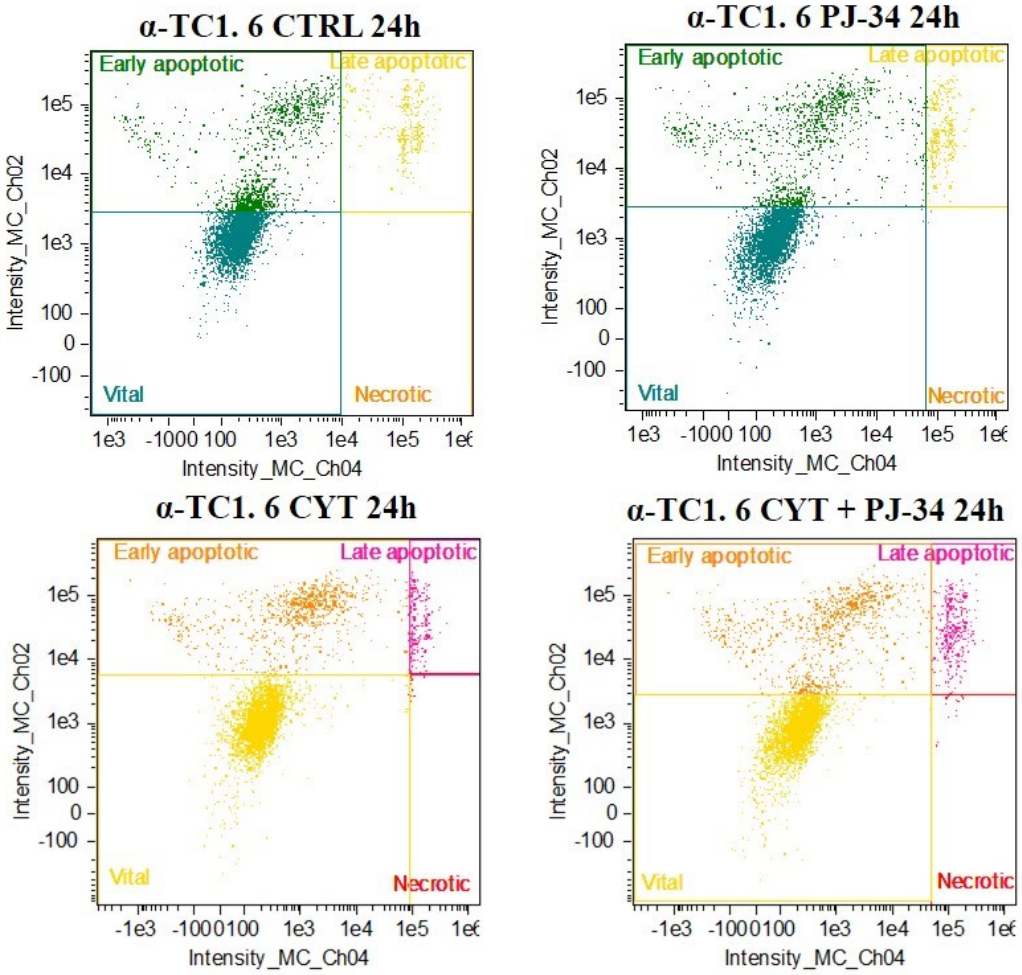

Figure 8a. Representative pictures of flow cytometry analysis on α-TC1.6 cells, at 24h. In square CTRL α-TC1.6 cells at steady state at 24h. In square 10μM PJ-34 α-TC1.6 cells after 24h treatment with PARP inhibitor PJ-34. In square CYT α-TC1.6 cells treated, for 24h, with cytokines (TNFα 25 U/ml, IFNγ 25 U/ml, Il-1β 0.1 U/ml). In square CYT + PJ-34 α-TC1.6 cells after 24h of treatment with cytokines in presence of 10μM PJ-34. Each square includes cells that stain negatively for both Annexin V and PI and are considered undamaged (Vital cells); cells stained with Annexin V, but are PI negative and are considered early apoptotic cells; cells that are both Annexin V and PI positive and are considered late apoptotic and cells that are PI positive and Annexin V negative and are considered necrotic cells.

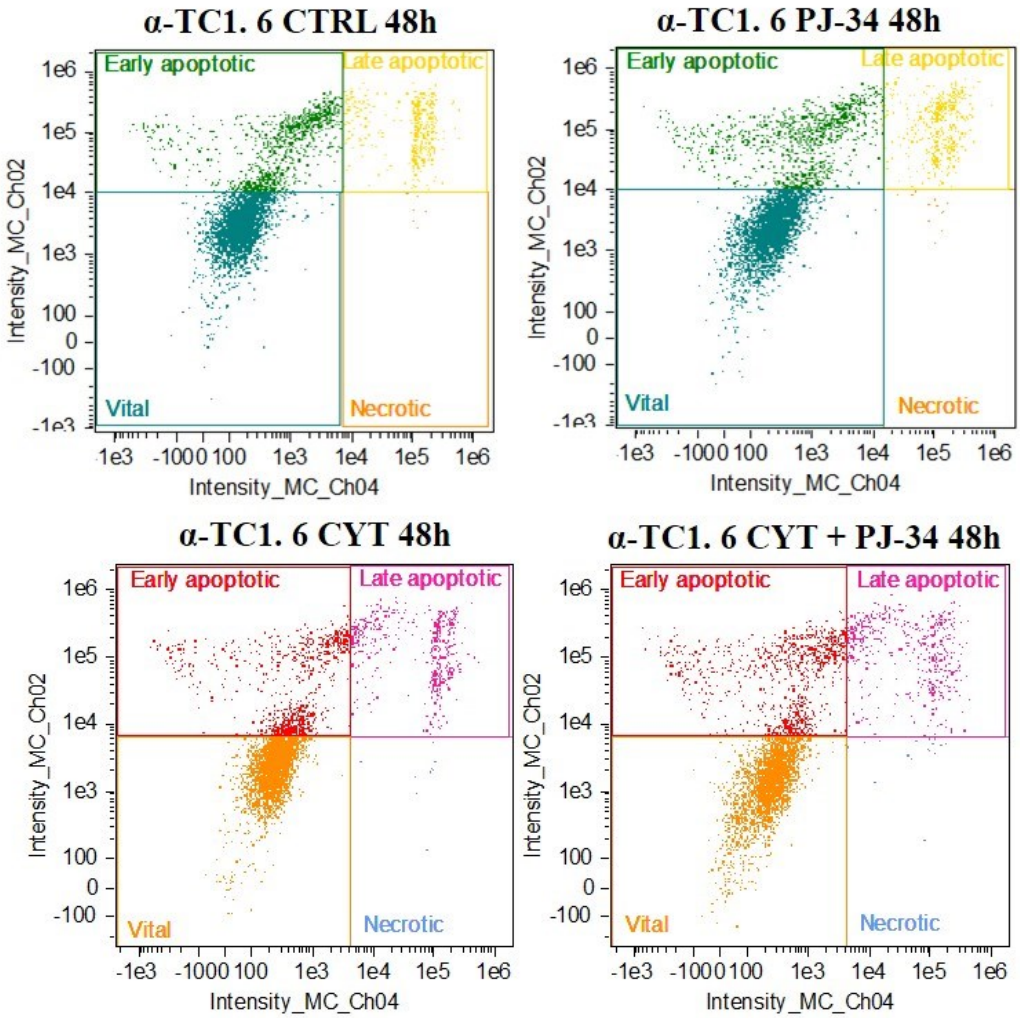

Figure 9b. Representative pictures of flow cytometry analysis on α-TC1.6 cells, at 48h. In square CTRL α-TC1.6 cells at steady state at 48h. In square 10μM PJ-34 α-TC1.6 cells after 48h treatment with PARP inhibitor PJ-34. In square CYT α-TC1.6 cells treated, for 48h, with cytokines (TNFα 25 U/ml, IFNγ 25 U/ml, Il-1β 0.1 U/ml). In square CYT + PJ-34 α-TC1.6 cells after 48h of treatment with cytokines in presence of 10μM PJ-34. Each square includes cells that stain negatively for both Annexin V and PI and are considered undamaged (Vital cells); cells stained with Annexin V, but are PI negative and are considered early apoptotic cells; cells that are both Annexin V and PI positive and are considered late apoptotic and cells that are PI positive and Annexin V negative and are considered necrotic cells.

Figures 8a and 8b show the distribution of the α-TC1.6 cell population in 4 squares, depending of their stained with apoptosis markers (Annexin V and PI). How it is possible to note, at 24h as well as at 48h, the α-TC1.6 cell distribution was similar in each square, indicating, once again, the resistance of the pancreatic α-TC1.6 cells to apoptotic death, induced by inflammatory cytokines (TNF-α 25 U/ml; IFN-γ 25 U/ml and IL-1β 0,1 U/ml). In Figure 10 it has been reported the histograms of the data of cytometry analysis.

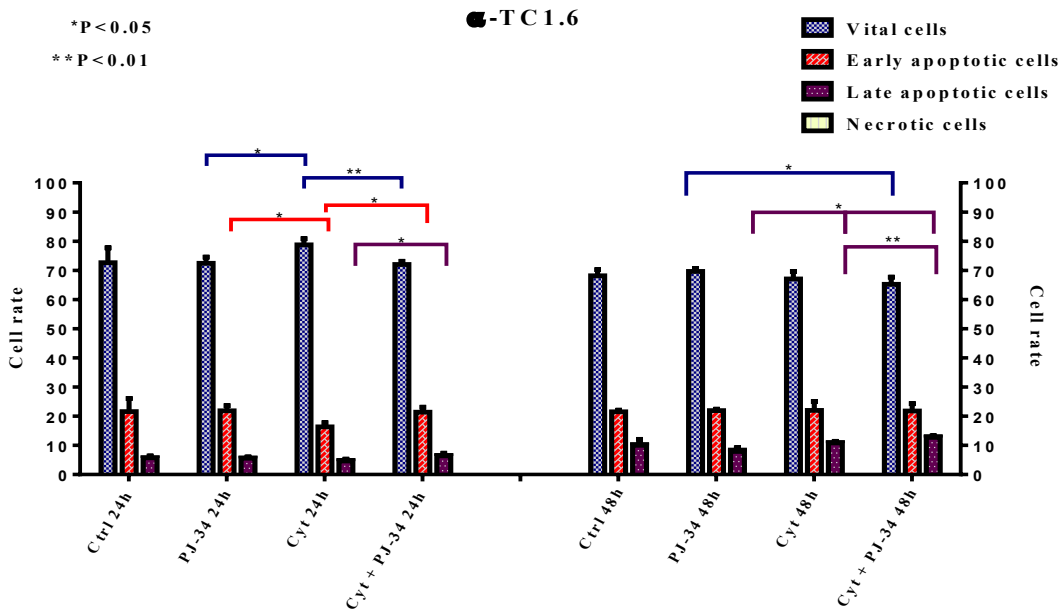

Figure 9. Cytometry analysis on pancreatic α-TC1.6 cell lines. Histograms show the rate of vital, early apoptotic, late apoptotic and necrotic α-TC1.6 cells, at the steady state (control); with the addiction of 10µM PJ-34; with cytokines alone (TNF-α 25 U/ml; IFN-γ 25 U/ml and IL-1β 0,1 U/ml) or in presence of 10µM PJ-34 (added simultaneously) at 24h, 48h. Analysis by Student's T-test *P ≤ 0.05; **P≤ 0.01.

Figure 9 shows the relative rates of α-TC1.6 vital, early apoptotic, late apoptotic and necrotic cells for each of experimental conditions, at both time points (24h and 48h). There are not significant differences among the vital, early apoptotic, late apoptotic and necrotic cells rates of α-TC1.6 cells at the steady state compared to the α-TC1.6 cells grown with 10µM PJ-34, for 24h. However, it is possible to observe a significant enhancement (P<0.05) of the rate of vital cells among the cells treated with 10µM PJ-34 and those treated with inflammatory cytokines (TNF-α 25 U/ml; IFN-γ 25 U/ml and IL-1β 0,1 U/ml). The rate of α-TC1.6 vital cells was restored to control value after the addiction of 10µM PJ-34 to the cytokines. The figure 6 showed also a statistically significant reduction of the rates of early apoptotic cells in α-TC1.6 cells treated with cytokines (TNF-α 25 U/ml; IFN-γ 25 U/ml and IL-1β 0,1 U/ml) compared to the control and to α-TC1.6 cells treated with 10µM PJ-34, for 24h. The addiction of 10µM PJ-34to the cytokines (TNF-α 25 U/ml; IFN-γ 25 U/ml and IL-1β 0,1 U/ml) cause a

statistically significant reduction of the rates of early apoptotic cells, reproducing the same situation present in the control and PJ-34 conditions. Concerning to the rate of late apoptotic cells, after 24h, the addiction of 10μM PJ-34 to the cytokines (TNF-α 25 U/ml; IFN-γ 25 U/ml and IL-1β 0,1 U/ml) determined a significant increase of the rate of late apoptotic α-TC1.6 cells compared to α-TC1.6 cells treated for the same time with cytokines (TNF-α 25 U/ml; IFN-γ 25 U/ml and IL-1β 0,1 U/ml).

At 48h, there are statistically significant difference among the rates of vital α-TC1.6 cells treated with 10μM PJ-34 with and without cytokines (TNF-α 25 U/ml; IFN-γ 25 U/ml and IL-1β 0,1 U/ml). In fact, 10μM PJ-34 added to cytokines (TNF-α 25 U/ml; IFN-γ 25 U/ml and IL-1β 0,1 U/ml) determined a reduction of the rate of vital cells against to PJ-34 alone. Regarding the rates of early apoptotic α-TC1.6 cells are similar in every experimental condition. Conversely, there are a statistically significant increment of the rates of late apoptotic cells among α-TC1.6 cells treated with 10μM PJ-34 alone compared to α-TC1.6 cells grown with cytokines alone (TNF-α 25 U/ml; IFN-γ 25 U/ml and IL-1β 0,1 U/ml) and with cytokines (TNF-α 25 U/ml; IFN-γ 25 U/ml and IL-1β 0,1 U/ml) in presence of 10μM PJ-34. Furthermore, we can observe a more significant increment ($P<0.01$) of rates of late apoptotic cells among the α-TC1.6 cells treated, for 48h, with cytokines (TNF-α 25 U/ml; IFN-γ 25 U/ml and IL-1β 0,1 U/ml) and α-TC1.6 cells treated with cytokines (TNF-α 25 U/ml; IFN-γ 25 U/ml and IL-1β 0,1 U/ml) in presence of 10μM PJ-34, for the same experimental time. Finally, since the rates of necrotic α-TC1.6 cells were very low, in both time points, they didn't appear in the graphic.

3.5.2 Effect of PJ-34 on apoptotic β-TC1 cells death: flow cytometry analysis

To demonstrate the protective role of PARP-14 in α-TC1.6, we tested the effects of PJ-34 on β-TC1 cells by flow cytometry analysis.

Representative data of the Annexin V-FITC/propidium iodide (PI) flow cytometry results, at 24h and 48h, are shown in Figure 10a and 10b.

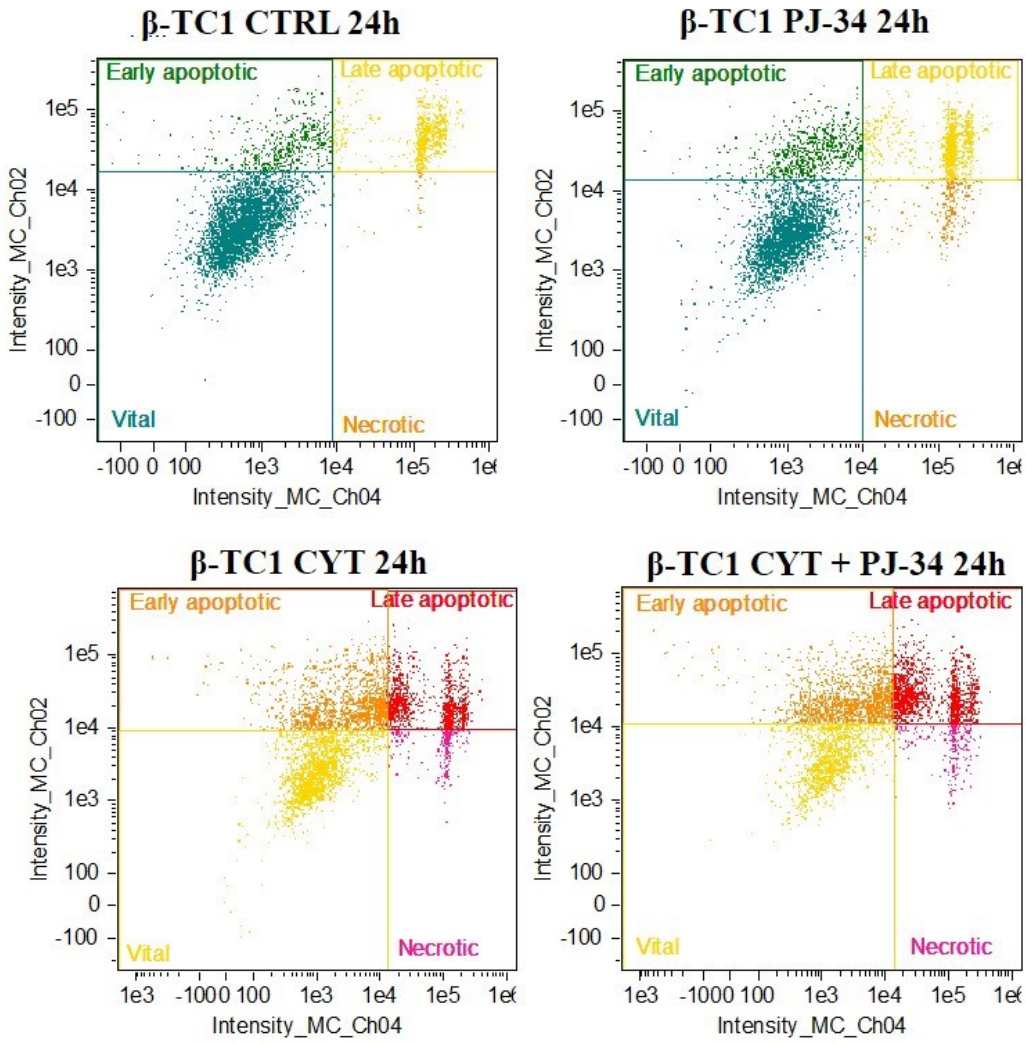

Figure 10a. Representative pictures of flow cytometry analysis on β-TC1 cells, at 24h. In square CTRL, β-TC1 cells grown for 24h with normal medium. In square 10μM PJ-34 β-TC1 cells after 24h of treatment with PARP inhibitor PJ-34. In square CYT β-TC1cells treated, for 24h, with cytokines (TNFα 25 U/ml, IFNγ 25 U/ml, Il-1β 0.1 U/ml). In square CYT + PJ-34 β-TC1cells after 24h of treatment with cytokines in presence of 10μM PJ-34. Each square includes cells stained negatively for both Annexin V and PI and are considered undamaged (Vital cells); cells stained with Annexin V, but are PI negative and are considered early apoptotic cells; cells that are both Annexin V and PI positive and are considered late apoptotic and cells that are PI positive and Annexin V negative and are considered necrotic cells.

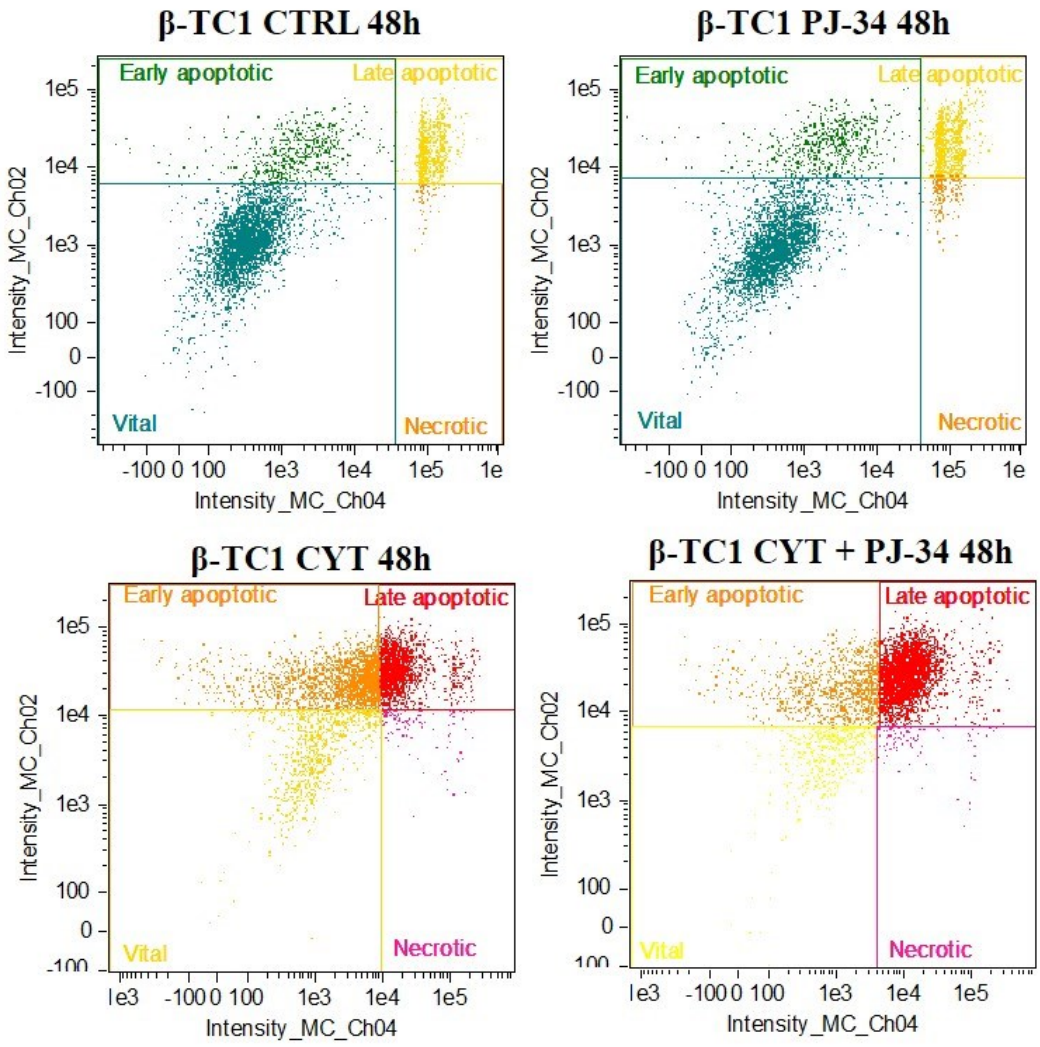

Figure 10b. Representative pictures of flow cytometry analysis on β-TC1 cells, at 48h. In square CTRL, β-TC1 cells grown for 48h with normal medium. In square 10μM PJ-34 β-TC1 cells after 48h of treatment with PARP inhibitor PJ-34. In square CYT β-TC1cells treated, for 48h, with cytokines (TNFα 25 U/ml, IFNγ 25 U/ml, Il-1β 0.1 U/ml). In square CYT + PJ-34 β-TC1cells after 48h of treatment with cytokines in presence of 10μM PJ-34. Each square includes cells stained negatively for both Annexin V and PI and are considered undamaged (Vital cells); cells stained with Annexin V, but are PI negative and are considered early apoptotic cells; cells that are both Annexin V and PI positive and are considered late apoptotic and cells that are PI positive and Annexin V negative and are considered necrotic cells.

The scatter plots of both pancreatic cell lines (figure 8a and 8b; 10a and 10b) show a very important differences between the distribution of β-TC1 and α-TC1.6 cell population, particularly after cytokines treatment. In fact, as α-TC1.6 cells, the distribution of β-TC1 cell population treated with 10μM PJ-34 was similar compared to the control, at 24h as well as at 48h. However, the most significant differences in the distribution of β-TC1 cell population occur when β-TC1 cell grown in presence of

cytokines (TNF-α 25 U/ml; IFN-γ 25 U/ml and IL-1β 0,1 U/ml), with or without 10µM PJ-34. In these cases, most of β-TC1 cell population is scattered within the upper quadrants, proving that this cells are stained with Annexin V going through an apoptotic death.

In figure 11 are reported the cytometry results. The histograms represent the rates of vital, early apoptotic, late apoptotic and necrotic β-TC1 cells in different experimental conditions (control, PJ-34, cytokines (TNF-α 25 U/ml; IFN-γ 25 U/ml and IL-1β 0,1 U/ml) and cytokines + PJ-34) at 24h and 48h.

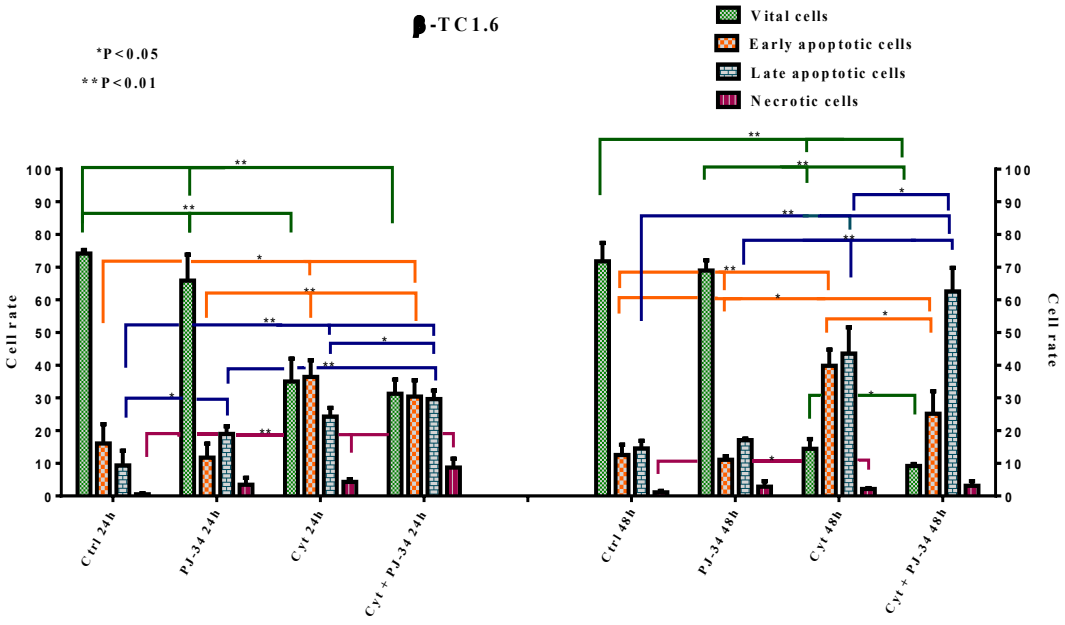

Figure 11. Cytometry analysis on pancreatic β-TC1 cell lines. Histograms show the rate of vital, early apoptotic, late apoptotic and necrotic β-TC1 cells, at the steady state (control); with the addiction of 10µM PJ-34; with cytokines alone or in presence of 10µM PJ-34, at 24h, 48h. Analysis by Student's T-test *P ≤ 0.05; **P≤ 0.01.

As shown in figure, there is statistically significant decrease of the rates of vital β-TC1 cells among the β-TC1 cells at the steady state and β-TC1 cells treated, for 24h, with 10µM PJ-34 compared to β-TC1 cells treated, with the same time, with cytokine alone (TNF-α 25 U/ml; IFN-γ 25 U/ml and IL-1β 0,1 U/ml) and in presence of 10µM PJ-34.

This decrease is associated to a statistically significant increase of the rates of early apoptotic cells in β-TC1 cells treated with cytokines (TNF-α 25 U/ml; IFN-γ 25 U/ml and IL-1β 0,1 U/ml) in presence and absence 10μM PJ-34 compared to the control ($P<0.05$) and to the β-TC1 cells grown with 10μM PJ-34 alone ($P<0.01$). Concerning to the late apoptotic cell, after 24h, we can observe a statistically significant increase among the control compared to PJ-34 condition. However, this increment is more significant among the control compared to the cytokines (TNF-α 25 U/ml; IFN-γ 25 U/ml and IL-1β 0,1 U/ml) with and without PJ-34. There are also statistically significant differences of the rates of late apoptotic cells among the β-TC1 cells treated, for 24h, with 10μM PJ-34 alone compared to β-TC1 cells treated with cytokines (TNF-α 25 U/ml; IFN-γ 25 U/ml and IL-1β 0,1 U/ml) and 10μM PJ-34. Furthermore, it is possible to note a significant increment of the rates of late apoptotic cells among the β-TC1cells grown with cytokines (TNF-α 25 U/ml; IFN-γ 25 U/ml and IL-1β 0,1 U/ml) compared to the β-TC1cells grown with cytokines (TNF-α 25 U/ml; IFN-γ 25 U/ml and IL-1β 0,1 U/ml) in presence of 10μM PJ-34. Finally, after 24h, the treatment with cytokines alone (TNF-α 25 U/ml; IFN-γ 25 U/ml and IL-1β 0,1 U/ml) or in presence of 10μM PJ-34 cause a statistically significant enhancement of the rates of necrotic β-TC1 cells compared to the control.

The histograms showed on the right represent the trend of the rates of vital, early apoptotic, late apoptotic and necrotic β-TC1 cells, after 48h of treatments. There is a statistically significant reduction of the rates of vital cell among the β-TC1 cells at the steady state and in the PJ-34 condition compared to the cytokines alone (TNF-α 25 U/ml; IFN-γ 25 U/ml and IL-1β 0,1 U/ml) and in presence of 10μM PJ-34. A statistically significant reduction of the rates of vital cell occurs also when β-TC1 cells are treated with cytokines (TNF-α 25 U/ml; IFN-γ 25 U/ml and IL-1β 0,1 U/ml) in

presence of 10μM PJ-34 compared to β-TC1 cells grown with cytokines alone (TNF-α 25 U/ml; IFN-γ 25 U/ml and IL-1β 0,1 U/ml). Referring to the early apoptotic cells we can observe a statistically significant enhancement of this rates among the control and PJ-34 condition compared to β-TC1 cells grown with cytokines alone ($P<0.01$) and in presence of 10μM PJ-34 ($P<0.05$). Furthermore, the addiction of 10μM PJ-34 to the cytokines (TNF-α 25 U/ml; IFN-γ 25 U/ml and IL-1β 0,1 U/ml) determined a statistically significant increment of the rates of early apoptotic cell compared to the β-TC1 cells treated with cytokines alone (TNF-α 25 U/ml; IFN-γ 25 U/ml and IL-1β 0,1 U/ml). A similar trend was observed for the late apoptotic cells. In fact, as early apoptotic cells, there is a statistically significant enhancement of the rates of late apoptotic cells among the β-TC1 cells at the steady state and β-TC1 cells treated with 10μM PJ-34 compared to β-TC1 cells treated with cytokines alone (TNF-α 25 U/ml; IFN-γ 25 U/ml and IL-1β 0,1 U/ml) and with cytokines (TNF-α 25 U/ml; IFN-γ 25 U/ml and IL-1β 0,1 U/ml) with 10μM PJ-34. In addition, the rates of the late apoptotic cells increase in statistically significant manner in the β-TC1 cells grown in presence of both cytokines (TNF-α 25 U/ml; IFN-γ 25 U/ml and IL-1β 0,1 U/ml) and 10μM PJ-34 compared to β-TC1 cells grown with cytokines alone (TNF-α 25 U/ml; IFN-γ 25 U/ml and IL-1β 0,1 U/ml). The last rates regard the necrotic cells. In this case, there is a statistically significant increase among the rates of necrotic cell of the control compared to those of the cytokines condition.

3.6 Graphical Abstract

The figure shows our proposed model, which postulates that PARP-14 activation by phosphorylated JNK-2 could contribute to the survival of α-TC1.6 cells. In both pancreatic cell lines (α-TC1.6 cells and β-TC1 cells), binding of cytokines to their specific receptors activates the Mitogen-Activated Protein Kinase (MAPK) signalling cascade: this culminates with the Stress-Activated Protein Kinases (SAPK) / Jun N-terminal Kinases (JNK) activation.

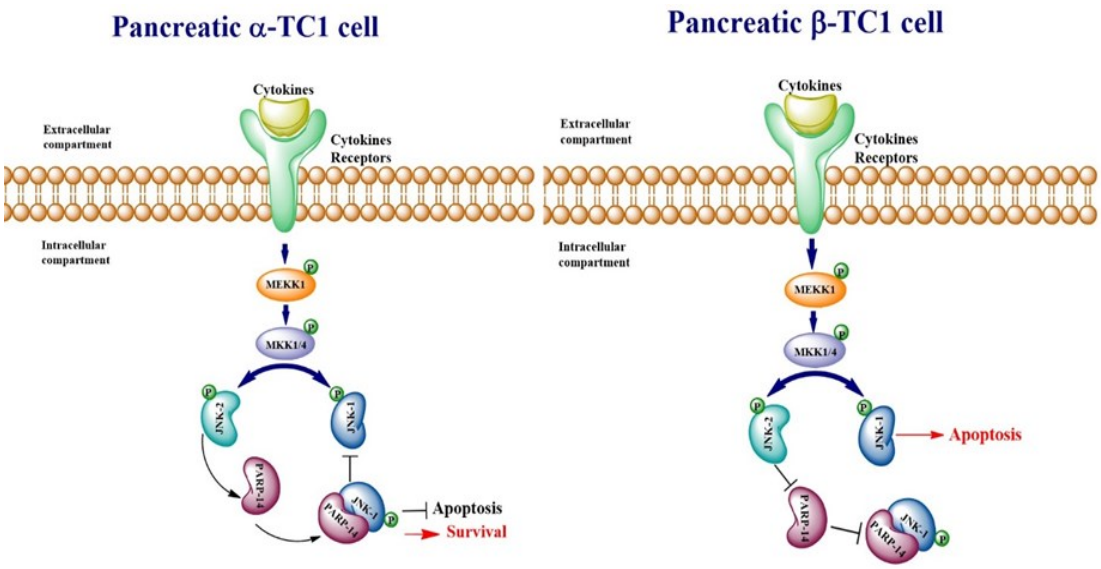

JNK-1 is involved in different cellular activity as cell differentiation and proliferation, apoptosis, neurodegeneration, inflammatory conditions and cytokine production. Under inflammatory stimuli, the pancreatic α-TC1.6 cell line overexpresses PARP-14. Therefore, in these cells, the phosphorylated JNK-2 activates PARP-14 that binds and inhibits JNK-1, promoting cell survival. Conversely, in the presence of an inflammatory environment, the pancreatic β-TC1 cell line doesn't express high levels of PARP-14: then, in these cells, JNK-1 can trigger apoptotic death.

4. Discussion

Poly(ADP)ribose polymerases (PARPs), also known as ADP-ribosyl transferases (ARTDs), comprise a large family of proteins that catalyse the transfer of ADP-ribose units from NAD+ to a number of acceptor proteins. PARP-14 is a member of the macro-PARP, one branch of the large family of PARP-like proteins also designated as B aggressive lymphoma proteins (BAL1, 2a/2b, 3, or PARP-9, PARP-14, and PARP-15) (Cho S.H. et al., 2009). In fact, PARP-14 contains three copies of the macrodomains that were first identified in the non-classical histone macroH2A (mH2A) (Mehrotra P. et al., 2011). Since mH2A participates in the inactivation of the X chromosome (Xi) and macrodomains are associated to histone deacetylases (HDACs), it is possible that the macrodomains found in PARP-14 may function to repress transcription. However, it has been shown that PARP-14 enhances Stat6-dependent transcription instead of repressing it (Goenka S. and Boothby M., 2006). According to this evidence, PARP-14 does function as a repressor first by recruiting HDAC 2 and 3. However, in the presence of IL-4 the ADP-ribosyl transferase activity of PARP-14 is activated, which results in relieving its repressive function: this indicate that the ADP-ribosyl transferase function of PARP-14 is extremely important for its transcriptional enhancement functions (Mehrotra P. et al., 2011). Although, the physiologic functions of PARP-14 and other members of the BAL (macro-PARP) family are not clear, Cho et al. reported that PARP-14 mediated IL-4–induced B-cell protection against apoptosis after irradiation or growth factor withdrawal. Furthermore, they demonstrated that the induction of several B-cell survival factors (Pim-1; Mcl-1) by IL-4 depended on PARP-14 (Cho S.H. et al., 2009). PARP-14 expression has been also shown to promote B-cell lymphomagenesis through supporting cell survival signals in mice (Cho S.H. et al., 2011).

Recently it has been shown that in multiple myeloma (MM) PARP-14 acts as a physiological downstream effector of the JNK-2-dependent prosurvival signaling, by binding to JNK-1 and inhibiting its activity. It was also found that expression of PARP-14 is correlated with disease progression and poor prognosis in MM (Barbarulo A. et al., 2013). Signaling via JNK is involved in induction of apoptosis, cell proliferation, transformation and survival through phosphorylation and regulation of its substrates (Bogoyevitch M.A. and Kobe B., 2006). In particular, JNK-1 is a pro-apoptotic factor, thus its inhibition could promote cell survival. Indeed, this study showed that JNK-2 is a master regulator of survival of myeloma cells, and defined a new regulatory pathway linking JNK-2 to JNK-1 through regulation of a novel survival factor of B-lineage cells, PARP-14 (Barbarulo A. et al., 2013; Cho S.H. et al., 2009). The interaction between PARP-14 and JNK-1 regulates negatively the proapoptotic activity of JNK-1, promoting cell survival. Therefore, this study describes a novel regulatory pathway in myeloma cells through which JNK-2 promotes survival and suggests that selective inhibition of PARP14 might be of therapeutic value (Barbarulo A. et al., 2013). Pharmacological inhibition of key proteins involved in the response to DNA damage has emerged as an effective tool for cancer treatment, given that the resistance of cancer cells to DNA damaging agents originates from the modulation of DNA repair pathways (Peralta-Leal A. et al., 2009). Recently, we demonstrated that PARP-1 inhibition was able to impair the migration of endothelial cells induced by conditioned medium from glioma cells, showing an antiangiogenic effect of PARP inhibitor PJ-34 (Motta C. et al., 2015). Furthermore, PARP inhibitors exert a protective effect towards a number of inflammatory conditions (Giansanti V. et al., 2010).

According to this mechanism of PARP inhibitors, in our previous studies we demonstrated the effects of DPQ and PJ-34 on human glioblastoma (GBM) cells in a

proinflammatory state induced by Lipopolysaccharide (LPS) and Interferon-γ (INF-γ). In that case, we demonstrated that DPQ and PJ-34 reduced cell inflammation and damage following PARP-1 overexpression, while they increased cell survival, similar to other well characterized drugs (Scalia et al., 2013). In our previous study we also showed the protective effect of PARP inhibition on rat primary astroglial cells cultures, under LPS/IFNγ induced proinflammatory conditions (Spina-Purrello V. et al., 2008). PARPs inhibitors are designed to compete with NAD+ at the enzyme active site. Although they universally inhibit PARP-1, most of them have the potential to inhibit other enzymes that use NAD+, including other members of the PARP family, mono-ADP-ribosyl-transferases and sirtuins; however, the extent to which they do so is largely unknown (Rouleau M. et al., 2010). Thus, the PARP-1 inhibitor PJ-34 was considered a pan-PARP inhibitor, since it is able to bind and inhibit other PARPs, including PARP-14. These observations led us to investigate whether one or more of PARP family members are involved in immune-mediated diabetes.

It is well known that the etiology of the immune-mediated diabetes stems from a progressive autoimmune assault, in which macrophages and T cells secrete proinflammatory cytokines, as IL-1β, IFN-γ, and TNF-α as well as nitric oxide (NO), which provoke cell death. Therefore, in our experimental design, we treated mouse pancreatic β-TC1 and α-TC1.6 cell lines with a cocktail of inflammatory cytokines for two time points (24h and 48h). Although pancreatic α and β cells derive from common endocrine precursors (Ngn3+ cells), after their differentiation they have a different physiological response to external stimuli, including the exposition to inflammatory environment. In particular, in presence of inflammatory cytokines pancreatic α-cells are resistant to the apoptotic death, whereas pancreatic β-cells are very susceptible.

Therefore, we sought to study the molecular mechanism responsible of the pancreatic α-TC1.6 cells resistance to apoptotic death.

By RT-PCR analysis we found that PARP-14 was the only PARP differentially expressed between the pancreatic β-TC1 and α-TC1.6 cell lines. Indeed, it was more overexpressed in α-TC1.6 cells then in β-TC1 cells. Confocal microscopy analysis confirmed the RT-PCR results, showing high expression levels of the protein in α-TC1.6 cells under inflammatory stimuli, at both time points. Thus we hypothesized the involvement of PARP-14 in α-TC1.6 cells resistance to the apoptotic death in presence of an inflammatory insult. However, we observed an overexpression of PARP-14 protein also in β-TC1 cells, only at 24h of treatment with cytokines. This could be due to an attempt of the β-TC1 cells to resist the apoptotic death.

The pan-PARP inhibitor PJ-34, a PARP inhibitor that is able to inhibit also PARP-14, was introduced in the subsequent experiments to further investigate on the possible role of PARP-14 in the α-TC1.6 cells. Therefore, the exposition of α-TC1.6 cell to the cytokines cocktail, at 24h as well as 48h, did not induce any change in cell viability, demonstrating the resistance of α-TC1.6 cells to apoptotic death. On the other hand, after 48h, the treatment with PJ-34 added to the cytokines determined a significant reduction of α-TC1.6 cell viability compared to the treatment with cytokines alone, supporting our hypothesis on protective role of PARP-14 in the pancreatic α-TC1.6 cells. Conversely, the treatment with cytokines of the β-TC1 cells caused a significant reduction of cell viability at both 24h and 48h, confirming the susceptibility of the β-TC1 cells to the apoptotic death.

Our hypothesis on the protective role of PARP-14 was strengthened by caspase-3 assay results. Indeed, according to MTT analysis, at 24h, in the pancreatic α-TC1.6 cells, there were not significant differences of the caspase-3 activity between our

experimental conditions. At 48h, the PJ-34, added to the cytokines, was able, once again, to enhance the of caspase-3 activity, indicating that the inhibition of the protective protein PARP-14 leads the α-TC1.6 cells to apoptotic death. The apoptotic death of β-TC1 cells in presence of inflammatory environment was further confirmed by this assay, that showed a significant increment of caspase-3 activity after both 24h and 48h of treatment cytokines, compared to the control and PJ-34 condition. Furthermore, the addition of PJ-34 to the cytokines caused a significant increase of caspase-3 activity compared to the treatment with cytokines alone, only at 24h. This could be explained through the fact that PJ-34 is a pan-PARP inhibitor, therefore it inhibits different protein belonging to PARP family, including PARP-14 and other PARP that could be essential to the β-TC1 cell survival.

Flow cytometry experiments allowed us to studied the amount of vital, early apoptotic, late apoptotic, and necrotic cells. The results showed a significant increase of the amounts of vital cells and a significant decrease of the amount of early apoptotic cells in α-TC1.6 cells, treated for 24h with cytokines alone compared to the PJ-34 condition. This could indicate that in presence of inflammatory environment, α-TC1.6 cells express protective factors that protect them from apoptotic death, induced by cytokines. Thus, we can speculate that one of this factors could be PARP-14 protein. Indeed, after 24h, its inhibition by PJ-34 added to the cytokines leads to a significant decrease of the numbers of vital cells and a significant increase of the amount of early and late apoptotic cells compared to the cytokines condition, reproducing the same situation present in the control and in PJ-34 condition. At 48h, we can note that the treatment with PJ-34 added to the cytokines determined a significant reduction of the amounts of vital cells and a significant increase of the amounts of late apoptotic cell compared to the PJ-34 alone. These results show that when α-TC1.6 cells were

stimulated with the cytokines, the inflammatory stimuli induced the expression of survival factors, including PARP-14, that can be inhibited by PJ-34. Conversely, when PJ-34 was added to the normal medium, the α-TC1.6 cells did not overexpress PARP-14, thus its inhibitor cannot act.

Concerning β-TC1 cells, it is important to note the drastic reduction of the amounts of vital cells and the high levels of the amounts of early apoptotic, late apoptotic and necrotic cells after treatment with cytokines, compared to the control and PJ-34 condition, at 24h as well as 48h. This, once again, confirms the strong susceptibility of pancreatic β-TC1 cell line to inflammatory environment. The addition of PJ-34 to the cytokines determined at both time points a significant increment of the rate of the late apoptotic cells compared to the treatment with cytokines alone. This shows a consistency of the results of all the experiments, since the MTT and caspase-3 assay demonstrated that the addition of the inhibitor PJ-34 determined an increase of β-TC1 apoptotic death, probably for its ability to inhibit the basal levels of the protective protein PARP-14 and other PARPs important to β-TC1 cells physiology.

5. Conclusion

In conclusion, our results show a strong relationship between PARP-14 and α-TC1.6 cells survival after inflammatory insult. Indeed, the treatment with the pan-PARP inhibitor PJ-34, added to cytokines cocktail, has proven effective to reduce α-TC1.6 apoptosis resistance. Therefore, here we showed a new protective factor against the apoptotic death of pancreatic cells, paving the way to the understanding of the molecular mechanisms underlying the pancreatic α-TC1.6 survival in a context of immune-mediated diabetes. However, further study will be needed to demonstrate the interaction between PARP-14 and JNK-1 and to investigate the pathway involved in α-TC1.6 cell survival.

References

Albert M.L., 2004. Death-defying immunity: do apoptotic cells influence antigen processing and presentation? Nat Rev Immunol. 4(3):223-31

Baccala R., Hoebe K., Kono D.H., Beutler B., Theofilopoulos A.N., 2007. TLR-dependent and TLR-independent pathways of type I interferon induction in systemic autoimmunity. Nat. Med. 13,543–551

Barbagallo D., Piro S., Condorelli A.G., Mascali L.G., Urbano F., Parrinello N., Monello A., Statello L., Ragusa M., Rabuazzo A.M., Di Pietro C., Purrello F., Purrello M., 2013. miR-296-3p, miR-298-5p and their downstream networks are causally involved in the higher resistance of mammalian pancreatic α cells to cytokine-induced apoptosis as compared to β cells. BMC Genomics 14:62

Barbarulo A., Iansante V., Chaidos A., Naresh K., Rahemtulla A., Franzoso G., Karadimitris A., Haskard D.O., Papa S., Bubici C., 2013. Poly(ADP-ribose) polymerase family member 14 (PARP14) is a novel effector of the JNK2-dependent pro-survival signal in multiple myeloma. Oncogene 32(36):4231-42

Blachère N.E., Darnell R.B., Albert M.L., 2005. Apoptotic cells deliver processed antigen to dendritic cells for cross-presentation. PLoS Biol. 3(6):e185

Bogoyevitch M.A. and Kobe B., 2006. Uses for JNK: the many and varied substrates of the c-Jun N-terminal kinases. Microbiol Mol Biol Rev.

Bolli G.B., Tsalikian E., Haymond M.W., Cryer P.E., Gerich J.E., 1984. Defective glucose counterregulation after subcutaneous insulin in noninsulindependent diabetes mellitus. Paradoxical suppression of glucose utilization and lack of compensatory increase in glucose production, roles of insulin resistance, abnormal neuroendocrine responses, and islet paracrine interactions. Journal of Clinical Investigation 73 1532–1541

Brody L.C., 2005. Treating cancer by targeting a weakness. N Engl J Med 353: 949–950

Cardozo A.K., Ortis F., Storling J., Feng Y.M., Rasschaert J., Tonnesen M., Van Eylen F., Mandrup-Poulsen T., Herchuelz A., Eizirik D.L., 2005. Cytokines downregulate the sarcoendoplasmic reticulum pump Ca2+ ATPase 2b and deplete endoplasmic reticulum Ca2+, leading to induction of endoplasmic reticulum stress in pancreatic beta-cells. Diabetes 54(2):452-61

Chadwick B.P., Valley C.M., Willard H. F., 2001. Histone variant macroH2A contains two distinct macrochromatin domains capable of directing macroH2A to the inactive X chromosome. Nucleic. Acids Res. 29, 2699–2705

Chakravarthy S., Gundimella S. K., Caron C., Perche P. Y., Pehrson J. R., Khochbin S., Luger K., 2005. Structural characterization of the histone variant macroH2A. Mol. Cell. Biol. 25, 7616–7624

Chiarugi A., 2002. Inhibitors of poly(ADP-ribose) polymerase-1 suppress transcriptional activation in lymphocytes and ameliorate autoimmune encephalomyelitis in rats. Br. J. Pharmacol. 137, 761–770

Cho S.H., Ahn A.K., Bhargava P., Lee C.H., Eischen C.M., McGuinness O. Boothby M., 2011. Glycolytic rate and lymphomagenesis depend on PARP14, an ADP ribosyltransferase of the B aggressive lymphoma (BAL) family. Proc Natl Acad Sci USA; 108:15972–15977

Cho S.H., Goenka S., Henttinen T., Gudapati P., Reinikainen A., Eischen C.M., Lahesmaa R., Boothby M., 2009. PARP-14, a member of the B aggressive lymphoma family, transduces survival signals in primary B cells. Blood. 113(11):2416-25

Clark J.B. and Pinder S., 1969. Control of the steady-state concentrations of the nicotinamide nucleotides in rat liver. Biochem J 114:321–30

Clark J.B., Ferris G.M., Pinder S., 1971. Inhibition of nuclear NAD nucleosidase and poly ADP-ribose polymerase activity from rat liver by nicotinamide and 50-methyl nicotinamide. Biochim Biophys Acta 238:82–5

Cnop M., Welsh N., Jonas J.C., Jörns A., Lenzen S., Eizirik D.L., 2005. Mechanisms of pancreatic beta-cell death in type 1 and type 2 diabetes: many differences, few similarities. Diabetes 54 (Suppl. 2), s97–s107

Cobo-Vuilleumier N. and Gauthier B.R., 2012. PARP-1 and cytokine-mediated β-cell damage: a nick in the Okamoto model? Am J Physiol Endocrinol Metab 303: E170–E171

Colyer R.A., Burdette K.E., Kidwell W.R., 1973. Poly ADP-ribose synthesis and DNA replication in synchronized mouse L-cells. Biochem Biophys Res Commun 53:960–6

Costanzi C. and Pehrson J.R., 1998. Histone macroH2A1 is concentrated in the inactive X chromosome of female mammals. Nature 393, 599–601

Cryer P.E., 2002. Hypoglycaemia: the limiting factor in the glycaemic management of Type I and Type II diabetes. Diabetologia 45 937–948

D'Amours D., Desnoyers S., D'Silva I., Poirier G.G., 1999. Poly(ADP-ribosyl)ation reactions in the regulation of nuclear functions. Biochem J. 342(Pt 2): 249–268

Devendra D., Jasinski J., Melanitou E., Nakayama M., Li M., Hensley B., Paronen J., Moriyama H., Miao D., Eisenbarth G.S., Liu E., 2005. Interferon-alpha as a mediator of polyinosinic:polycytidylic acid-induced type 1 diabetes. Diabetes 54(9):2549-56

Dinneen S., Alzaid A., Turk D., Rizza R., 1995. Failure of glucagon suppression contributes to postprandial hyperglycaemia in IDDM. Diabetologia 38 337–343

Dogusan Z., García M., Flamez D., Alexopoulou L., Goldman M., Gysemans C., Mathieu C., Libert C., Eizirik D.L., Rasschaert J., 2008. Double-stranded RNA induces pancreatic beta-cell apoptosis by activation of the toll-like receptor 3 and interferon regulatory factor 3 pathways. Diabetes 57(5):1236-45

Drescher K.M. and Tracy S.M., 2008. The CVB and etiology of type 1 diabetes. Curr Top Microbiol Immunol. 323:259-74

Dunning B.E., Foley J.E., Ahre´n B., 2005. Alpha cell function in health and disease: influence of glucagon-like peptide-1. Diabetologia 48 1700–1713

Eizirik D. L., Colli M. L., Ortis F., 2009. The role of inflammation in insulitis and β-cell loss in type 1 diabetes. Nat. Rev. Endocrinol. 5, 219–226

Eizirik D. L., Mandrup-Poulsen T., 2001. A choice of death the signal-transduction of immune mediated beta-cell apoptosis. Diabetologia 44, 2115–2133

Eizirik D.L., Cardozo A.K., Cnop M., 2008. The role for endoplasmic reticulum stress in diabetes mellitus. Endocr Rev. 29(1):42-61

El-Khamisy S.F., Masutani M., Suzuki H., Caldecott K.W., 2003. A requirement for PARP-1 for the assembly or stability of XRCC1 nuclear foci at sites of oxidative DNA damage. Nucleic Acids Res 31: 5526–5533

Foulis A.K., Farquharson M.A., Meager A., 1987. Immunoreactive alpha-interferon in insulin-secreting beta cells in type 1 diabetes mellitus. Lancet. 2(8573):1423-7

Giansanti V., Donà F., Tillhon M., Scovassi AI., 2010. PARP inhibitors: new tools to protect from inflammation. Biochem Pharmacol.

Giarratana N., Penna G., Amuchastegui S., Mariani R., Daniel K.C., Adorini L., 2004. A vitamin D analog down-regulates proinflammatory chemokine production by pancreatic islets inhibiting T cell recruitment and type 1 diabetes development. J Immunol. 173(4):2280-7

Goenka S. and Boothby M., 2006. Selective potentiation of Stat-dependent gene expression by collaborator of Stat6 (CoaSt6), a transcriptional cofactor. Proc Natl Acad Sci U S A.

Gromada J., Ma X., Hoy M., Bokvist K., Salehi A., Berggren P.O., Rorsman P., 2004. ATP-sensitive KC channel-dependent regulation of glucagon release and electrical activity by glucose in wild-type and SUR1K/K mouse alpha-cells. Diabetes 53 (Suppl 3) S181–S189

Grunnet L.G., Aikin R., Tonnesen M.F., Paraskevas S., Blaabjerg L., Størling J., Rosenberg L., Billestrup N., Maysinger D., Mandrup-Poulsen T., 2009. Proinflammatory cytokines activate the intrinsic apoptotic pathway in beta-cells. Diabetes 58:1807–1815

Hakmé A., Huber A., Dollé P., Schreiber V., 2008. The macroPARP genes Parp-9 and Parp-14 are developmentally and differentially regulated in mouse tissues. Dev Dyn. 237(1):209-15

Hultcrantz M., Hühn M.H., Wolf M., Olsson A., Jacobson S., Williams B.R., Korsgren O., Flodström-Tullberg M., 2007. Interferons induce an antiviral state in human pancreatic islet cells. Virology. 367(1):92-101

Kent S.C., Chen Y., Bregoli L., Clemmings S.M., Kenyon N.S., Ricordi C., Hering B.J., Hafler D.A., 2005. Expanded T cells from pancreatic lymph nodes of type 1 diabetic subjects recognize an insulin epitope. Nature 435(7039):224-8

Kim H.S., Han M.S., Chung K.W., Kim S., Kim E., Kim M.J., Jang E., Lee H.A., Youn J., Akira S., Lee M.S., 2007. Toll-like receptor 2 senses beta-cell death and contributes to the initiation of autoimmune diabetes. Immunity. 27(2):321-33

Ladurner A.G., 2003. Inactivating chromosomes: a macro domain that minimizes transcription. Mol. Cell 12, 1–3

Lang K.S., Recher M., Junt T., Navarini A.A., Harris N.L., Freigang S., Odermatt B., Conrad C., Ittner L.M., Bauer S., Luther S.A., Uematsu S., Akira S., Hengartner H., Zinkernagel R.M., 2005. Toll-like receptor engagement converts T-cell autoreactivity into overt autoimmune disease. Nat Med. 11(2):138-45

Liadis N., Murakami K., Eweida M., Elford A.R., Sheu L., Gaisano H.Y., Hakem R., Ohashi P.S., Woo M., 2005. Caspase-3-dependent beta-cell apoptosis in the initiation of autoimmune diabetes mellitus. Mol Cell Biol. 25(9):3620-9

Lindahl T., Satoh M.S., Poirier G.G., Klungland A., 1995. Post-translational modification of poly(ADP-ribose) polymerase induced by DNA strand breaks. Trends Biochem Sci 20: 405–411

Liu D., Cardozo A.K., Darville M.I., Eizirik D.L., 2002. Double-stranded RNA cooperates with interferon-gamma and IL-1 beta to induce both chemokine expression and nuclear factor-kappa B-dependent apoptosis in pancreatic beta-cells: potential mechanisms for viral-induced insulitis and beta-cell death in type 1 diabetes mellitus. Endocrinology 143(4):1225-34

Liu D., Darville M., Eizirik DL., 2001. Double-stranded ribonucleic acid (RNA) induces beta-cell Fas messenger RNA expression and increases cytokine-induced beta-cell apoptosis. Endocrinology 142(6):2593-9

MacDonald P.E., De Marinis Y.Z., Ramracheya R., Salehi A., Ma X., Johnson P.R., Cox R., Eliasson L., Rorsman P., 2007. A K ATP channel-dependent pathway within alpha cells regulates glucagon release from both rodent and human islets of Langerhans. PLoS Biology 5 e143

Medzhitov R., 2008. Origin and physiological roles of inflammation. Nature 454, 428–435

Mehrotra P., Riley J.P., Patel R., Li F., Voss L., Goenka S., 2011. PARP-14 functions as a transcriptional switch for Stat6-dependent gene activation. J Biol Chem. 286(3):1767-76

Motta C., D'Angeli F., Scalia M., Satriano C., Barbagallo D., Naletova I., Anfuso C.D., Lupo G., Spina-Purrello V., 2015. PJ-34 inhibits PARP-1 expression and ERK phosphorylation in glioma-conditioned brain microvascular endothelial cells. Eur J Pharmacol. 761:55-64

Nadal A., Quesada I., Soria B., 1999. Homologous and heterologous asynchronicity between identified alpha-, beta- and delta-cells within intact islets of Langerhans in the mouse. Journal of Physiology 517 85–93

Nakayama M., Abiru N., Moriyama H., Babaya N., Liu E., Miao D., Yu L., Wegmann D.R., Hutton J.C., Elliott J.F., Eisenbarth G.S., 2005. Prime role for an insulin epitope in the development of type 1 diabetes in NOD mice. Nature 435(7039):220-3

Okamoto H. and Takasawa S., 2002. Recent advances in the Okamoto model: the CD38-cyclic ADP-ribose signal system and the regenerating gene protein (Reg)-Reg receptor system in beta-cells. Diabetes 51 Suppl 3:S462-73

Peralta-Leal A., Rodríguez-Vargas J.M., Aguilar-Quesada R., Rodríguez M.I., Linares J.L., de Almodóvar M.R., Oliver F.J., 2009. PARP inhibitors: new partners in the therapy of cancer and inflammatory diseases. Free Radic Biol Med. 47(1):13-26

Purnell M.R. and Whish W.J., 1980. Novel inhibitors of poly(ADP-ribose) synthetase. Biochem J. 185:775–7

Quesada I., Nadal A., Soria B., 1999. Different effects of tolbutamide and diazoxide in alpha, beta-, and delta-cells within intact islets of Langerhans. Diabetes 48 2390–2397

Quesada I., Todorova M.G., Alonso-Magdalena P., Beltra M., Carneiro E.M., Martin F., Nadal A. and Soria B., 2006b. Glucose induces opposite intracellular Ca2C concentration oscillatory patterns in identified α- and β-cells within intact human islets of Langerhans. Diabetes 55 2463–2469

Quesada I., Todorova M.G., Soria B., 2006a. Different metabolic responses in α-β-, and δ-cells of the islet of Langerhans monitored by redox confocal microscopy. Biophysical Journal 90 2641–2650

Quesada I., Tudurí E., Ripoll C., Nadal A., 2008. Physiology of the pancreatic alpha-cell and glucagon secretion: role in glucose homeostasis and diabetes. J Endocrinol. 199(1):5-19

Rasschaert J., Ladrière L., Urbain M., Dogusan Z., Katabua B., Sato S., Akira S., Gysemans C., Mathieu C., Eizirik D.L., 2005. Toll-like receptor 3 and STAT-1 contribute to double-stranded RNA+ interferon-gamma-induced apoptosis in primary pancreatic beta-cells. J Biol Chem. 280 (40):33984-91

Rouleau M., Patel A., Hendzel M.J., Kaufmann S.H., Poirier G.G., 2010. PARP inhibition: PARP1 and beyond. Nat Rev Cancer.

Ruf A., de Murcia G., Schulz GE., 1998. Inhibitor and NAD^+ binding to poly(ADPribose) polymerase as derived from crystal structures and homology modeling. Biochemistry 37:3893–900

Ruf A., Mennissier de Murcia J., de Murcia G., Schulz G.E., 1996. Structure of the catalytic fragment of poly(AD-ribose) polymerase from chicken. Proc Natl Acad Sci USA 93:7481–5

Scalia M., Satriano C., Greca R., Giuffrida-Stella A.M., Rizzarelli E., Spina-Purrello V., 2013. PARP-1 inhibitors DPQ and PJ-34 negatively modulate proinflammatory commitment of human glioblastoma cells. Neurochem Res 38:50-58

Scheuner D. and Kaufman R.J., 2008. The unfolded protein response: a pathway that links insulin demand with beta-cell failure and diabetes. Endocr Rev. 29(3):317-33

Shah P., Basu A., Basu R., Rizza R., 1999. Impact of lack of suppression of glucagon on glucose tolerance in humans. American Journal of Physiology 277 E283–E290

Shah P., Vella A., Basu A., Basu R., Schwenk W.F., Rizza R.A. 2000. Lack of suppression of glucagon contributes to postprandial hyperglycemia in subjects with type 2 diabetes mellitus. Journal of Clinical Endocrinology and Metabolism 85 4053–4059

Shall S., 1975. Proceedings: experimental manipulation of the specific activity of poly(ADP-ribose) polymerase. J Biochem 77:2

Skowera A., Ellis R.J., Varela-Calviño R., Arif S., Huang G.C., Van-Krinks C., Zaremba A., Rackham C., Allen J.S., Tree T.I., Zhao M., Dayan C.M., Sewell A.K., Unger W.W., Drijfhout J.W., Ossendorp F., Roep B.O., Peakman M., 2008. CTLs are targeted to kill beta cells in patients with type 1 diabetes through recognition of a glucose-regulated preproinsulin epitope. J Clin Invest. 118(10):3390-402

Spina-Purrello V., Patti D., Giuffrida-Stella A.M., Nicoletti V.G., 2008. Parp and cell death or protection in rat primary astroglial cell cultures under LPS/IFNgamma induced proinflammatory conditions. Neurochem Res. 33(12):2583-92

Steffen J.D., Brody J.R., Armen R.S., Pascal J.M., 2013. Structural Implications for Selective Targeting of PARPs. Front Oncol. 20;3:301

Suarez-Pinzon W.L., Mabley J.G., Power R., Szabo C., Rabinovitch A., 2003. Poly (ADP-ribose) polymerase inhibition prevents spontaneous and recurrent autoimmune diabetes in NOD mice by inducing apoptosis of islet-infiltrating leukocytes. Diabetes 52:1683–1688

Uchigata Y., Yamamoto H., Kawamura A., Okamoto H., 1982. Protection by superoxide dismutase, catalase, and poly(ADP-ribose) synthetase inhibitors against alloxan- and streptozotocin-induced islet DNA strand breaks and against the inhibition of proinsulin synthesis. J Biol Chem 257:6084–6088

Uchigata Y., Yamamoto H., Nagai H., Okamoto H., 1983. Effect of poly(ADP-ribose) synthetase inhibitor administration to rats before and after injection of alloxan and streptozotocin on islet proinsulin synthesis. Diabetes 32:316–318

Underhill C., Toulmonde M., Bonnefoi H., 2011. A review of PARP inhibitors: from bench to bedside. Ann Oncol. 22(2):268-79

Vives-PI M., Somoza N., Fernández-Alvarez J., Vargas F., Caro P., Alba A., Gomis R., Labeta M.O., Pujol-Borrell R., 2003. Evidence of expression of endotoxin receptors CD14, Toll-like receptors TLR4

and TLR2 and associated molecule MD-2 and of sensitivity to endotoxin (LPs) in islet beta cells. Clin. Exp. Immunol. 133, 208–218

Wahlberg E., Karlberg T., Kouznetsova E., Markova N., Macchiarulo A., Thorsell A.G., Pol E., Frostell Å., Ekblad T., Öncü D., Kull B., Robertson G.M., Pellicciari R., Schüler H., Weigelt J., 2012. Family-wide chemical profiling and structural analysis of PARP and tankyrase inhibitors. Nat Biotechnol. 30(3):283-8

Wen L., Peng J., Li Z., Wong F.S., 2004. The effect of innate immunity on autoimmune diabetes and the expression of Toll-like receptors on pancreatic islets. J Immunol. 172(5):3173-80

Wong F.S., Karttunen J., Dumont C., Wen L., Visintin I., Pilip I.M., Shastri N., Pamer E.G., Janeway C.A. Jr., 1999. Identification of an MHC class I-restricted autoantigen in type 1 diabetes by screening an organ-specific cDNA library. Nat Med. (9):1026-31

Yamamoto H., Uchigata Y., Okamoto H., 1981. Streptozotocin and alloxan induce DNA strand breaks and poly(ADP-ribose) synthetase in pancreatic islets. Nature 294: 284–286

Ylipaasto P., Kutlu B., Rasilainen S., Rasschaert J., Salmela K., Teerijoki H., Korsgren O., Lahesmaa R., Hovi T., Eizirik D.L., Otonkoski T., Roivainen M., 2005. Global profiling of coxsackievirus- and cytokine-induced gene expression in human pancreatic islets. Diabetes 48(8):1510-22

Zhou H., Zhang T., Oseid E., Harmon J., Tonooka N., Robertson R.P., 2007. Reversal of defective glucagon responses to hypoglycemia in insulindependent autoimmune diabetic BB rats. Endocrinology 148 2863–2869.